UNIVERSITY OF OKLAHOMA

GRADUATE COLLEGE

# STRUCTURAL ANALYSIS OF A NATURALLY FRACTURED CARBONATE FIELD IN THE SOUTH-EAST GULF OF MÉXICO.

A THESIS

SUBMITTED TO THE GRADUATE FACULTY

in partial fulfillment of the requirements for the

Degree of

MASTER OF SCIENCE

By

LAURA BEATRIZ SÁNCHEZ FLORES
Norman, Oklahoma
2018

STRUCTURAL ANALYSIS OF A NATURALLY FRACTURED CARBONATE FIELD IN THE SOUTH-EAST GULF OF MÉXICO

A THESIS APPROVED FOR THE
CONOCOPHILLIPS SCHOOL OF GEOLOGY AND GEOPHYSICS

BY

_____
Dr. Shankar Mitra, Chair

_____
Dr. Kurt Marfurt

_____
Dr. Roger Slatt

*To my first and endless love, my Mom: Laura Flores.*
*My example of persistence and encouragement.*

**Acknowledgments**

I would like to express my gratitude to PEMEX Exploración y Producción and to CONACYT-SENER-Hidrocarburos for permitting me to realize my long-held dream of completing a postgraduate degree in Geology. Thank you for the support and funding of my work. I am deeply indebted to my PEMEX supervisors: Antonio Escalera Alcocer, Guillermo Mora Oropeza, Dr. Faustino Monroy Santiago, Leonardo E. Aguilera Gómez, Ignacio Pereznegrón Zarco. Especially thank you to my PEMEX advisor and friend Rolando H. Peterson for his guidance and encouragement in all moment. Thank you PEMEX and CNH for the permission to use the data in my thesis. Thanks, also to my many friends in PEMEX and helpful contributors: Antonio Cervantes, Gerardo Leyva, Rodrigo Portillo, Alberto Abarca, Arely Villaveitia, Javier Cortazar, Rubi Bravo and Juana O. Salas. And, of course, my thanks to the PEMEX administrative and human resources staff: Erika Carmona, Monica Aldape, and Alma Silvia for keeping me focused and headed in the right direction!

I am very appreciative of all the members of the faculty at the University of Oklahoma who welcomed me and assisted me throughout my studies and research, especially my advisor, Dr. Shankar Mitra who gave continuing guidance as I developed my thesis and during his Structural Geology courses. A special thanks to Dr. Kurt Marfurt and Dr. Roger Slatt, for their classes on Seismic Interpretation and Reservoir Characterization, courses which formed the basis of my work. I also wish to thank Dr. Lynn Soreghan for her support and example. Thanks also to the administrative staff of the Geology Department at OU, especially to Rebecca Fay, Ginny Gandy and Lisa Mitchel who were there to deal with my concerns and doubts.

To my dear friends in Oklahoma: Orquidea Trejo, Paula Perilla, Robinson Carvallido, Rafael Pires de Lima, Catherine Schipul, Puntira Henglei, Ashley Horton, Laura Hernández, Daniela, Henry, Hernán, Shipra Shina, Yuli, Saurab, Lenon, Andreina, Bryan, David, Richard, Carlos, Emilio, Jian Jun, Jie, for your friendship and support in all the moments.

Special Thank you to my beloved family: Gerardo Pineda, Laura Flores, Juan Manuel Sánchez, Marcela, Paulina and Juan Manuel, know how much I treasure your presence in my life!

## Table of Contents

## List of Tables

## List of Figures

# ABSTRACT

Fractured carbonates produce more than 85% of hydrocarbon production in Mexico. A large number of the producing fields are located in the South Gulf Salt Province (SGSP) in Campeche Bay within the Upper Jurassic Kimmeridgian and Cretaceous carbonates. Multidisciplinary analysis involving structural and stratigraphic interpretation, integrated with fracture analysis is needed to efficiently produce from these fields. This study focuses on the structural geology and fracture analysis of two structures (A and B) in the area. As well as in the inquiring of the most important mechanisms involved in the formation of the most critical hydrocarbon traps and principal reservoirs.

The structures formed during four main periods of deformation, including (1) upper Jurassic to early Cretaceous extension (D1), (2) Eocene-Oligocene compression (D2), (3) Middle-Upper Miocene compression (D3), and (4) late Miocene to Recent extension (D4). The deformation resulted in broad faulted detachment folds superimposed on salt pillows. Numerous secondary faults related to episodes D2-D4 are mapped on the structures. Although a number of fracture sets related to the multiple episodes of deformation are present, the main sets of open conductive fractures are transverse (type1), and longitudinal (type 2). The principal factors controlling the presence of the naturally fractured carbonate reservoirs are related to the lithology, and local deformation discussed.The interpreted structural geometry, evolution, and fracture patterns will be critical for future production from the Cretaceous reservoirs.

# CHAPTER 1. Introduction.

The Campeche Basin is the most developed petroliferous zone in México. The study area is located in this basin, at the south-east of the Gulf of Mexico, about 88.7 km to the north of Villahermosa and 80 km to the south-southeast of Ciudad del Carmen, Campeche, México. (**Figure 1. 1**). The South Gulf Salt Province (SGSP) has been developed in the oil industry and includes the oil provinces of the Chiapas Fold Belt, Southeast Basins and Deep Gulf of Mexico. In addition, SGSP is divided into sub-provinces as explained in the tectonic settings section of the next chapter.

In México, more than 85% of the hydrocarbon production comes from naturally fractured carbonate reservoirs (F. Monroy et al. 2012, PEMEX, personal communication). This type of reservoir has formed as a result of complex structural deformation in the study area, located in the Chiapas Fold Belt province. This province involves three or more deformational events, including both extensional and compressional episodes. Additionally, salt and shale diapirism is involved. The understanding of these reservoirs in the Campeche Basin is essential to the proposal of new exploratory prospects.

Most of the oil of this region has been developed from Mesozoic carbonate rocks in carbonate slopes, base of slope, and basal carbonate debris flow facies as a response to the regional tectonics and the impact of the Chicxulub meteorite on the Yucatán Peninsula (Grajales Nishimura et al., 2000; Murillo-Muñetón et al., 2002)(Grajales-Nishimura et al., 2000; Murillo-Muñetón et al., 2002)(Grajales-Nishimura et al., 2000; Murillo-Muñetón et al., 2002)(Grajales-Nishimura et al., 2000;

Murillo-Muñetón et al., 2002). Trapping mechanisms include Upper Jurassic, Cretaceous and Tertiary stratigraphic traps in carbonate and clastic facies, and numerous structural traps associated with the Neogene and Paleogene movements and the Upper Jurassic salt diapirism (Magoon et al., 2001).

## 1.1 Objectives.

The objectives of this study are:

1) To develop a structural interpretation of two structures, analyzing the principal deformation events responsible for their origin and architecture, to explain the possible relationship and evolution of faults and fractures to deformational events, and to determine the most important structural elements responsible for hydrocarbon trap formation in the area; and

2) To construct a 3D structural model for the purpose of understanding the 3D structural deformation of the Mesozoic units, analyzing the correlation between the deformation, stratigraphy and fracturing within the Cretaceous. This analysis is used to resolve the uncertainty about the main controls that created the natural fracture systems in the two structures. This objective is applied to the Cretaceous, because is the most important fractured play in the area.

## 1.2 Methodology.

The study utilizes a multi-disciplinary analysis involving four steps to develop the stated objectives:

1) Structural interpretation of the area using three-dimensional depth migrated seismic, acquired using Ocean Bottom Cable (OBC) during 2011-2013. The final Reverse Time Migration (RTM) volume was processed and integrated with well data in 2015. Interpretation of horizons of interest, such as the top of the Upper Cretaceous, Upper Jurassic Kimmeridgian, and the top and base of the autochthonous salt (principal detachment surface in the area) was followed by the interpretation of unconformities, detachment surfaces, and compartmentalized zones. The interpreted horizons and wells located in the different zones were correlated to determine the evolution and relation of the structures with the deformational events.

2) Structural attributes were analyzed by applying OU AASPI software and other commercial software for seismic interpretation, to define and compare which attributes best enhance the principal unconformities as faults and structural or stratigraphic features, and subsequently adjust and correlate the results with well data. The possible application of attributes to identify major fractured zones or distribution of lithology and petrophysical properties in the 3D model were also investigated.

3) Three cross sections were constructed to understand and represent the structural geometry of the folds and interpreted the ages of the principal deformational events involved.

4) Fracture analysis in cores, thin sections, well logs and petrophysics were used to determine the generation of the most critical naturally open fracture systems with the purpose of extrapolating this information to new exploratory prospects.

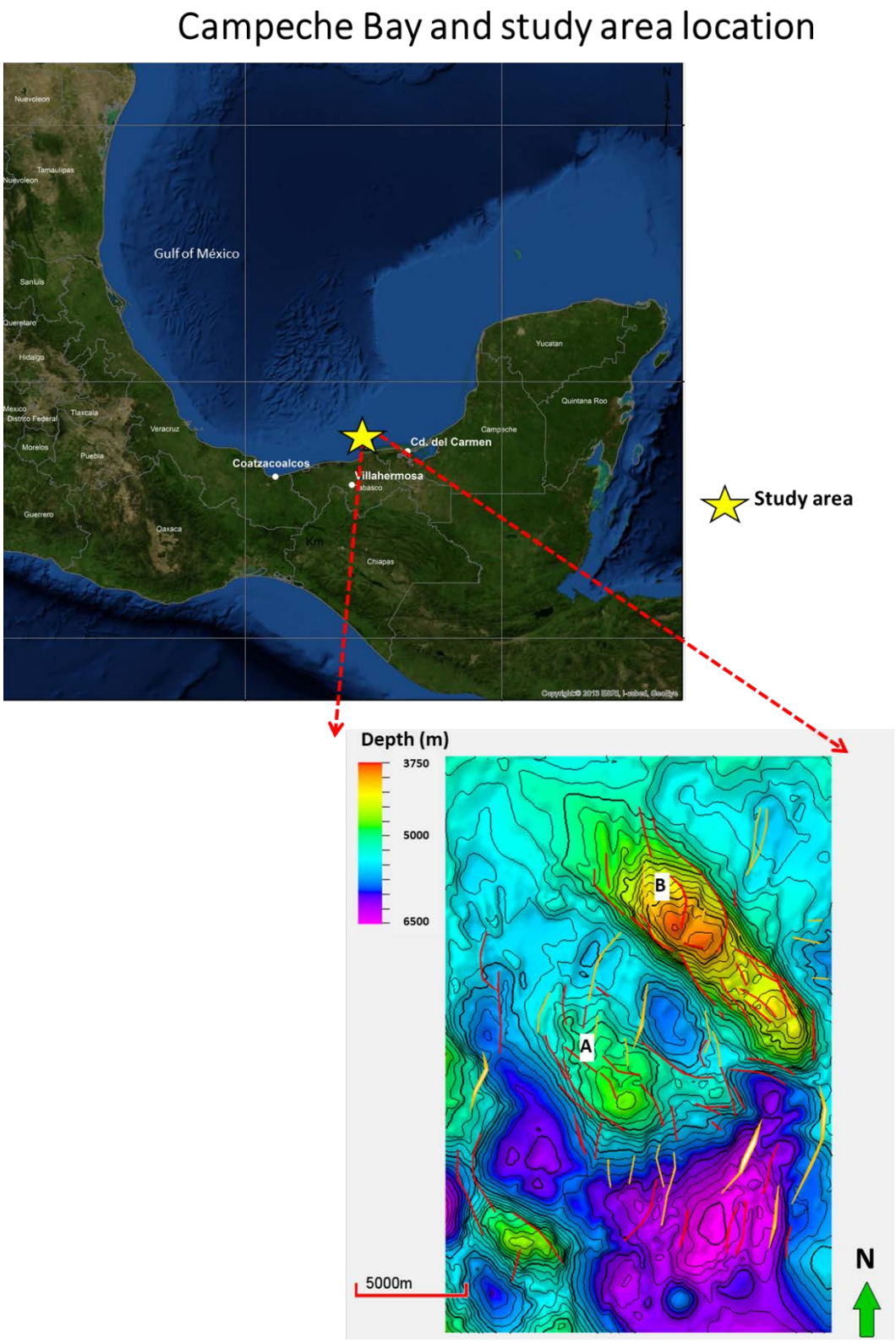


**Figure 1. 1** Campeche Bay and study area location showing the structures analyzed (A and B).

## CHAPTER 2. Regional Geology.

### Tectonic evolution of the region.

The tectonic evolution of the South Gulf Salt Province SGSP involves four general phases:

1) Late Triassic to Middle-Late Jurassic continental rifting, resulting in the opening of the Gulf of Mexico basin, developing of large grabens and widespread deposits of Jurassic salt (Salvador, 1991b, Padilla y Sanchez, 2007); 2) Late Jurassic to Cretaceous gravitational linked system deformation (Rivera et al., 2011); 3) two Eocene-Middle Miocene principal compressional events; and 4) a regional extensional – contractional linked system in the Late Miocene to present day (Rivera et al., 2011). Regional uplifts are related to the Laramide Orogeny pulse (Eocene-Oligocene) and the Chiapaneca Orogeny (Miocene).

This tectonism has persisted until the Recent period. (Figure 2. 1).

The Campeche Bay area, specifically the South Gulf Salt Province (SGSP), has been characterized by the presence of the Callovian salt, one of the most critical controls building the architecture of the deformational structures, for example, the development of detachment folds and faulted detachment folds.

Rivera et al. (2011) outlined five principal deformation events (Figure 2. 1).

**1. D0 - Middle Jurassic Rifting**. Regional widespread salt deposition.

**2. D1 - Gravitational linked extensional system (Upper Jurassic – Cretaceous)**. Composed by three different domains: a) thin-skinned tectonics with extensional component represented by half grabens and salt rollers. b) transitional

component and c) down-dip compressional domain, represented by salt pillows, subtle folded structures and diapirism at the center and north part of the basin.

**3. D2 (Eocene-Oligocene)**: formed in southwest-northeast direction, this episode is best observed close to the Chiapas fold Belt province and the central part of the province, forming canopies, salt sheets, walls, squeezers and active diapirism related to the Laramide Orogeny.

**4.- D3 Contractional (Miocene):** formed in the same direction as D2, this is the most critical pulse causing the fold development and significant fold-thrust structural hydrocarbon traps related to the Chiapaneca Orogeny. (Figure 2. 1)

**5.- D4: Extensional-Contractional linked system (Miocene-Recent):** caused by the gravitational movement towards the center of the basin because of a high sedimentation rate associated with a massive salt evacuation and the basement inclination with different detachment levels like allochthonous salt and tertiary horizons.

## Structural evolution model

Four principal deformation events (D1-D4) have been recognized:

**D1** = Gravitational extension (upper Jurassic – Cretaceous)

**D2** = Contractional (Eocene-Oligocene).

**D3** = Contractional (Miocene).

**D4** = Extensional (Miocene-Recent):

(PEMEX Rivera et al. 2011).

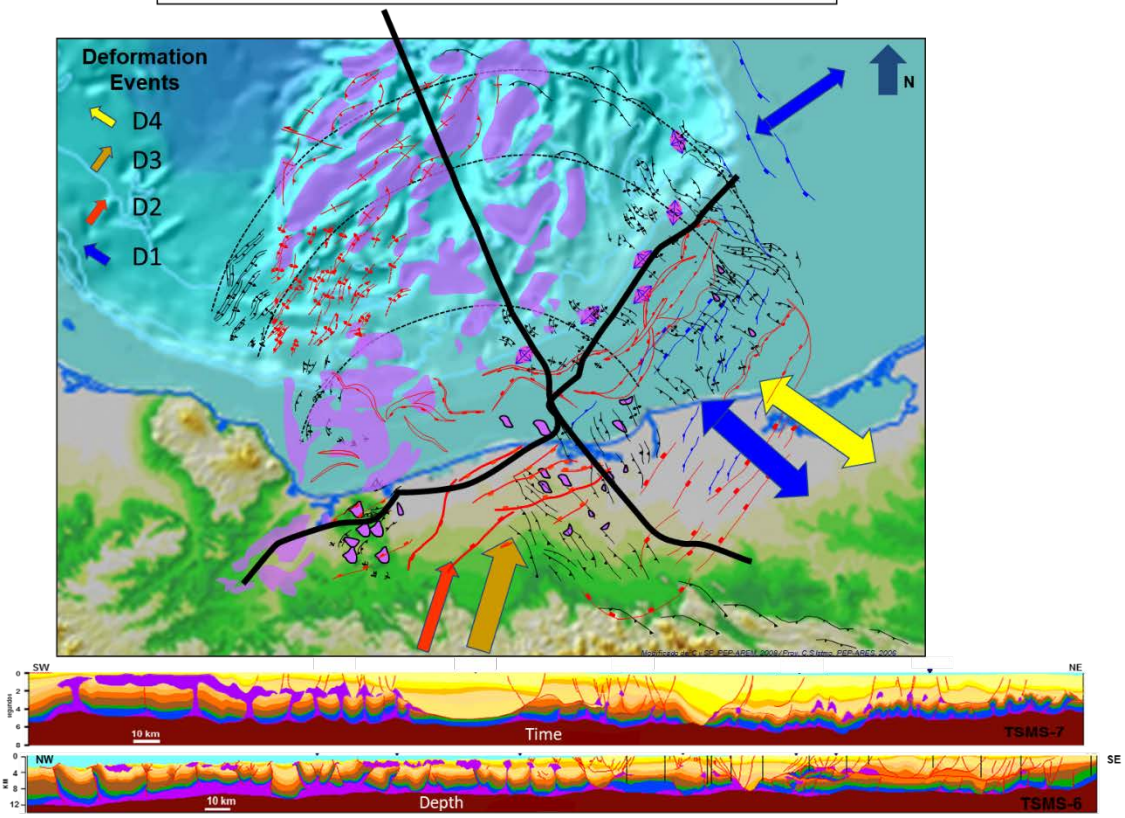


**Figure 2. 1** Regional Structural Evolution model of Campeche Bay, showing the principal deformation events and their direction and showing the principal deformed structures in two regional sections: SW-NE and NW-SE. (modified, adapted, and updated from PEMEX, 1994, 1995, 2006, 2007, 2009 by Rivera et al., 2011).

# CHAPTER 3. Stratigraphy and tectonics.

## 3.1 Stratigraphy and its relationship to the tectonic evolution.

***General stratigraphy of the SGSP province.***

**Triassic-Jurassic**

The regional sedimentation history in the South Gulf Salt Province (SGSP) region of the GOM starts with the deposition of continental red beds during the late Triassic – early Jurassic. These deposits are observed in some of the outcrops in the Chiapas localities (Padilla y Sanchez, 2007). During this time, the Callovian salt deposition occurred because of the marine water invasion of the Pacific (Salvador, 1987, 1991b), covering a vast expanse of land with a low rise and restricted water circulation. This invasion originated high salinity concentration caused by evaporation, generating extensive salt and evaporites deposition across the basin. (Padilla y Sanchez, 2007). In the SGSP province, the oldest rocks that drilled in the Marine zone date from Upper Jurassic Oxfordian.

During the extensional deformation stage (D1), the restricted sedimentary environment continued, limiting the sedimentary deposition and architecture to broadly extended oolitic banks (Padilla y Sanchez, 2007).

Angeles-Aquino and Cantu-Chapa (Angeles-Aquino and Cantu-Chapa, 2001) formally proposed names that have been accepted for this area. They are referred as the Ek-Balam Group, Akimpech formation, and Edzna formation, corresponding to the Upper Jurassic (Oxfordian, Kimmeridgian, and Tithonian respectively).

**Upper Jurassic Oxfordian, Ek-Balam Group** (Angeles-Aquino and Cantu-Chapa, 2001; Cantú-Chapa, 2009) or unit **(A)** named by Angeles Aquino in 1987. The

development of wide shallow marine water of abundant clastic and detrital sediments from the Yucatan platform and surrounding volcanic areas occurred in the GOM on very irregular topography. Exemplified by sands, limolites (horizontally layered claystones), bentonites, sandstones with some carbonates, and evaporites (anhydrite and salt) intercalations which occasionally present hydrocarbon impregnation. The thickness varies from 57 to 440 m.

The Oxfordian is an important reservoir and source rock in the region. It is sub-divided into three members: a) the Lower member: marly to sandy wackestone – packstone of pelletoids, with quartz cement and evaporites which grades to bentonites. b) the Middle member: intercalation of calcareous sandstones, mudstone and bentonitic shales and broad, massive sand bodies, and c) the Upper member: sandy carbonates with evaporites in sharp contact with the overlying Akimpech Formation.

**Upper Jurassic Kimmeridgian, Akimpech formation:** These rocks are the most important reservoirs for the Upper Jurassic. They consist of wide shallow platforms of broad carbonate sedimentation and oolitic banks. The sedimentation of this period was controlled by several factors: topographic highs caused by the salt movement during down building, and development of salt pillows, and diapirs, the warm climate, and the presence of listric normal faults dipping to the west with decollement in the autochthonous salt. Resulting high-energy sedimentological conditions increase the porosity and the presence of the oolitic banks deposits (Portillo and Peterson, 2017).

Figure 3. 1 shows the facies and thickness distribution controlled by salt walls and diapirism in the west of the area.

The lithology of this formation is composed of a cyclic sequence of carbonates and clastic facies divided in four members**: B, C, D, E.** Thickness varies from 95 – 1272 m:

1) The Lower terrigenous **(B)** member: shale and bentonitic sandy shales and limolites, some anhydrite intercalations. The thickness varies from 75 to 408 m. 2) The Lower calcareous member **(C):** microcrystalline to mesocrystalline dolomites, pelletoids packstone with incipient dolomitization and isolated mudstone interbeds with shale and limolites intercalations. It varies in thickness from 37 to 267 m. 3) The Upper terrigenous member **(D):** claystone, mudstones, and sandy shale interbedded among carbonates with a thickness variation of 23 to 387 m. 4) The Upper calcareous member **(E)**: mesocrystalline and microcrystalline Dolomites, which originally were packstones, ooid, and peloid grainstones or mudstone-wackestone Oolitic banks. Thickness varies from 52 to 373 m.

**Upper Jurassic Tithonian, Edzna formation**: This is a transgressive environment with probably some local regressive stages of a broad, shallow marine ramp from slope to basin, composed of shales, marls, and carbonates. The subsidence velocity was slower than the previous stages, originating stable sedimentation. The subsidence and the temperate weather created a propitious habitat for an abundance of organisms.

The Edzna formation is divided into three members (Angeles-Aquino and Cantu-Chapa, 2001) that can vary in their facies in different areas of the Gulf and are composed of 1) lower member **(F)** shaly carbonates: radiolarian mudstone-wackestone, which varies to shale facies; 2) Middle **(G)** claystone and 3) Upper **(H)** bentonitic shale

that varies to marls or clay micro-dolomite. The average thickness of the Tithonian is 295 m.

**Cretaceous Period.**

The Campeche Sound was a passive-margin regime from Late Cretaceous to Early Cenozoic. (Murillo-Muñetón et al., 2002). During the **Cretaceous**, the subsidence velocity changed continuously, generating an alternation of platform carbonates and shaly carbonates.

The deposits contain some of the principal reservoirs of the entire marine zone. The most important reservoir is the K/T(Cretaceous-Tertiary) boundary carbonate Breccia. The Breccia has different possible formation causes, one of them attributed and related to the boundary of the "Chicxulub" crater, a meteorite impact event (Murillo-Muñetón et al., 2002).

Another of the reservoirs are the fractured carbonates originated primarily from the Late Cenozoic tectonic processes (Laramie and Chiapaneca orogenies) and present in most of the oil fields. Cretaceous units are composed basically of carbonates that are dolomitized, brecciated or fractured depending on the zone.

In México, the Cretaceous Period is divided into three zones: Lower, Middle, and Upper Cretaceous.

The Lower Cretaceous **(Berriasian - Aptian)** has an average thickness of 460 m and is composed of bentonitic mudstone lightly dolomitized and micro dolomite with some shale intercalations. It displays good secondary porosity in fractures and dissolution if dolomitized. Accessory minerals include pyrite and chert. (Angeles-Aquino, 2006).

The Middle Cretaceous **(Albian – Cenomanian)** has an average thickness of 176 m and is composed of mudstone – wackestone of bioclasts, intraclasts, and exo-clasts. It is bentonitic and dolomitized in parts with a very low primary porosity and represents the most important fractured reservoir. Accessory minerals include pyrite, chert, authigenic quartz, and bentonite (Angeles-Aquino, 2006).

The Upper Cretaceous **(Turonian – Maastrichtian)** has a thickness of 272 m and is composed of mudstone– wackestone with bioclasts or intraclasts, micro-dolomites**,** bentonitic mudstone**,** and intercalations of marls, shales, and bentonites. Stylolites are frequent. Accessories are pyrite, chert, and bentonite. It possesses good primary and secondary porosity, depending on the facies and the area.

The K-T Breccia **(Upper Cretaceous-Paleocene).** This formation has an average thickness of 205 m. It is the most important reservoir of the marine zone. However, the K-T Breccia is not present in all the structures but is present in the north-east part of the Campeche Basin in a slope environment. These slope breccias consist of dolomitized, calcareous, angular fragments of assorted sizes cemented by a beige carbonate mudstone. Bentonite layers occur locally. The zone changes laterally to marly limestones and in some areas, the breccia is not present (Cantu-Chapa and Landeros-Flores, 2001). The origin of the carbonate breccias is considered to be either due to solution-collapse related to subaerial exposure, or deposition of the talus in a deep-water setting (Murillo-Muñetón et al., 2002).

**Tertiary Period**.

Regionally, the major compressive tectonic deformation that affected the SGSP (South Gulf Salt Province) and responsible for the hydrocarbon trap formation, occurred during this Period, from late Eocene to Miocene, when compression and strike-slip faulting took place (Murillo-Muñetón et al., 2002). A final trans-tensional tectonic event that resulted in extensive normal faulting affected this region during Pliocene-Pleistocene Time (Murillo-Muñetón et al., 2002).

**Paleocene:** This layer is made up of bentonitic wackestone- packstone with lithoclasts or bioclasts, sometimes lightly dolomitized, intercalated with bentonitic shales.

**Eocene - Upper Pliocene:** The depositional setting during this Period underwent a considerable change in the sedimentation since the clastics were the maximum input of sediments caused by the Laramide Orogeny, where the formation of the Sierra Madre Oriental caused large depocenters in the Gulf. Also important was the Chiapaneca Orogeny, which generated significant volumes of sediments while the Yucatan block deposition of shallow water carbonates continued. (Padilla y Sanchez, 2007). Also present are shales with intercalations of bentonites, some isolated detritical flows from the Eocene in some areas, and some sand reservoirs in the Lower Miocene and Lower Pliocene.

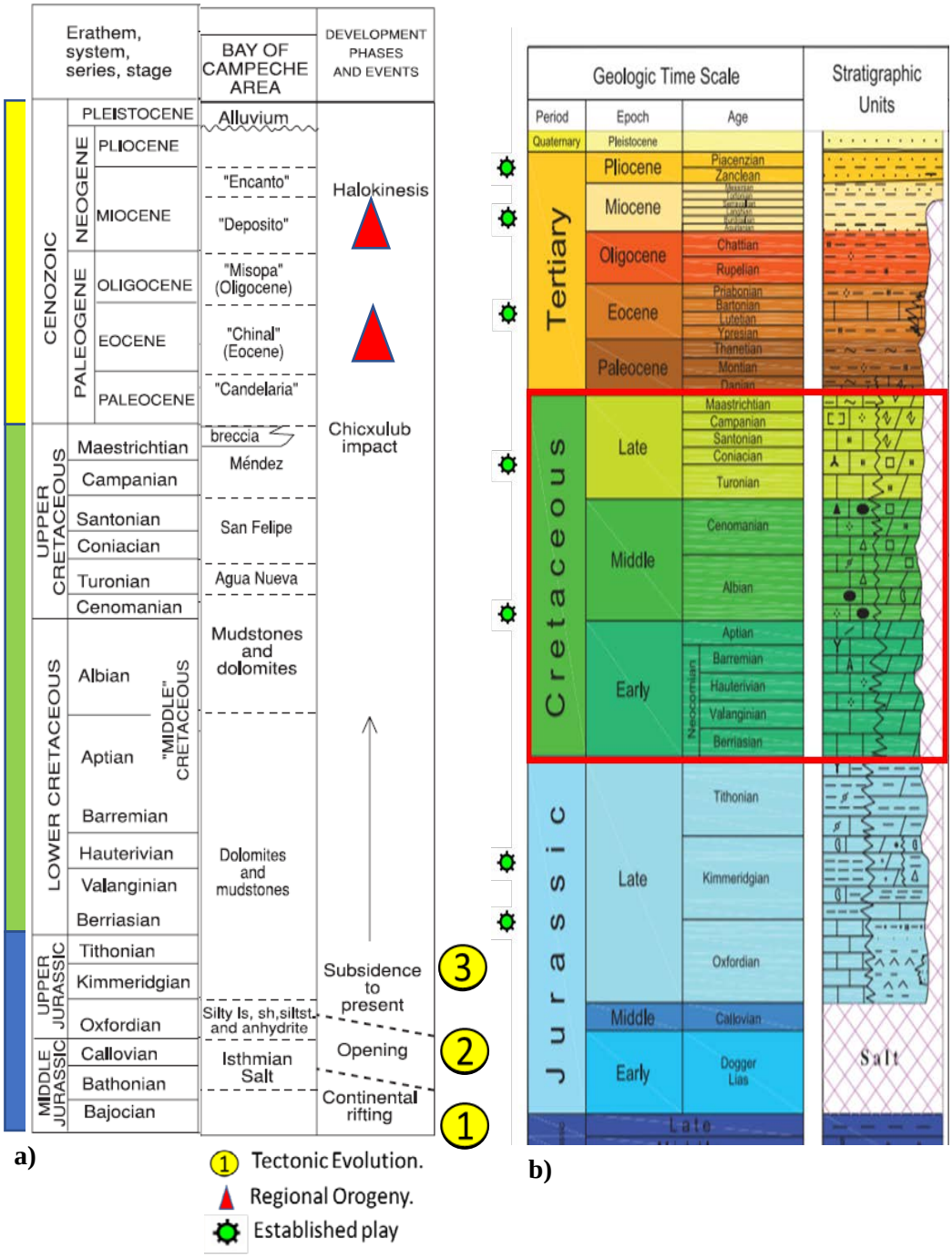


**Figure 3. 1** a) Stratigraphic chart (modified from Salvador, 1991a, development phases of the southern Gulf of Mexico. 1-3 Late Triassic through Jurassic tectonic evolution: (1) Late Triassic to Middle Jurassic: large grabens; (2) Middle to early Late Jurassic: widespread of Jurassic salt deposits. (3) Late Jurassic to present-day regional subsidence; Two Regional Orogenies in chronologic order: Laramide and Chiapaneca. b) Regional stratigraphic chart of the marine zone (modified from Ortuño et al., 2006)

# CHAPTER 4. Petroleum system.

## 4.1 Source Rock.

Pimienta-Tamabra is an enormous, potential and supercharged petroleum system located in the southern Gulf of Mexico, from which significant reserves of oil and gas have been produced for more than 30 years in the Campeche Basin (**Figure 4. 1**). The effectiveness of this system results from the largely widespread distribution of good to excellent thermally mature, Upper Jurassic source rock which superposes and underlies numerous stratigraphic and structural traps that contain carbonate and clastic reservoirs. The expulsion of oil and gas fluids from the Upper Jurassic source rock occurred when the thickness of overburden rock exceeded approximately five kilometers. This burial event started during the Eocene, in some areas culminated in the Miocene, and continues to a lesser extent today. The expelled hydrocarbons started to migrate laterally and then upward as a gas-saturated 35-40°API oil (Magoon et al., 2001).

In general, the Upper Jurassic source rock includes the Oxfordian, Kimmeridgian, and Tithonian intervals that are primarily marine calcareous and shale-rich rocks, (Holguin et al., 1994, Medrano et al., 1996b, Mello and Guzmán-Vega, 1996 Guzmán-Vega and Mello, 1999 PEMEX internal reports). The Upper Jurassic source rock is below a variety of stratigraphic and structural traps that contain excellent carbonate Mesozoic reservoirs and some Tertiary siliciclastic reservoirs. Usually, these Mesozoic reservoirs contain excellent fractured carbonate rocks and in some areas of the basin, one of the most critical reservoirs: the K-T breccias(Cretaceous-Tertiary).

The lateral and vertical oil and gas migration through fractures is significant. Risk or uncertainty is with the lateral seals when the reservoirs are connected. The carbonate reservoirs have good continuity and are laterally connected, also implying a lateral migration risk.

### 4.2- Campeche Basin 10 Petroleum criticals of Upper Jurassic Tithonian (Pimienta-Tamabra) source rock generation.

A 1D basin analysis model was conducted using BMOD software using data of the well A-1 of the study area and based on the Magoon et al. (2001) source rock information getting the next results for the 10-critical factor analysis for the Petroleum Systems.

Ten critical parameters of the Petroleum System are found in the study area:

1.- Quantity: The effectiveness of this system results from good to excellent thermally mature source rock, since TOC values can vary from 1 to more than 5% in the Campeche Basin, with an average TOC content of about 3% for Tithonian source rocks (Magoon et al., 2001).

2.- Quality (Organo-facies) Van Krevelen Class Type: The majority of oil samples in the Bay of Campeche area are from Upper Jurassic Tithonian source rock. The most representative organo-facies for this source rock is Type II high sulfur.

3.- Maturity: Cenozoic siliciclastic sedimentation created an overburden thickness sufficient to thermally mature the Upper Jurassic source rock. Figure 4. 4 shows that oil maturity starts during Miocene and Pliocene Time.

4.- Migration: The Upper Jurassic source rock is below a variety of stratigraphic and structural traps that contain excellent carbonate Mesozoic reservoirs and some

Tertiary siliciclastic reservoirs. Pathway connectivity: usually these Mesozoic reservoirs can contain very good fractured carbonates, and Breccias exist in some areas of the basin. For this reason, we expect to find good pathway connectivity. Expulsion of oil and gas from Upper Jurassic source rock occurred when the thickness of overburden rock exceeded 5 km. This burial event started during the Miocene and continues today.

5.- Speed and charge of migration: Based on tectonics and complex structural system of the basin, there could have a good migration speed.

6.- Reservoir Seal: The upper and lower seals are very effective since they contain a reasonable rate of SGR (shale/gouge ratio). The more significant risk or uncertainty is with the lateral seals when the reservoirs are connected since some of the reservoirs that are carbonates have good continuity and are laterally connected. Moreover, under the reservoirs, aquifers could be connected by regional faults.

7.- Rate of Leaking: Based on the complex tectonic evolution of the region, a reasonable rate of leaking can be assumed.

8.- In the Campeche Bay area, the Tithonian source-rock regionally ranges in thickness from 80 to 476 m (PEMEX, 1999b, internal report) and locally in the study area ranges from 216 m to 476 m. Therefore, it has a large thickness and an excellent container volume.

9.- Figure 4. 4 shows the timing of oil generation and oil peak in the early Paleogene. Expulsion-migration occurred during Miocene-recent time, and maturity occurred during Miocene-Pliocene. This results in excellent accumulation traps in the Cretaceous since the basin has a broad, widespread seal in the Tertiary. Timing of

deformation occurred prior to generation, expulsion, and migration. Because most of the oil and gas was generated and trapped during the Miocene, that is the critical moment.

10.- Economics. Based on the analysis of the geological risk, reservoir in well A-1 achieved an 85% grade, a geological risk of 47.2% and geologic certainty of 52.8% (**Figure 4. 5, Figure 4. 6**). These findings clearly suggest that continued drilling in exploration drilling is likely to result in discoveries and new prospects in Campeche Basin.

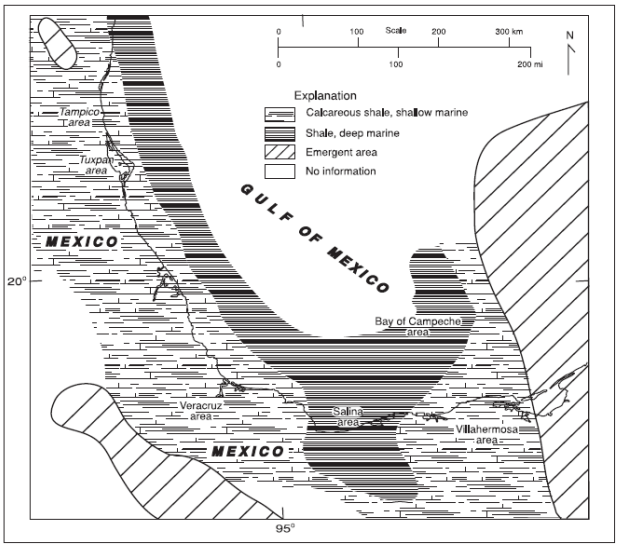


**Figure 4. 1** Map showing the Source Rock (Pimienta Tamabra) distribution: Tithonian lithofacies (modified from Salvador, 1991b).

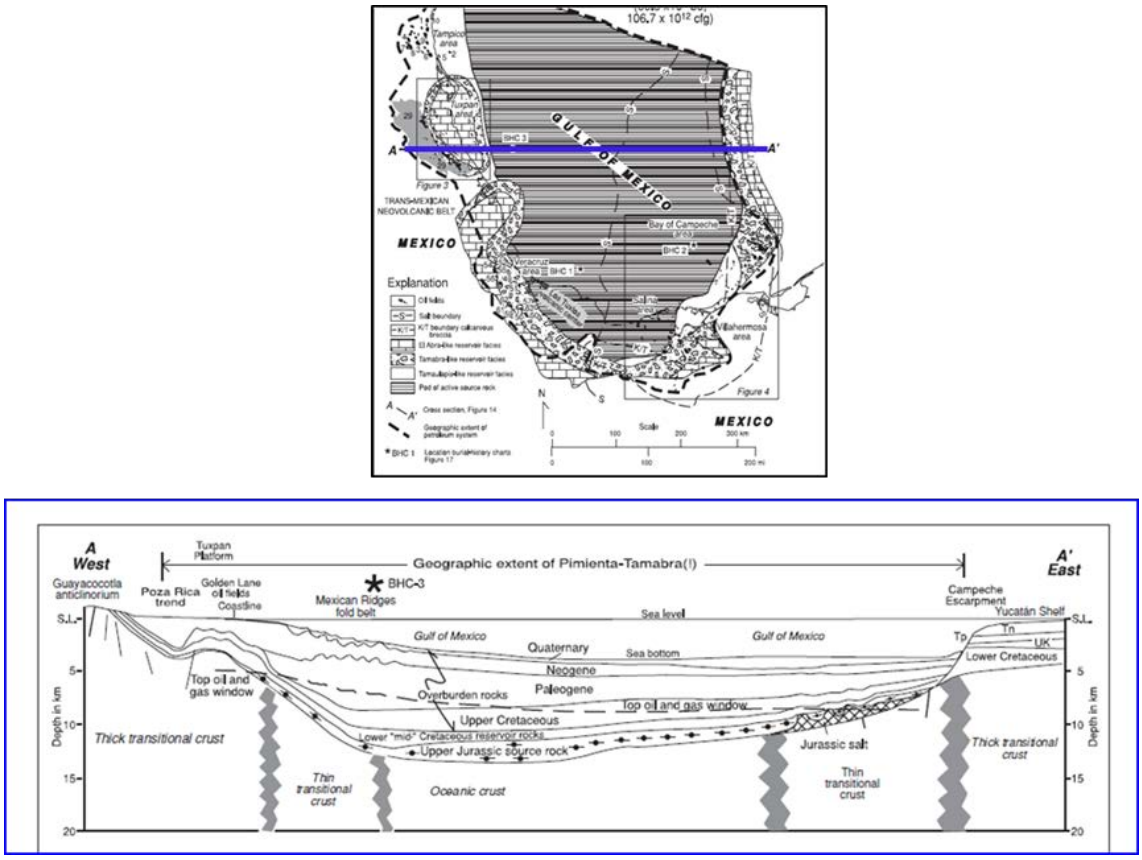


**Figure 4. 2** Regional cross section A-A', southern Gulf of Mexico, showing geographic extent of Pimienta-Tamabra, and essential elements of the petroleum system (Salvador 1991d).

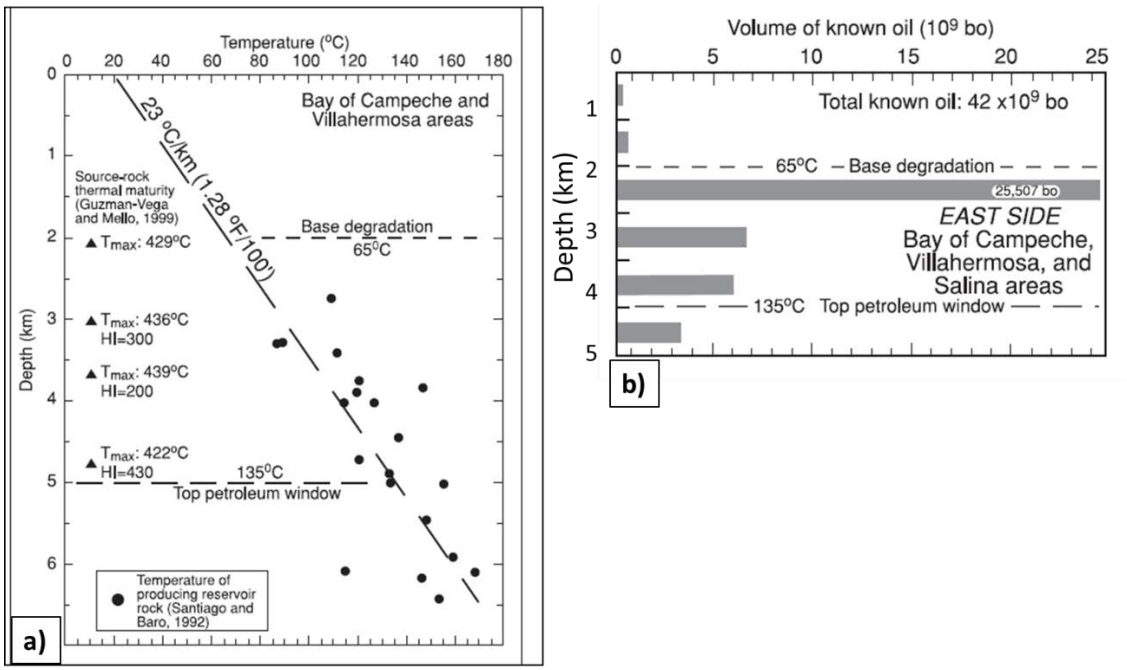


**Figure 4. 3** a) Geothermal gradient, the base of degradation, and top of petroleum window. Rock-Eval Tmax temperatures for the Upper Jurassic source rock (Guzmán-Vega and Mello, 1999). b) Histogram showing volume of known oil for each km most oil is produced between 2 and 3 km depth.

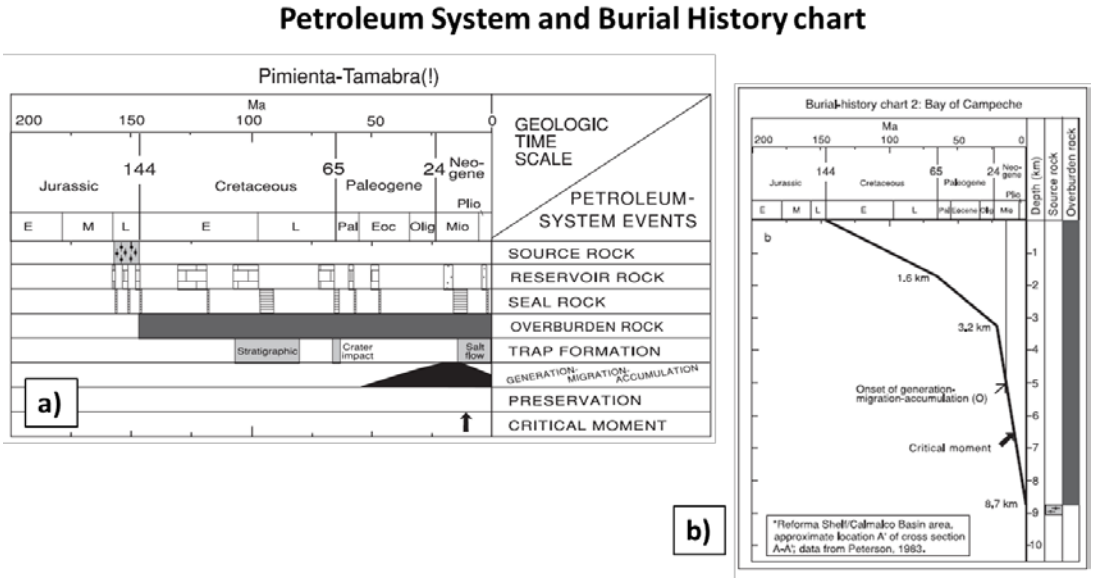


**Figure 4. 4** a) Events chart summarizing the petroleum system essential elements, processes, and critical moment for the Pimienta-Tamabra (L.B. Magoon et al., 2001). b) Burial-history charts of Bay of Campeche area, from cross sections of Salvador (1991d) and Peterson (1983).

The next two figures are based on an exercise made in the well A-1 in the software b-mod of Basin Analysis.

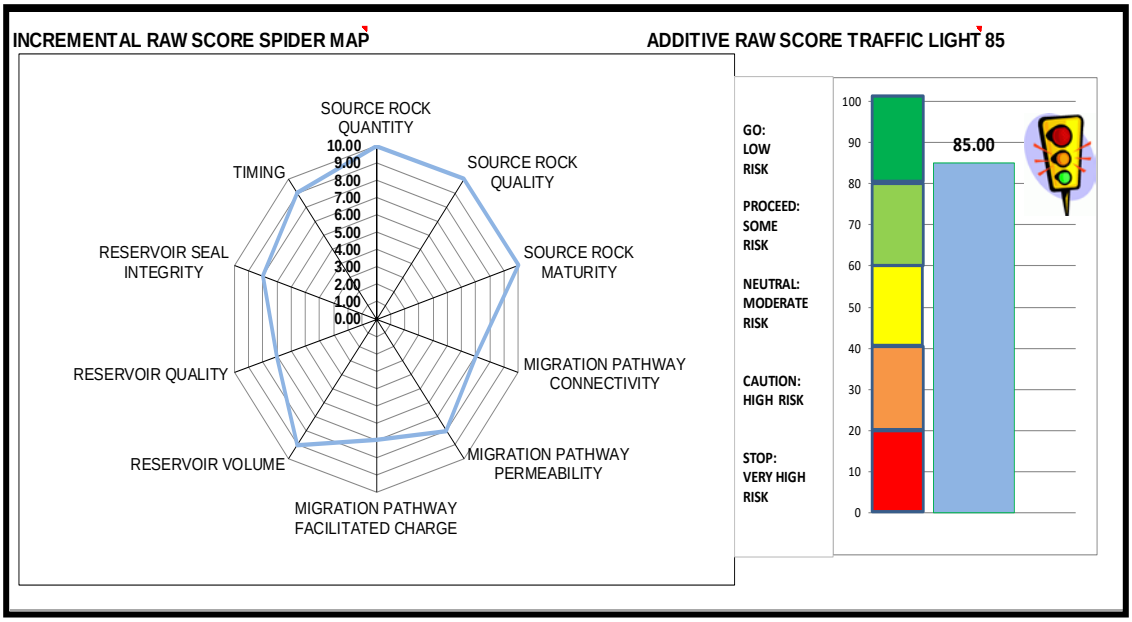


**Figure 4. 5** Results from the 10-petroleum system criticals analyzed in the b-mod software. Data from Campeche Basin, well A-1 of the study area, Getting a raw score for risk = 85% (low risk). Analyzed from a graph of J. Piggot 2016.

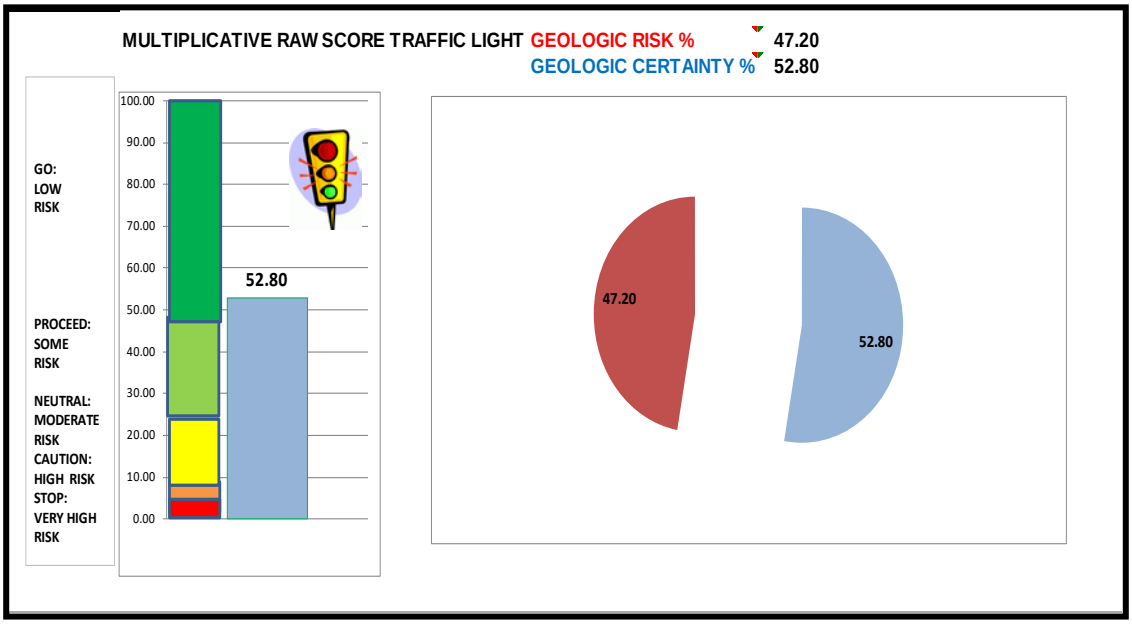


**Figure 4. 6** Results from the raw risk table analyzed from a graph of J. Piggot, 2016. Data from Campeche Basin, well A-1 of the study area, showing low geologic risk (47.2%) and a Geologic Certainty of 52.8%.

## CHAPTER 5. Local Stratigraphy.

The stratigraphy of this study area (structures “A” and “B”) (Figure 5.1), ranges in age from Upper Jurassic Kimmeridgian to the Pleistocene-Recent.

The most important reservoirs of the area correspond to:

1) The Oolitic banks and dolomites from the Upper Jurassic Kimmeridgian. In structure “A” are present and productive; while in structure “B” these reservoirs are not present.

2) The fractured carbonates from the Lower, Middle, and Upper Cretaceous. Structure “A” are hydrocarbon productive, and also Structure “B”, but only in the Upper Cretaceous.

The reason that field B is only productive in the Upper Cretaceous is because the oil/water contact (OWC) is very shallow, within the Upper Cretaceous strata. These reservoirs are identified and correlated with well logs and seismic data. All the information of these rocks come from subsurface data, and some of them correlate with outcrop formations. (**Figure 5. 1**).

To better understand the reservoir characteristics and compartmentalized zones, the local stratigraphy in the study area has been described only for the Mesozoic. This includes both Upper Jurassic Kimmeridgian and Cretaceous reservoirs, and the source rock (Upper Jurassic Tithonian).

According to the Regional Modeling, 2016 PEMEX report defines the sedimentary cycles as Milankovitch cycles, with fourth and fifth order sea level changes. This interpretation was made in a Cyclo-Log software using the following geophysical logs as input: Gamma-ray (GR), Delta T (DT Sonic log), Density (RHOB),

Neutron Porosity (NPHI), Resistivity (Rt), and caliper (CALI). The result of these cycles classification was the division of the Upper Jurassic in eight stratigraphic cycles and the Cretaceous in ten stratigraphic cycles.

These cycles were correlated in ten wells of the study area, using two analogous wells of the study area already classified in the (Peterson et al. 2016). The same sets of geophysical logs mentioned before (GR, DT, RHOB, NPHI, Rt, and CALI), were analyzed to correlate the cycles. Four stratigraphic sections are shown in (**Figure 5. 3** and **Figure 5. 7**).

## 5.1 Cycles classification.

***Upper Jurassic Kimmeridgian***.

The Kimmeridgian sequence is not completely drilled in the area. Six of the eight cycles exist in structure “B” and five cycles occur in structure “A”. This sequence begins with the cycle number 3. In the study area, the depositional environments were shallow water and correspond to a carbonate inner ramp of low energy with some local marine transgressions due to paleo-topography changes (Geologic Modeling, 2016 PEMEX internal report). (**Figure 5. 2**).

Figure 5. 4 exhibits transverse section I-I´ between “A” and “B” structures. Figure 5. 5 exhibits two longitudinal sections II-II´across “A” structure and III-III´across structure “B”. The hydrocarbon productive cycles are four, five and six. Their facies are dolo-mudstone to dolo-packstone-grainstone of ooids, with fractures and dissolution features.

***Cretaceous.***

The carbonates facies during the Mesozoic formed on a homoclinal carbonate ramp (Figure 5. 6).

The Cretaceous has been sub-divided into ten sedimentary cycles regionally described, with eight different litho-facies. The structures “A,” and “B” show nine sequences of the cycles. Cycle one and cycles three through ten are present. Only the second cycle is absent. These cycles correspond to the environment of deep marine basin facies, originated within moderate to low energy (shallow – deep water quiet open platform conditions). (Figure 5. 6).

The litho-facies varies from mudstone to packstone with a very high content of organic matter and a slight variation in the content of clay. Both structures “A” and “B”, contain the KT breccia. Some of the facies are dolomitized in the Lower Cretaceous strata in field “A”, in wells A-1, ADL, A-30 and in well A-50 only. In field “B”, the dolomitization is not present. Wells ADL and A-30 have a good percentage of dolomitization in the entire sequence.

Figure 5. 8 exhibits a transverse section I-I´ between “A” and “B” structures. Figure 5. 9 exhibits two longitudinal sections II-II´across “A” structure and III-III´across “B” structure. Hydrocarbon impregnation is observed in this unit in the cycles 5 through 10, and only the well B-1 presents hydrocarbon with water content in cycle 4.

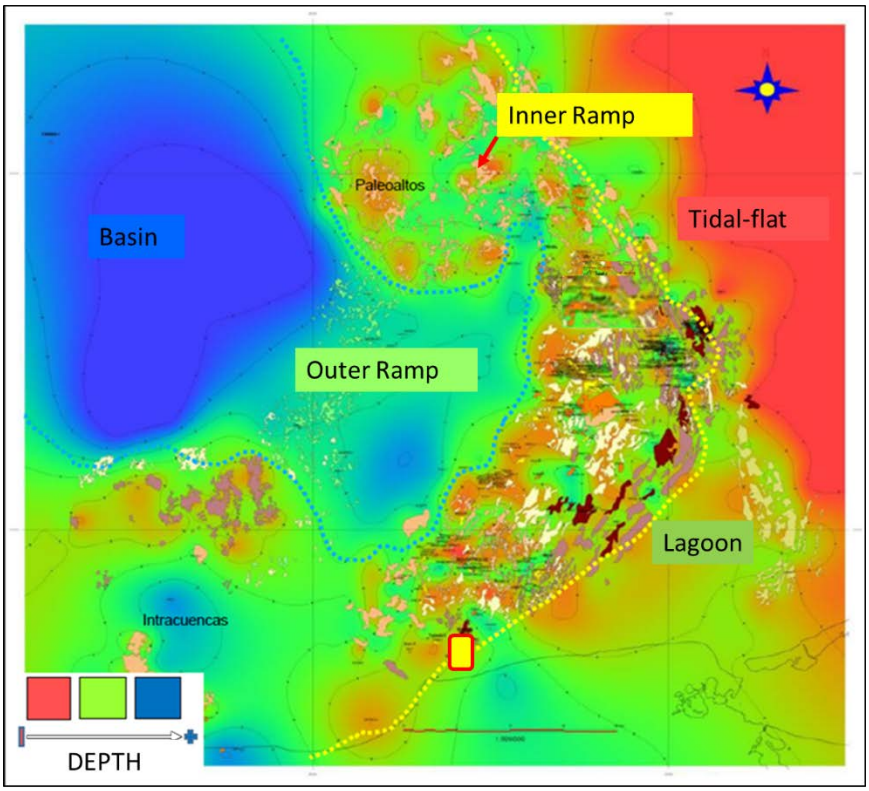


**Figure 5. 1** Upper Jurassic Kimmeridgian Paleo-environment Regional map of Campeche Sound (Modified from Aguilera & Prado, 2014).

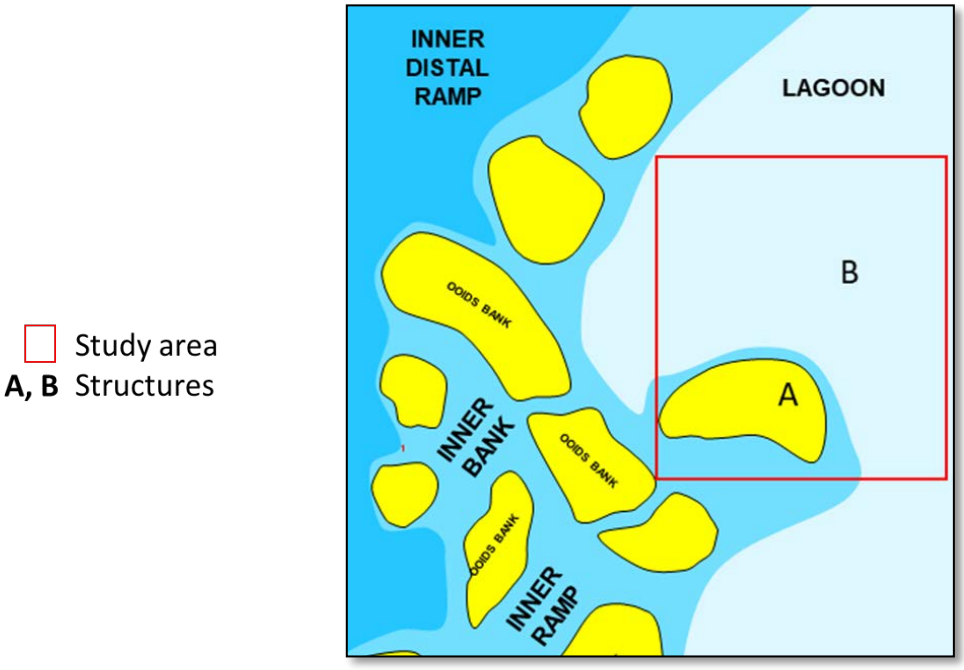


**Figure 5. 2** Upper Jurassic Kimmeridgian Ramp Model for the study area (PEMEX internal report, Regional Modeling 2010-2016).

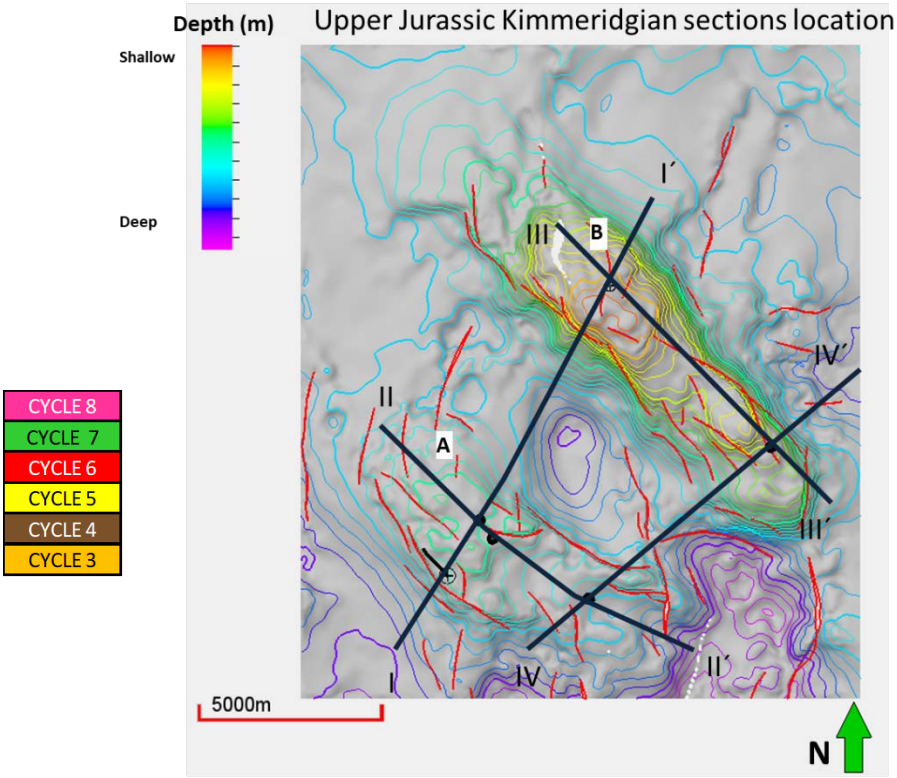


**Figure 5. 3** Four Stratigraphic sections to show the eight Cycles classification for the Upper Jurassic Kimmeridgian.

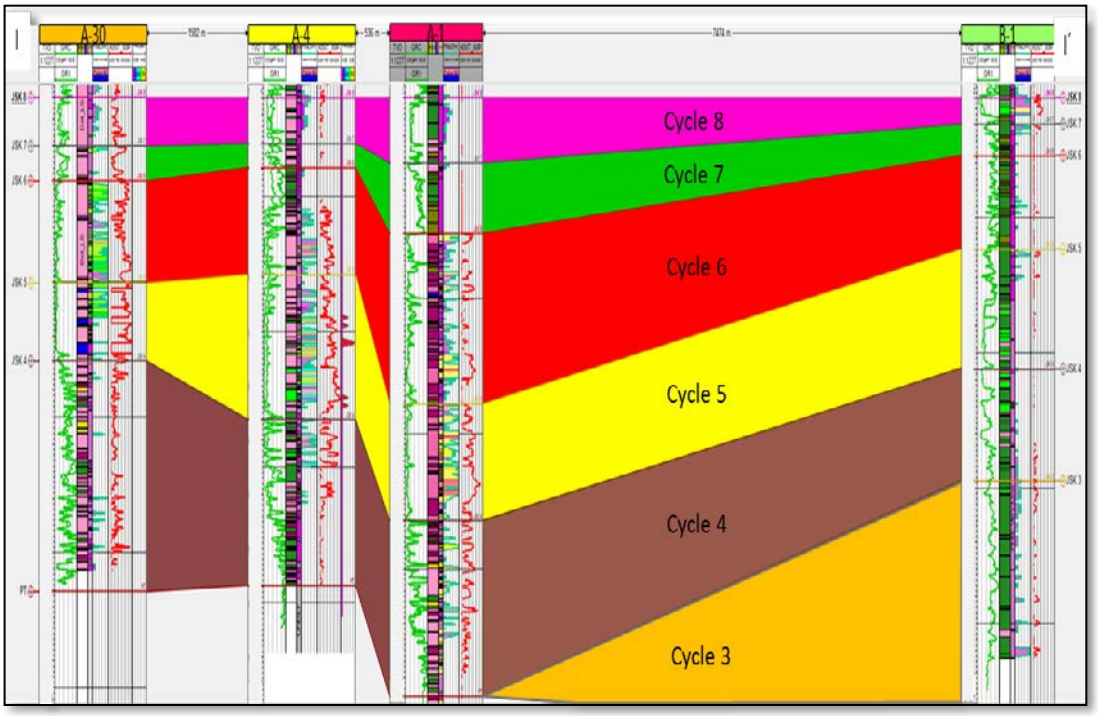


**Figure 5. 4** Stratigraphic section I–I´(SW-NE) showing the six Upper Jurassic Kimmeridgian (U.J.K.) cycles present in the study area. (Flatten at the top of U.J.K – cycle 8). Productive Jurassic Cycles in the study area: 4, 5 and 6.

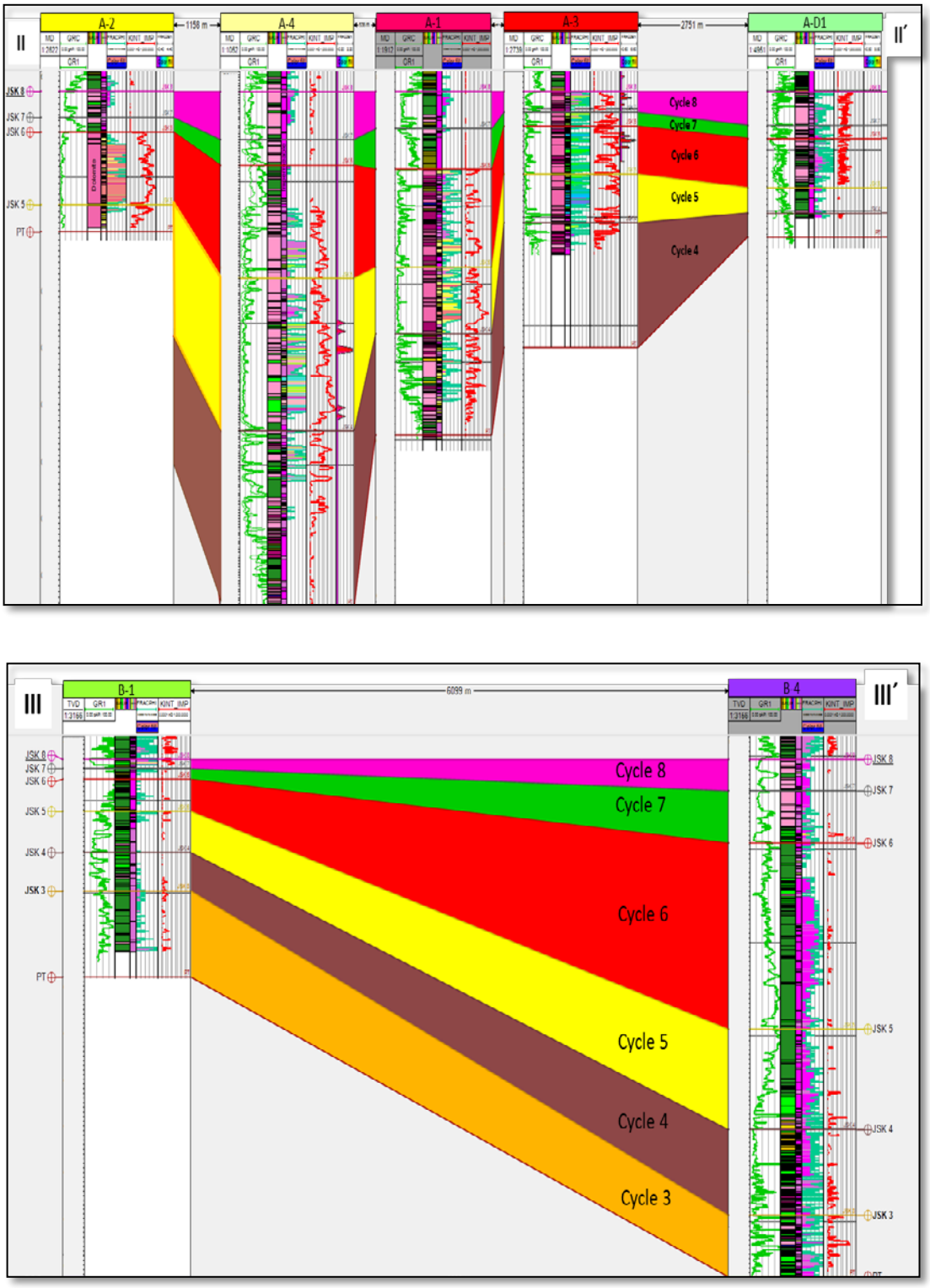


**Figure 5. 5** Stratigraphic section II-II´ and III- III´(both NW-SE) one parallel to "A" structure and the other parallel to the "B" structure, showing the six cycles.

a)

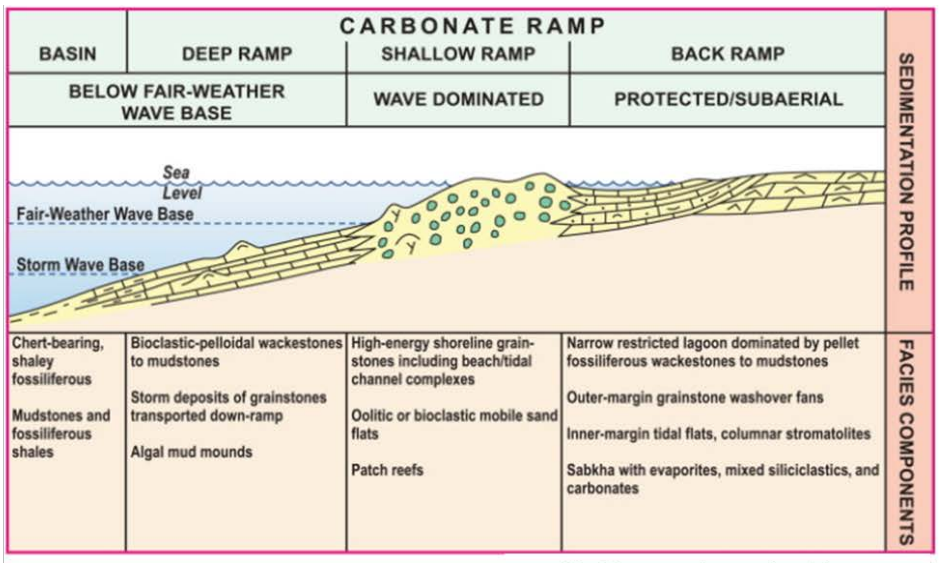


Modified from Tucker and Wright, 1990.

b)

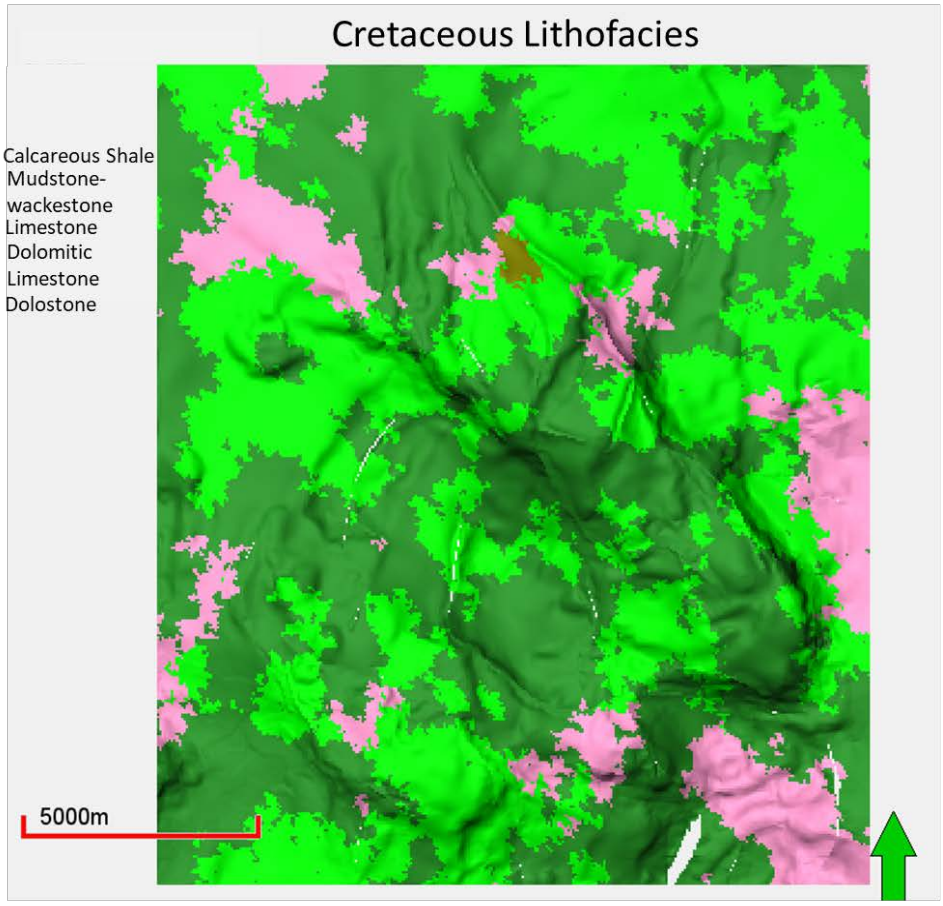


**Figure 5. 6** a) Carbonate Ramp depositional environment exhibits from Back Ramp environment to Deep ramp and Basin (Modified from Tucker and Wright, 1990). Cretaceous are formed in the basinal environment. b) Interpreted lithofacies of Cretaceous within the study area.

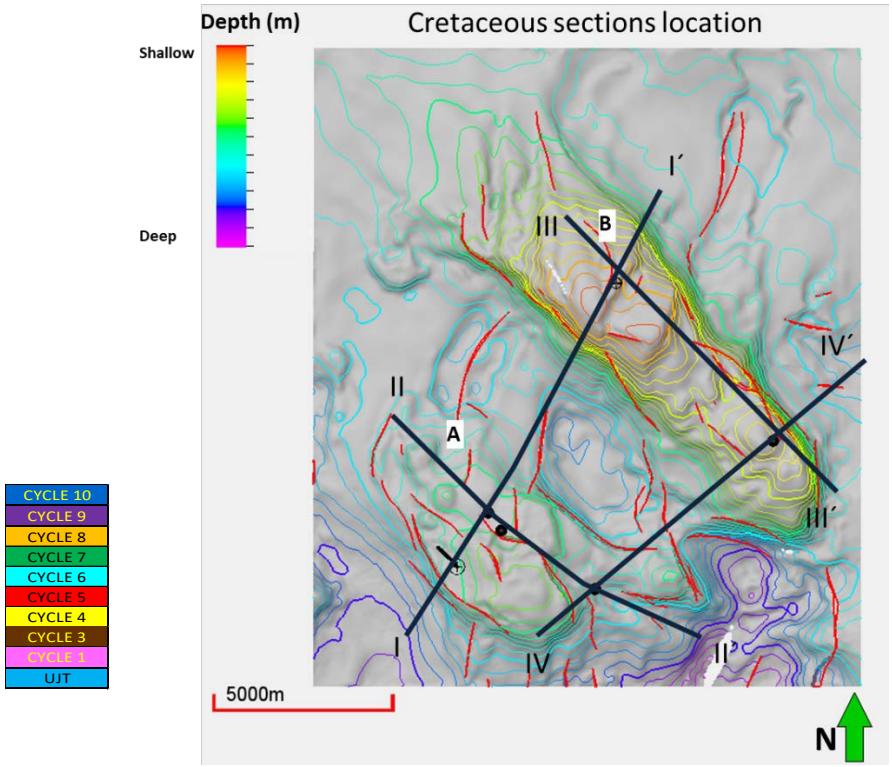


**Figure 5. 7** Four Stratigraphic sections showing the 10 Cycles classification for the Cretaceous.

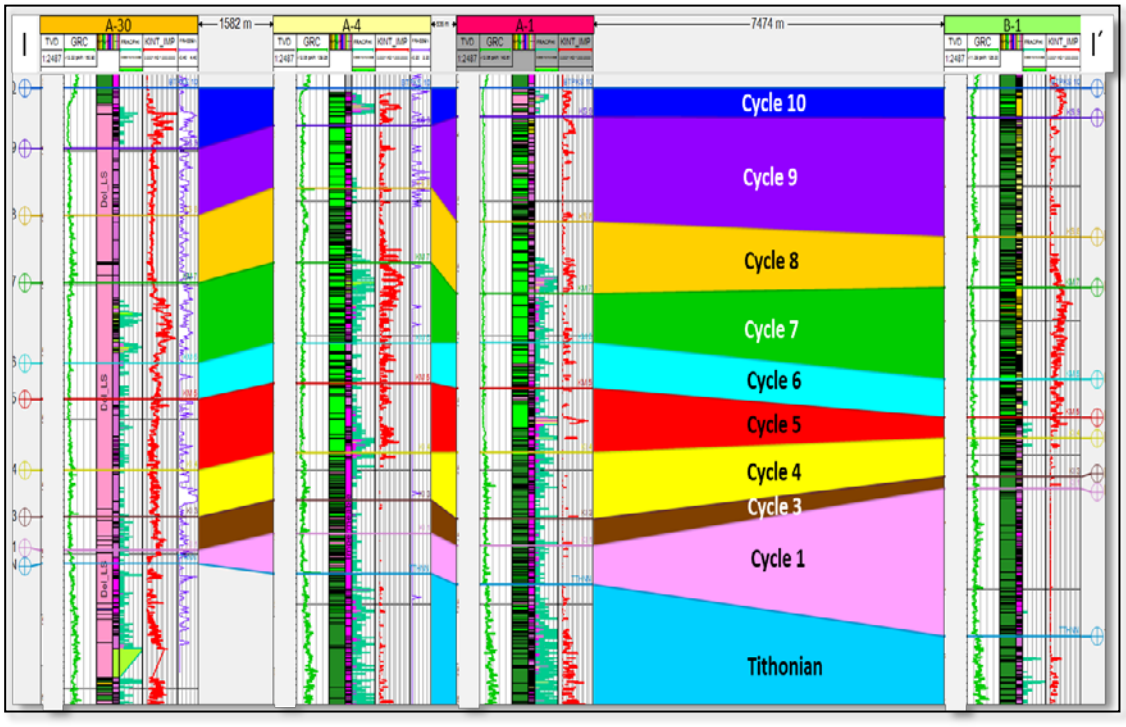


**Figure 5. 8** Stratigraphic section I–I´(SW-NE) showing the 10 Cretaceous cycles in the study area. (Flatten at the top of Cretaceous – cycle 10). Productive Cretaceous Cycles in the study area: 5, 6, 7, 8, 9 and 10.

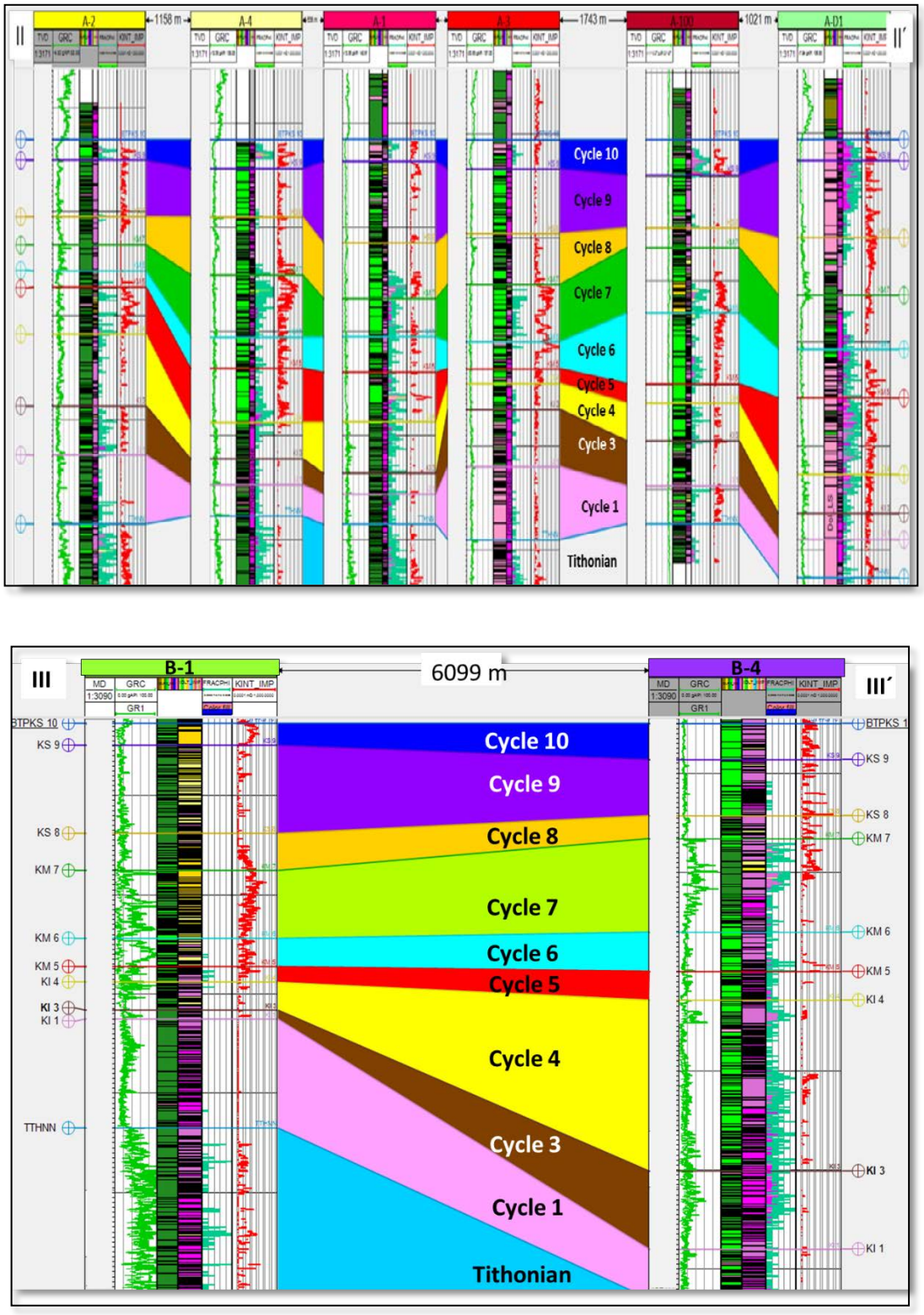


**Figure 5. 9** Stratigraphic section II-II´ and III- III´(both NW-SE) one parallel to A Structure and the other parallel to B structure, showing the ten cycles.

# CHAPTER 6. Three D Seismic.

## 6. 1 Data analysis and attributes.

The 3D seismic survey of the study area was acquired during 2011 – 2013 and Ocean Bottom Cable (OBC) acquisition and processed in 2015 using Pre-Stack Depth Migration (PSDM) using a reverse time migration algorithm.

**Table 1 Seismic data parameters.**

| Acquisition parameters | |
|---|---|
| Company | Geokinetics |
| Recording length | 10 seconds |
| Type of acquisition | OBC (Ocean Bottom Cable) |
| Bin Size | 15 by 25 m |
| Year | 2011 - 2013 |
| Cable length | 12,000 m |
| | |
| Processing parameters | |
| Company | ION GXT |
| Type of acquisition | PSDM (Post-Stack Depth Migration) Anisotropic Reverse Time Migration |
| Bin Size | 15 by 25 m |
| Year | 2015 |
| | |
| Seismic Quality | |
| Tertiary | Broad band with some footprint |
| Mesozoic | Narrow band, structurally complex |
| Salt bodies | Good top and flank of salt imaging |
| Sub Salt | Generally poor |

***Seismic data quality.***

In general, the seismic data are of good quality. Seismic noise is low, with the exception of some footprint seen in the shallower section (< 1350 m depth). However, this footprint does not affect the area of interest. (**Figure 6. 1**). Some artifacts were found close to the shale diapirism and in some places within the reservoir zone surrounding the fault discontinuities (**Figure 6. 2**).

The area of interest is in the Mesozoic section, with depths ranging between 4.5 and 7 km. The seismic resolution is significantly less than in the overlying Tertiary section (**Figure 6. 4)** for three reasons. First, there is more attenuation with deeper targets. Second, the velocities in the carbonate Mesozoic section are faster than the clastic Tertiary section resulting in longer wavelengths (and hence reduced spatial resolution). Third, small errors in velocity needed for depth migration can result in under- or over-focussing, resulting in attenuation of the higher frequency, short wavelength components of the data.

No obvious migration artifacts (such as migration operator aliasing) are seen in the data volume. However, multiples and other types of coherent noise that may be easy to recognize in time-migrated volumes, lose their periodicity in depth-migrated volumes and are much more difficult to recognize (Marfurt seismic imaging class notes).

Because of the tectonic complexity and the large size of the data volume, I computed a suite of seismic attributes to aid in the interpretation of faults, unconformities, and other geologic features of interest.

Geometric and spectral attributes were generated using the AASPI software (internal software of the geophysics consortium in the school of Earth and Energy, Geology and Geophysics at the University of Oklahoma). Some of the attributes generated included volumetric dip (**Figure 6. 6**), coherence, most positive and negative curvatures, aberrancy (**Figure 6. 9** and **Figure 6. 10**) and spectral components. Spectral balancing provided improved vertical rsolution, while structure oriented filter resulted in neglible changes. Some image processing atributes were also applied including fault

probability (**Figure 6. 8**), fault-enhancement, and skeletonization **(Figure 6. 9**). The attributes were run following the methodology shown in **Figure 6. 3** and **Figure 6. 4**. The seismic characteristics already mentioned, resulted in some difficulties in obtaining useful results from attributes. The difficulties stemmed from an attenuation of the seismic frequencies and very low resolution within the reservoir zone, which may have occurred during processing or seismic migration. However, attribute expression of very complex structures with high angle and steep reflector dips are rare.

Some anomalous results are shown in **Figure 6. 4** which represents a depth slice showing the aberrancy attribute, which measures the lateral change or gradient of curvature (Qi and Marfurt, 2017). The two sections analyzed in the study area, are perpendicular to both trends of structures “A” and “B.”

Since the dip extraction results were not satisfactory on this depth migrated seismic volume, none of the structural attributes such as Curvature, Coherence or Aberrancy worked (Marfurt, 2006; Chopra and Marfurt, 2015). Nevertheless, another commercial software was used to extract some of the principal discontinuities of the study area to locate faults. The attribute used was “Fault Likelihood”, which presented a better response to the seismic data in detecting or enhancing major unconformities such as faults and structural features. (**Figure 6. 7**).

Fault Likelihood attribute is an integrated suite of structural attributes of Decision Space (Halliburton software) that uses three attributes: Likelihood, Strike, and Dip (**Figure 6. 7**).

The Fault Likelihood attribute is an automated tracking method based on the fault-oriented semblance determined in elongated windows at numerous dips and azimuths (Hale, 2012). Other attributes usually measure semblance over regions that are not related to faults orientation. The window size to calculate this attribute is essential because it directly controls the sensitivity to noise and stratigraphic variations. Faults are zones of high disorder or low semblance; they can often appear to have low disorder when viewed in a small window, therefore the use of longer windows is recommended (Marfurt et al., 1999).

The likelihood attribute is defined as the inverse to the semblance; this means that where the semblance is minimum, the likelihood is maximum. This method can be handy for general interpretation and auto-tracking of faults or seismic horizons. (**Figure 6. 8)**.

This group of attributes (SOF filter and Fault likelihood) helped to better recognize the main fault traces within the seismic volume (**Figure 6. 9)**.

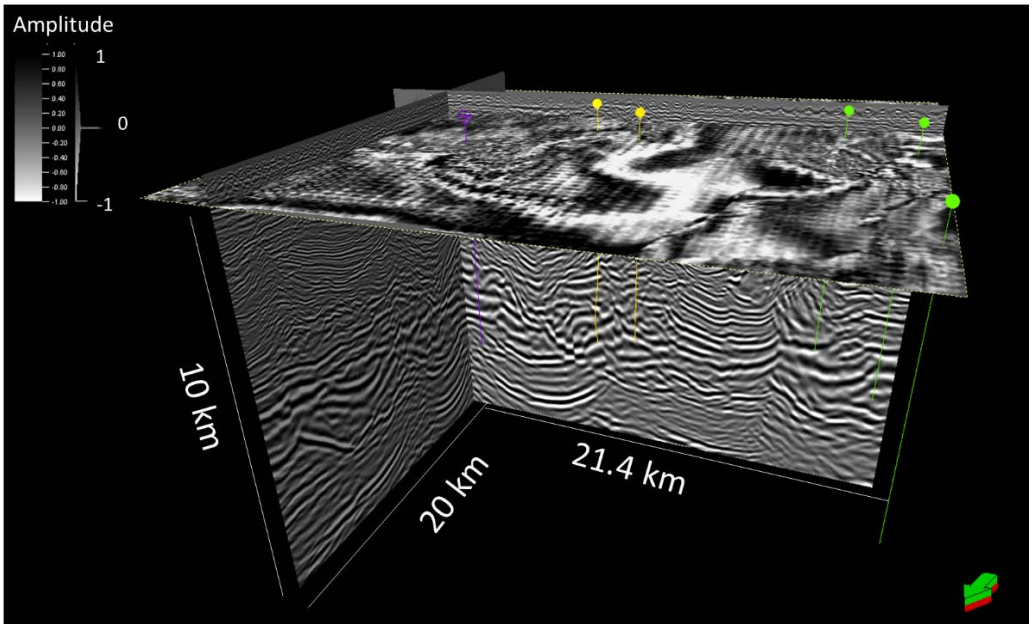


**Figure 6. 1** Depth slice at z=1000 m showing a North-South trending acquisition footprint pattern corresponding to the deployment of the ocean bottom cables. Note the "U-shaped" patterns on the shallow part of the vertical slice.

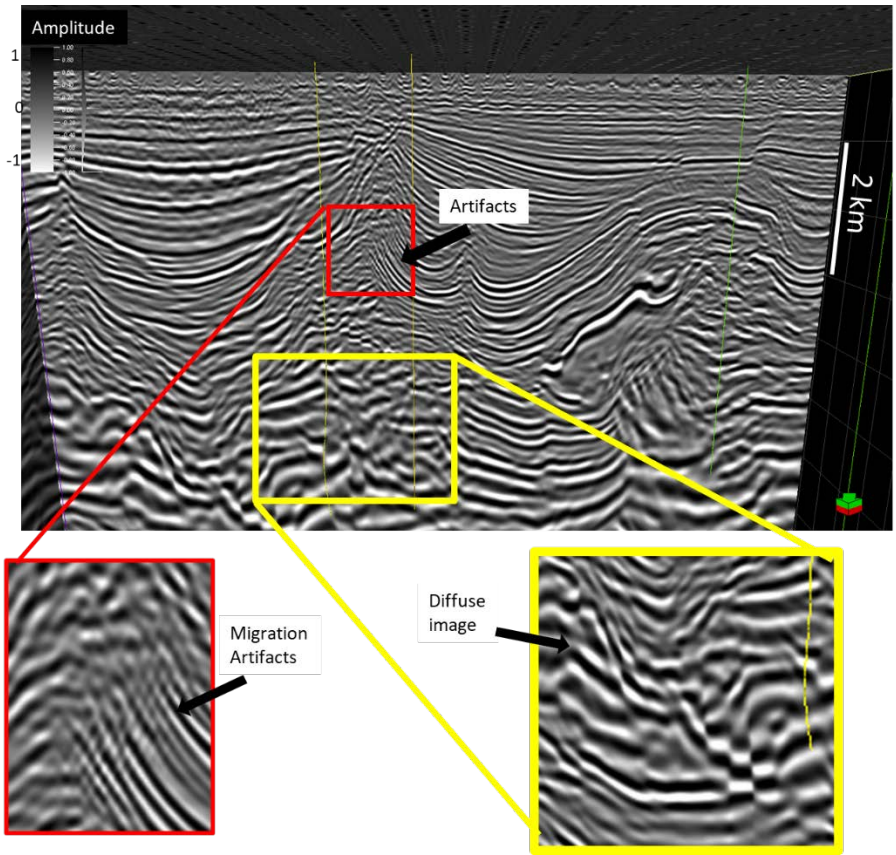


**Figure 6. 2** Expanded view of a representative vertical slice through the PSDM amplitude data showing some artifacts in the Mesozoic target level.

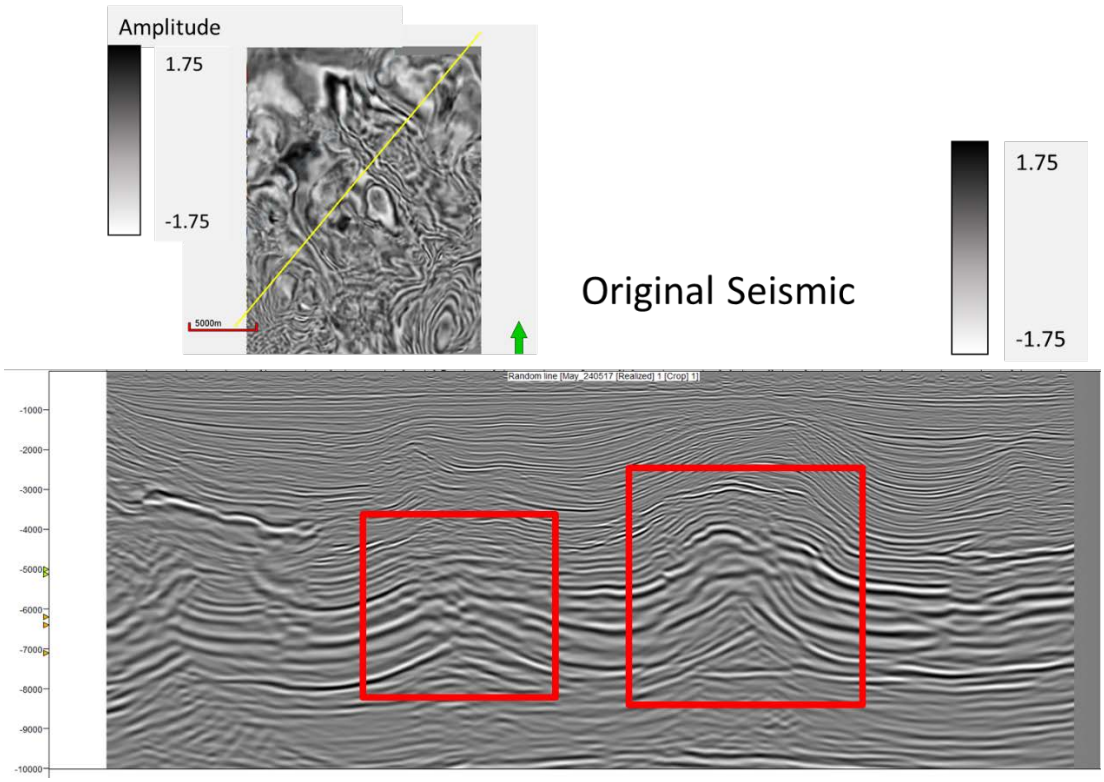


**Figure 6. 3** Original seismic data showing a very diffuse zone within the Mesozoic and along the principal fault traces.

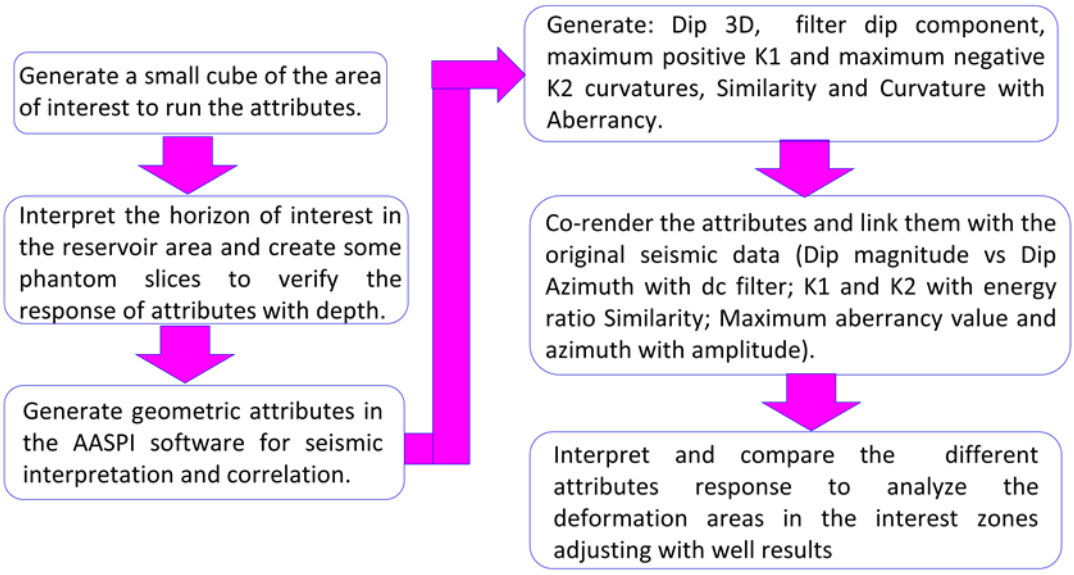


**Figure 6. 4** Methodology followed to extract some geometric attributes.

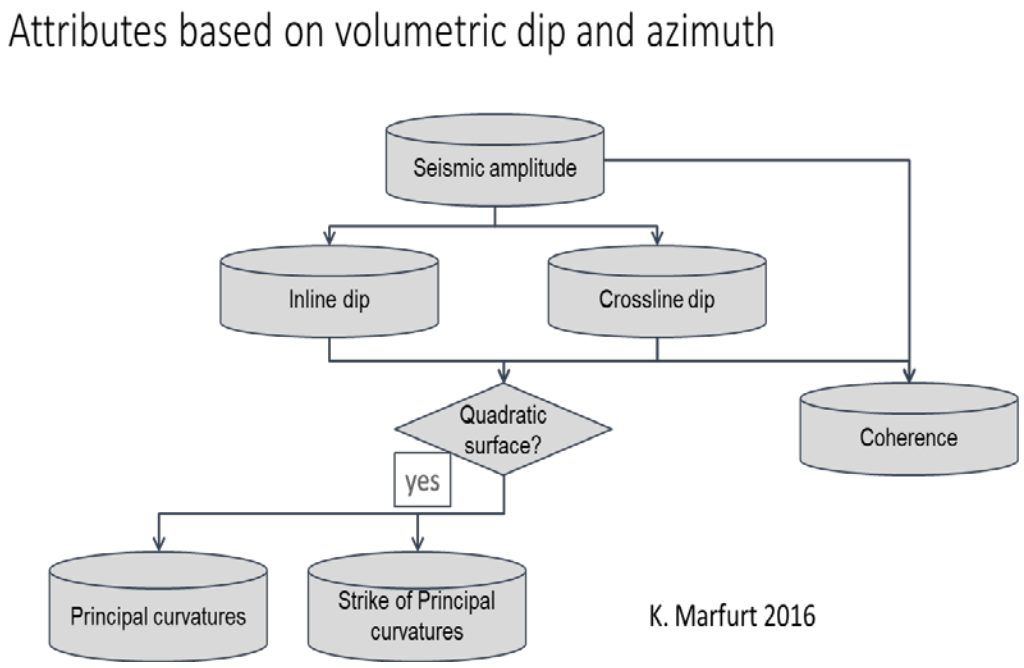


**Figure 6. 5** Methodology to get specific geometric attributes for structural interpretation (from AASPI software documentation.

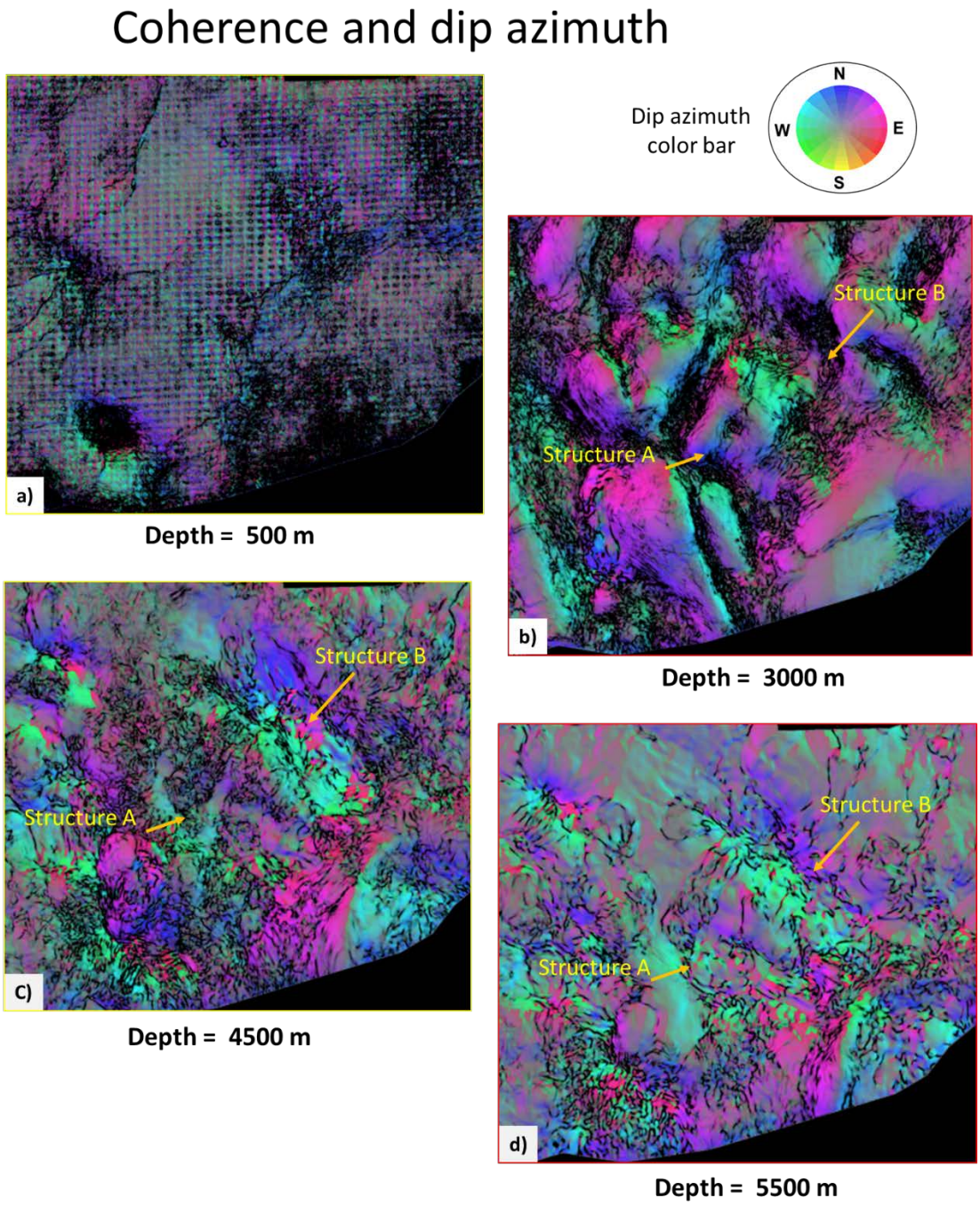


**Figure 6. 6** Different depth slides showing coherence attribute correndered with dip azimuth and dip magnitude (attributes from AASPI software). a) at 500 m showing footprints, b) depth slide at 3000 m (Tertiary), c) depth slide at 4500 m (Mesozoic at "B" structure), d) depth slide at 5500 m (Mesozoic in "A" structure).

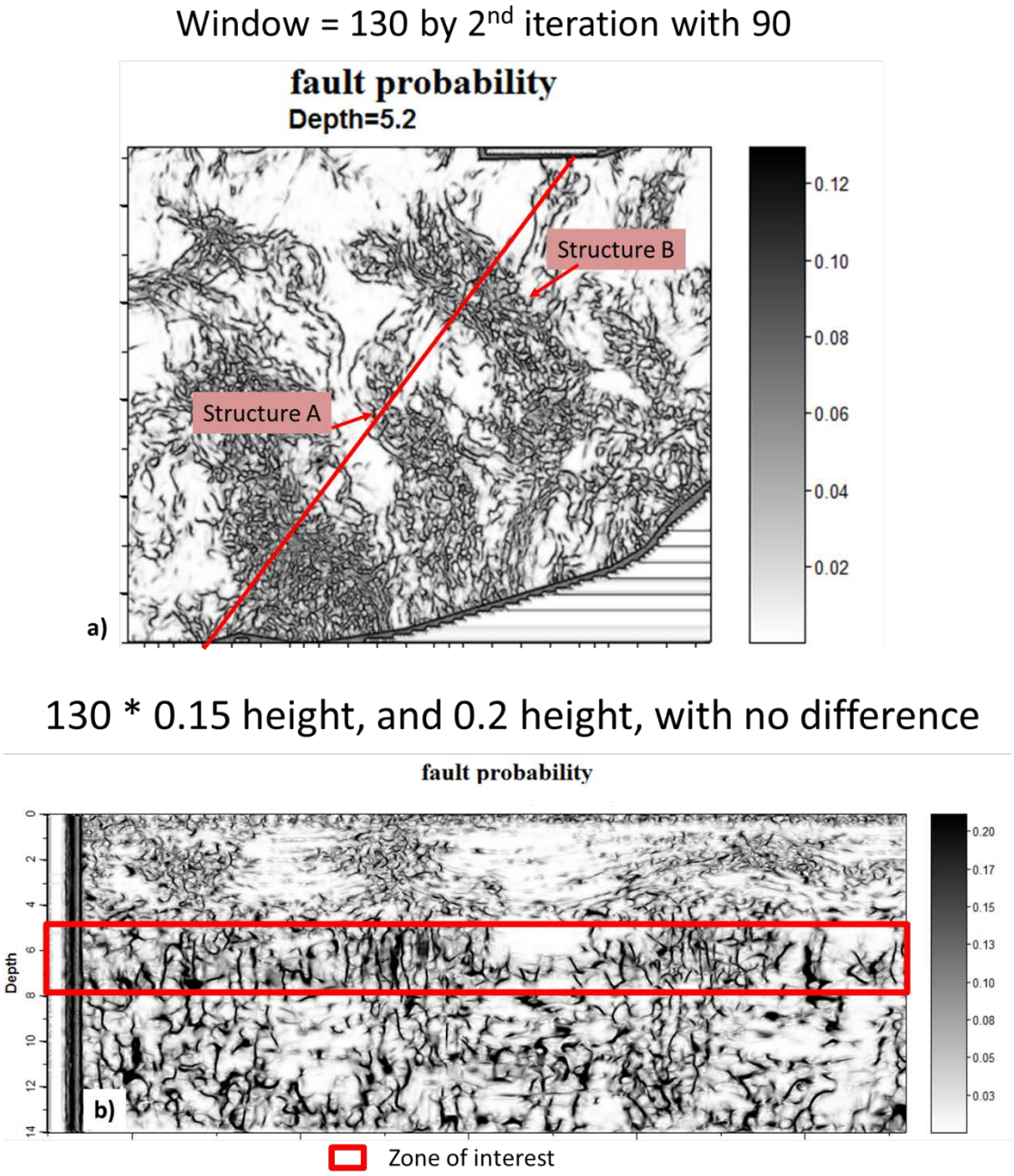


**Figure 6. 7** Fault probability attribute from AASPI software, was run in larger windows of 130 varying the height with no difference. a) Depth slice at 5200 m, b) random line across both structures “A” and “B”.

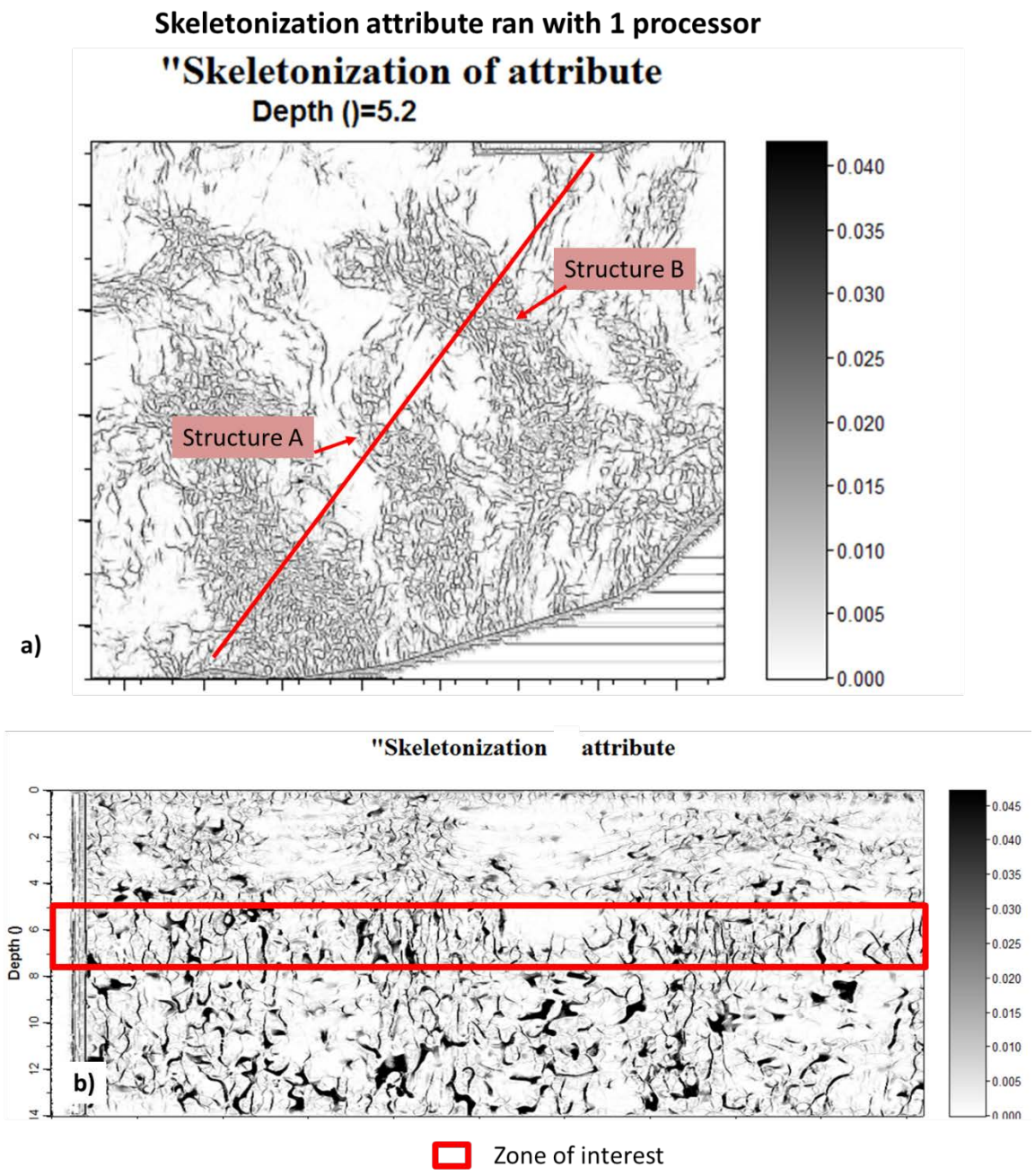


**Figure 6. 8** Skeletonization attribute from AASPI software, was run after fault probability attribute. a) Depth slice, b) random line across both structures “A” and “B”.

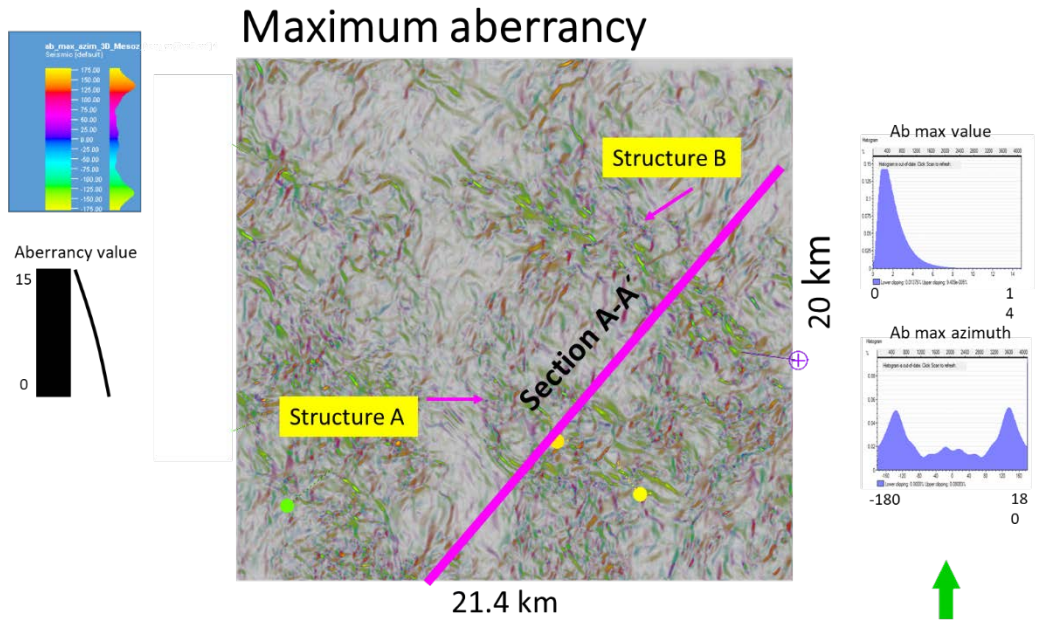


**Figure 6. 9** Depth slice shows the attribute of maximum Aberrancy (AASPI software attribute that measures the lateral change or gradient of the curvature on the seismic discontinuities).

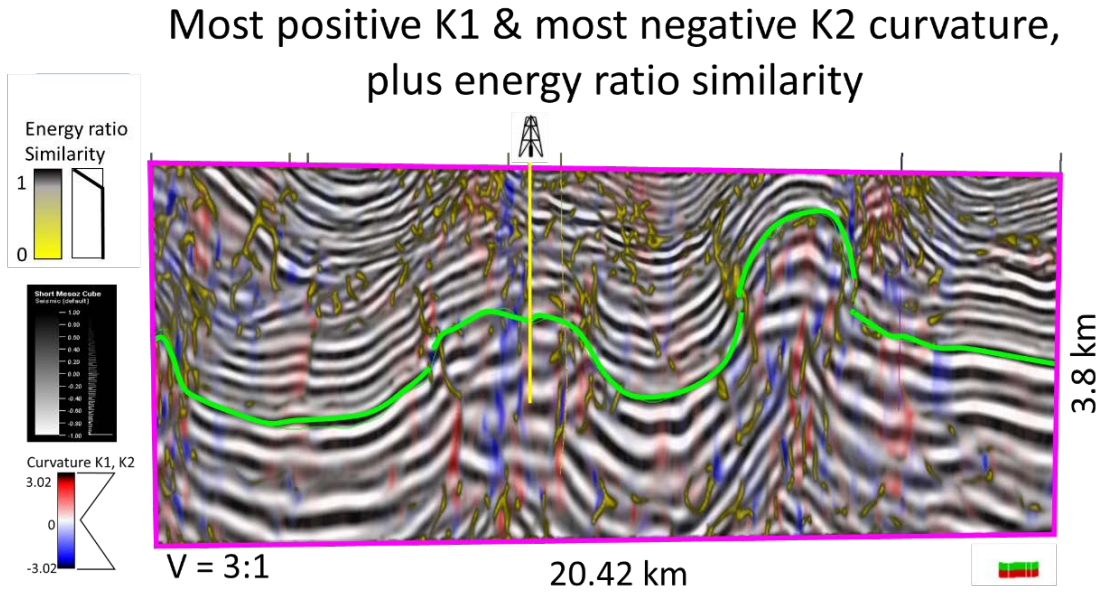


**Figure 6. 10** Cross-line Section A-A´ of the 3D seismic cube in depth showing three correndered attributes run in AASPI software (Energy ratio similarity plus most positive K1 and most negative K2 curvatures).

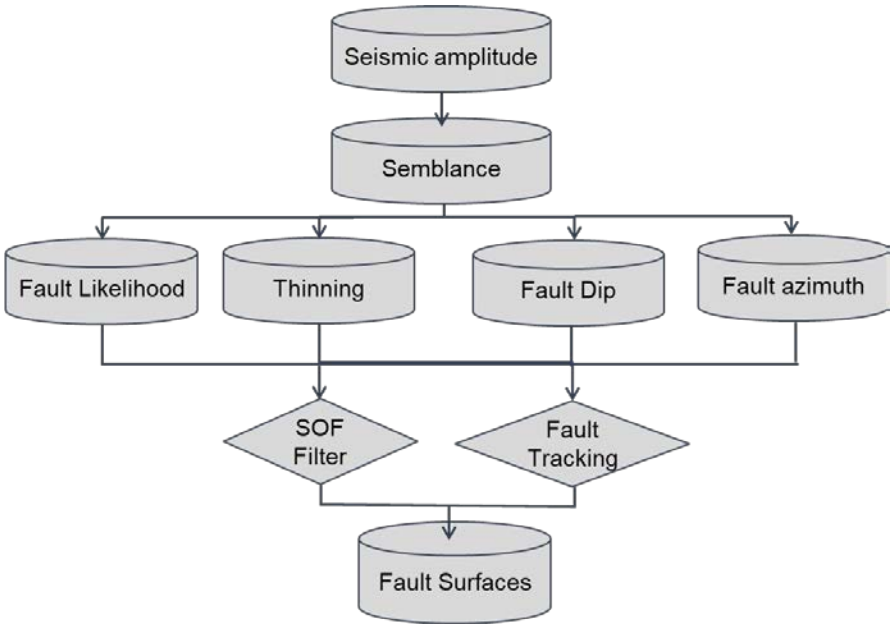


**Figure 6. 11** Methodology to extract the "Fault Tracking" volumetric attribute. (Modified from Halliburton, Decision Space).

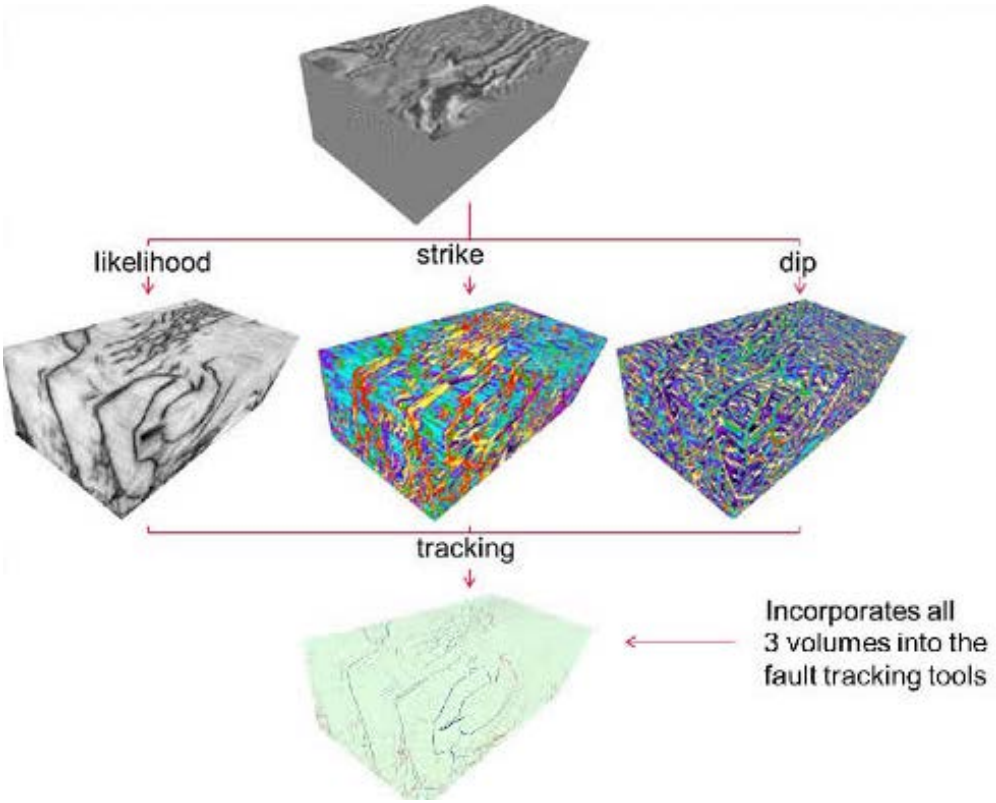


**Figure 6. 12** Three volumes are shown representing different geometric attributes (Likelihood, Strike, and Dip) to extract the final structural attribute "Tracking." (Decision Space, 2017).

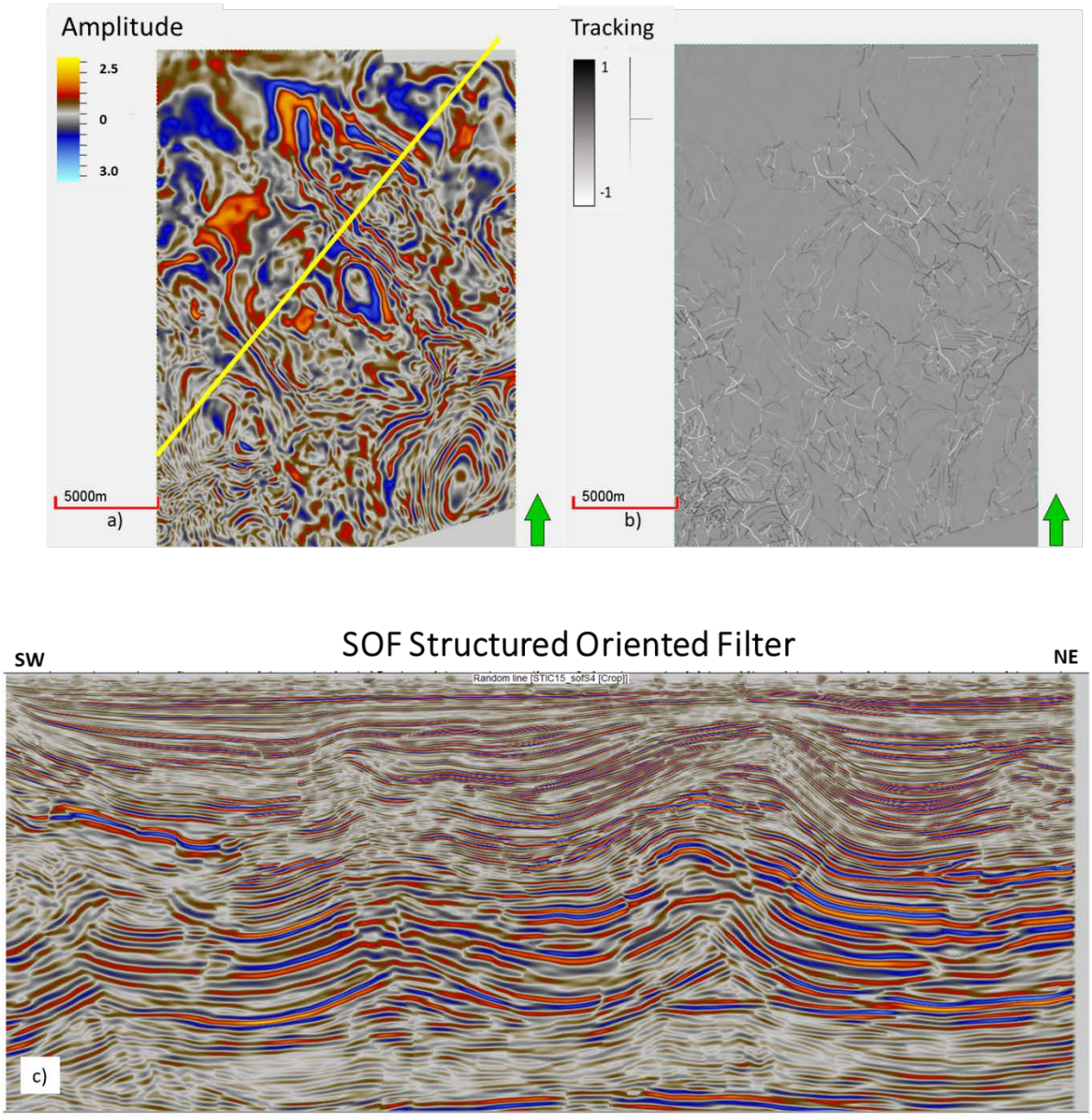


**Figure 6. 13** Study area showing two attributes from the suite of attributes "Fault Likelihood." a) Depth section showing the SOF Structural Oriented Filter b) Depth section of Tracking attribute from the same set of attributes. c) The random section in the SW-NE direction of SOF filter.

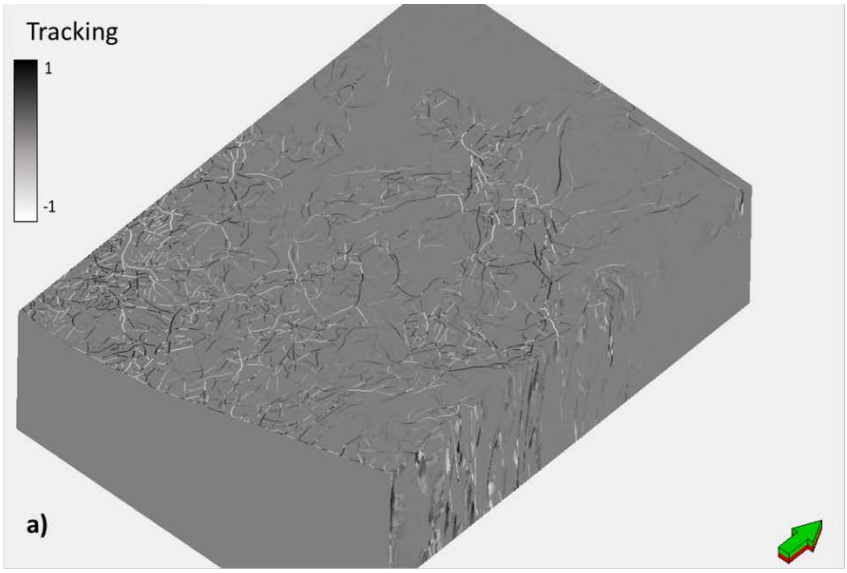


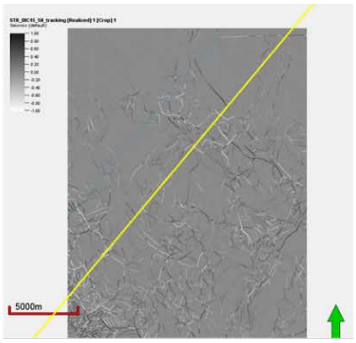


Tracking attribute from fault Likelihood

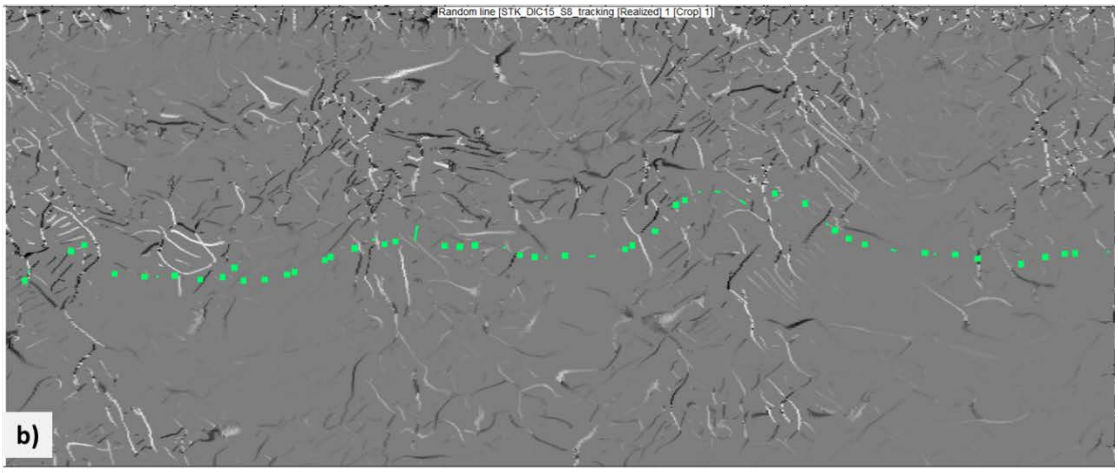


**Figure 6. 14** (a) A representative depth slice at z=5500 m through a fault likelihood attribute. This volume can be "tracked" to form fault objects. (b) Vertical random line AA' through the tracked fault likelihood volume showing major discontinuities. (Images generated using Halliburton's "Decision Space 2017" software).

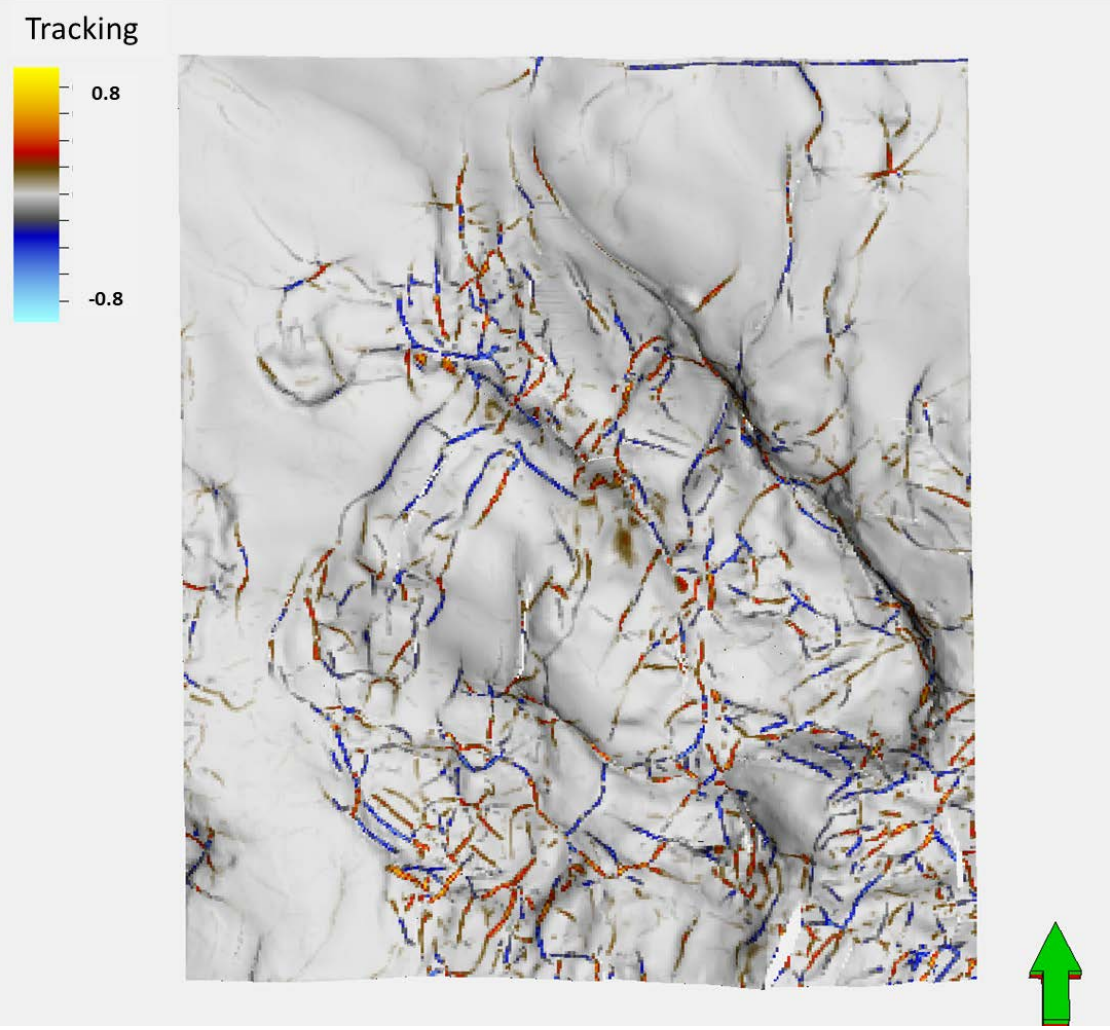


**Figure 6. 15** Horizon slice along the top Upper Cretaceous, (green horizon shown in the previous figure) through the tracked fault likelihood volume. In addition to aiding the structural interpretation, such images can be used to generate a variogram for geostatistical interpolation of petrophysical properties. The Tracking values represent an unconformity fault value for 8 and -8 and null value represented in white.

# CHAPTER 7. 3D Structural Interpretation.

The Regional structural geology of the study area is a tectonically driven system related to the four different deformation events D1 – D4 already explained in Chapter 2.

The seismic interpretation of the study area was conducted using the 3D seismic depth converted volume, integrated with well data. The geometry of the most significant structures in the area was obtained by interpreting a series of sequential random-lines, inlines, and crosslines at intervals of 20 lines in between. The interpretation of the lines both perpendicular and parallel to the trend of the structures yielded an overview of the most critical tectonic events involved in the formation and evolution of both extensional and contractional structures.

The geometry and kinematics of the principal faults and structural unconformities were mapped and correlated with some of the discontinuities mapped using the SOF Structural Oriented Filter (one of the outputs obtained from the Fault likelihood set of attributes). However, not all discontinuities observed using the filter were related to faults, some of them were joined stratigraphic and structural features and some of them were noise. The thrust faults are represented in red and the normal faults in yellow.

Four seismic horizons were interpreted based on the 3D seismic survey of the region (±240 km²): top of Upper Cretaceous, top of Upper Jurassic Kimmeridgian and top and base of autochthonous salt (principal detachment surface of the study area). Additionally, all Mesozoic faults possibly involved in causing fracturing in the

reservoirs of the study area were mapped. There were approximately a total of 400 faults interpreted for this study.

Two final structural maps resulted: Top of the Upper Cretaceous and Top of the Upper Jurassic Kimmeridgian which are the two principal reservoirs in the area and are shown in **Figure 7. 1**.

Structures “A” and “B”, have been affected by different superposed deformational events. The autochthonous salt acts as a principal detachment surface for both structures in the zone during extension and contraction (**Figure 7. 1**). Salt pillows and salt anticlines formed before the compressional events of the Eocene-Oligocene and the Miocene (Chiapaneca Orogeny).

## 7.1.- Structural Cross Sections

Three structural cross sections were analyzed in two different directions: NW-SE and SW-NE, based on the 3D seismic interpretation of random-lines, inlines and crosslines. Also, the interpretation of the most critical Tertiary tops were included (Upper Eocene, Upper Oligocene, Middle Miocene and Upper Pliocene), defining the age of the principal regional deformation events by analyzing the pre-growth, syn-growth, and post-growth cinematic units.

***NW-SE sections.***

The NW-SE sections were constructed parallel to the trend of the structures (“A” and “B”). These sections are oblique to the N-S trend of the normal faults but were used to show the normal fault system.

Structure “A” is shown in section I-I´ and structure “B” is shown in section II-II´.

**Section I-I´** (Figure 7. 2) runs parallel to the trend of structure "A." It provides a picture of how the extensional gravitational system developed a roll-over structure commencing with the basin-ward extension during the extensional stage.

Section I-I´, shows how the normal faults originated in the D1 event during the Upper Jurassic and continued in some parts of the area until the Middle-Upper Cretaceous. The section interprets a roll-over fold formed during extension. Significant displacement results in steepening of the dips of the beds in the rollover (Figure 7. 2). The faults detached in the autochthonous salt, triggering the block rotation in every major normal fault and separating the units into different tilted blocks. The highest parts of the tilted blocks define a shallow depositional environment of Inner Ramp carbonates, leading to the deposition of oolitic carbonate banks, which became the principal reservoirs of the Upper Jurassic Kimmeridgian.

**Section II-II´** (Figure 7.3)**:** this trend runs parallel to "B" structure, and reveals two different deformation styles.

Extensional deformation similar to structure "A" occurs of the south-east part structure "B" (well B-4). However, some of the normal faults have been re-activated to reverse faults during the Tertiary contractional events. In the north-west part of structure "B" (well B-1) a salt pillow structure formed.

***SW-NE section direction.***

The SW-NE section clearly reveals the contractional deformation events formed during two different episodes. These events resulted in the formation of the two structures A and B.

Section **III-III´** (**Figure 7. 4**), trends perpendicular to "A" and "B" structures. Both are faulted detachment folds formed during the deformational event D2 (Eocene-Oligocene) and re-deformed by the super-imposed shortening of event D3 (Chiapaneca Orogeny, Middle-Upper Miocene).

In the "B" structure, compression D2 was masked by the greater magnitude of the compression D3. At least three deformational events have deformed the structures. The structure has also undergone extension during the Upper Pliocene –Pleistocene-Recent.

## 7.2 Three-dimensional structural model.

The primary objective of the construction of the 3D structural model was to show the evolution and geometry of the structures during the deformational episodes. The model also helps to provide parameters of the critical deformation zones related to the fractured reservoirs.

In general, both structures "A" and "B" appear to have formed at the beginning of the deformational stage during the extension D1 as roll-over structures. At the end of the contractional deformational events, both are classified as faulted detachment folds, as determined by their characteristics visible in the seismic interpretation.

The north-west part of the structure “B,” site of well B-1, represents a symmetric detachment fold, faulted on both limbs, and cored by salt. Structures with this geometry are commonly referred to as pop-up structures. On the other hand, in the field “A” and the south-east side of the field “B” site of well B-4, the folds formed initially as a roll-over structure created by extension and then developed into faulted detachment folds.

The 3D structural model was defined within the area of 240 square kilometers, modeling the four interpreted horizons: upper Cretaceous (**Figure 7. 5**), upper Jurassic Kimmeridgian and top and base of autochthonous salt **(Figure 7. 6**). Additionally, 100 faults were modeled in conjunction with normal and thrust faults. The 3D structural model is shown in **Figure 7. 5, Figure 7. 6 and Figure 7. 7**.

**Structural models’ description.**

The description of the structures analyzed was based on the following observations:

***Symmetric Faulted Detachment Folds (Pop-up structures).***

Usually, a very low friction coefficient of salt layers induces a symmetric stress system. The lower friction promotes pop-up structures rather than asymmetric detachment folds. (Letouzey et al., 1995, Mitra, 2002). A pop-up structure is observable in Field “B,” site of well B-1.

***Roll-over anticlines.***

Rollover structures form in the hanging walls of listric faults and are primarily due to extension on a fault. Structures associated with listric faults formed during the extensional event D1. With the progressive deformation, an anticline developed.

These processes resulted in some local collapses at the top of the structures, forming new normal faults. These small collapses are present in the crest of the "A" structure, and some complex areas that are re-deformed by local fault inversion from normal to reverse faults such as in "B" structure, (**Figure 7. 3**).

***Faulted Detachment Fold model.***

Both structures are interpreted as Faulted Detachment Folds: the principal observable difference on these structures with the fault propagation fold and fault bent fold models is that faulting is secondary (**Figure 7. 9 and Figure 7. 10**). The faults have formed after, as a consequence of the initiation of the detachment folding (Mitra, 2003). Both structures exhibit the transition from folded to faulting. The fold geometries of both structures are more open, rounded, and symmetrical than the other fold models. (Davis and Engelder, 1985; Mitra, 2003). The structures have been developed over sedimentary units with significant thickness and competency contrasts since the basal layer is an incompetent unit, (autochthonous salt), overlain by competent siliciclastics and carbonates (Mitra 2003).

The fold wavelength is initially controlled by the thickness of the competent units (Currie et al., 1962), and the geometry and evolution are dependent on the mechanical stratigraphy, thickness, ductility, and sequence of the units (Davis and Engelder, 1985; (Mitra, 2003). The difference of the initial wavelength between both

structures is observed in **Figure 7. 4**. In structure "A," the autochthonous salt is thinner than in structure "B". The larger size of the "B" structure could be possibly related to the salt thickness variation and owing to its still active evolution.

### 7.3 Local Structural deformation events.

Structures in the study area developed during four main tectonic episodes. The detailed effects of these episodes on structures "A" and "B" are discussed briefly below:

**D1 Gravitational extension (Upper Jurassic – Cretaceous)**

During the Upper Jurassic, the depositional environment was a shallow marine ramp with a very low inclination (1-2°). During this time, gravitational extension occurred during the D1 episode. The extension was accompanied by the salt tectonics and tilting of the fault blocks towards the basin.

Extensional event D1 (**Figure 2. 3**), exhibits normal and occasionally listric normal faults. Some rollover structures formed during movement on the faults. A shallow marine environment formed on the highest parts of the tilted blocks, and a deeper depositional marine environment formed in the lowest parts of the model (**Figure 7. 8** and **Figure 7. 11**).

Oolitic banks and ooids formed in the shallowest parts at the top of the tilted blocks of the salt rollers, (between 1-5 meters depth). On the contrary, at the bottom of the structures, the deeper marine sediments were deposited according to the "Rampa Estructurada" (Structured ramp) model. The contrast between these two sedimentological environments can be observed in wells A-1 and ADL; shown in the first interpreted section I-I´, (Figure 7. 2). During the Upper Jurassic Kimmeridgian,

well A1 imaged the oolitic banks, while the other well ADL did not find this significant reservoir, because of its depositional settings of deeper facies or lower energy deposits. As a note, these wells have a difference in depth between their Kimmeridgian tops of 700 m.

Both structures “A” (represented by wells A1 and ADL) and structure “B,” (represented by well B-4) were affected by the D1 episode. D1 extension is exhibited in the interpreted cross-section I-I’ (Figure 7. 12). It follows the trend of the regional extension (SW-NE). D1 produced roll-over structures caused by extension and block tilting in the basinward direction.

The combination of the environment and extension, generated in almost all the wells of the structure “A” but not in well ADL, are the most critical traps for the formation of the oolitic and carbonated banks reservoirs of the Upper Jurassic Kimmeridgian. (Cross section I-I’, Figure 7. 12).

A good number of wells drilled in Field “A,” are productive in this Jurassic reservoir.

Structure B exhibits a different deformation style in its north-west section with the formation of a salt pillow, represented in well B-1 (section II-II´ of Figure 7. 12). The crest of the salt pillow probably was a shallower depocenter during the extension, which resulted in the development of a sedimentary environment for carbonate banks. In structure “B,” this facies was not productive due to the very shallow oil/ water contact in this structure.

**D2 Compressional deformation event Eocene-Oligocene.**

This contractional deformation is related to the Laramide Orogeny. The direction of this contraction was Southwest – Northeast. The deformation of the structures can be better observed in Section III-III´, (**Figure 7. 12**).

***Structure "A."***

The distinction between the two compressional events is better observed in structure "A," because in this structure, both episodes D2 and D3 are evident and separated by a large shale deposit located within the Upper Oligocene. This mobile shale responded as a plastic barrier between the compressional events D2 and D3. The geometric patterns observed in structure "A," suggest that the most critical reservoir traps within the Mesozoic carbonates formed principally by the D2 shortening as seen in the structural section III-III' (**Figure 7. 12)**. The main traps during the Cretaceous in structure "A" represent the most critical naturally fractured carbonate reservoir of the area, producing in nine of the twenty-one wells.

***Structure B.***

In structure "B," the compressional event D2 (Eocene-Oligocene) is not as clear because this event is masked by the second compressional event D3 (Chiapaneca Orogeny) which is of greater significance for this structure during the Middle-Upper Miocene. Therefore, it seems that the Mesozoic traps of this structure formed initially from extension D1 and continued to be contractionally deformed by the D2 and D3 events.

**D3 Compressional deformation (Middle - Upper Miocene) "Chiapaneca" Orogeny.**

The trend of this compression is South West – North East, the same as D2 (Eocene-Oligocene).

***Structure "A."***

The interpretation of structure "A," suggests that it was more affected by D3 in the upper part of the structure (Tertiary sediments) because of the two deformational domains separated by a thick shale horizon within the Upper Oligocene. The shale horizon acted as a second detachment level, and shale diapirism was developed over "A" structure, thus separating the two different structural domains (between the Mesozoic and the Tertiary).

Structure "A" was reactivated during this episode, but the most significant control of the reservoir traps was D2 episode. (**Figure 7. 12**).

***Structure "B".***

Structure "B" was more influenced than "A" by the Chiapaneca Orogeny or D3 compression. D3 developed a pop-up structure of higher relief than in structure "A." Some observations of "B" structure indicate that it is a deformational front which has been dramatically more affected than the surrounding structures which are significantly lower folds. Additionally, the interpretation suggests that this structure was deformed for a longer period than "A."

The higher relief of the structure also affected by the larger thickness of the salt in the pillow formed in the core. The critical nature of the contractional event D3 must be emphasized, since it exerted significant influence on the "B" structure. D3

reactivated the pre-existing folds and related traps originated during the D2 compression. Five wells have been drilled in the Upper Cretaceous fractured reservoirs in “B” structure, two of which are productive.

**D4 Extension (Pliocene):**

***Structure “A” and “B”.***

The D4 extensional system of the Pliocene Period affected both structures “A” and “B.” It was triggered in the study area by a gravitational movement towards the basin center because of a high sedimentation rate associated with a massive salt evacuation and the basement inclination. The faults detached in different detachment levels, including the allochthonous salt, Upper Jurassic Tithonian, and Tertiary horizons. The direction of this extension is SE-NW, the same direction as the first extensional deformation event D1. Moreover, D4 is probably the cause of the re-activation of some earlier-formed faults and fractures and responsible for keeping the conductive fractures open within the Cretaceous and Jurassic fractured reservoirs.

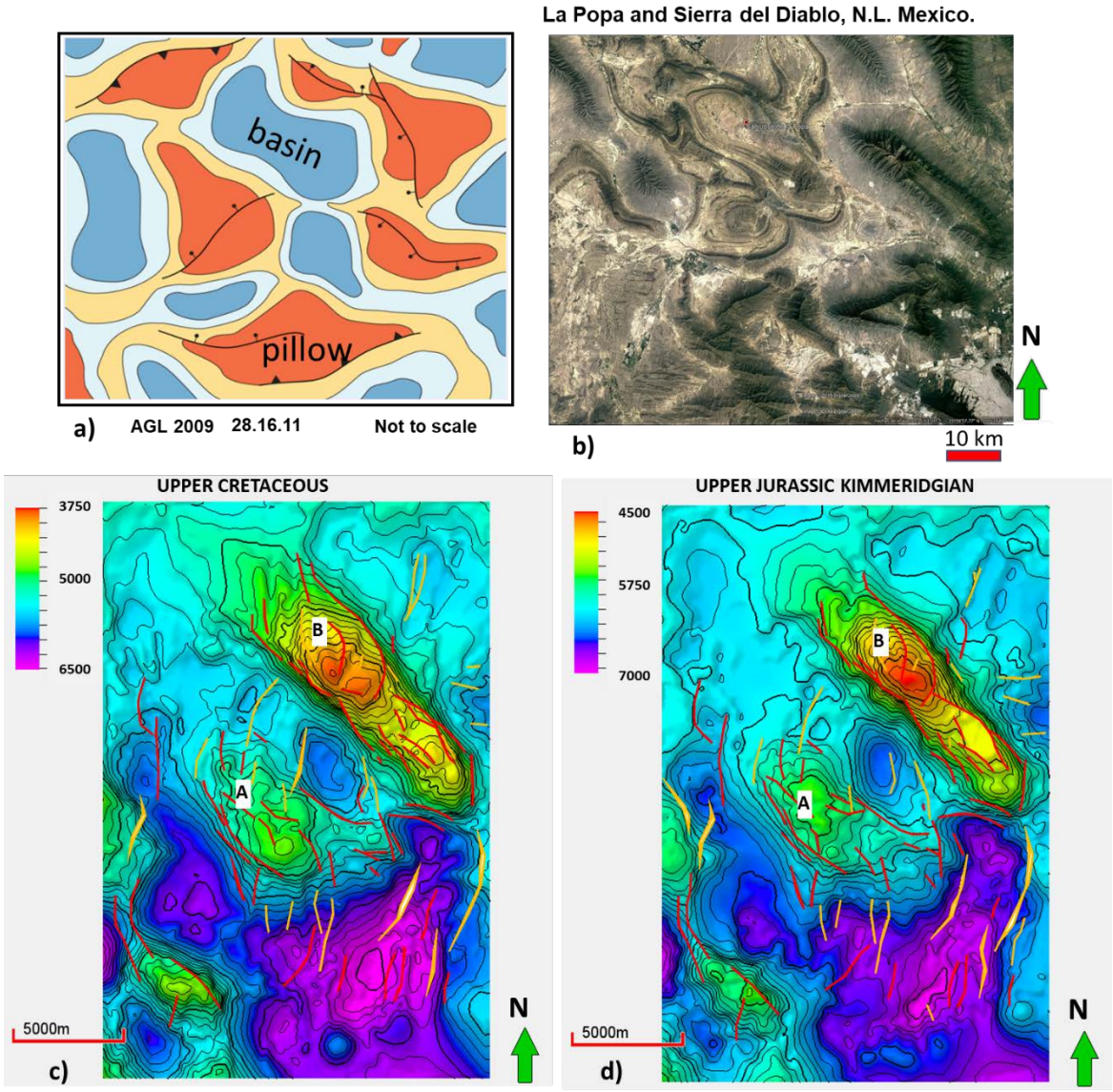


**Figure 7. 1** a) Analog model showing irregular shapes, sizes and distribution in geometries affected by salt pillows and salt anticlines (AGL 2009 Jackson, Hudec & McDonnell). b) Picture showing a real analog model in the salt province located in "La Popa," Nuevo León, México (Google earth). c) Upper Cretaceous structural configuration and d) Upper Jurassic Kimmeridgian configuration map. Highest depth represented by warm colors (red-green) and the most profound zones by cold colors (blue-purple). Thrust faults are represented in red and normal faults in yellow.

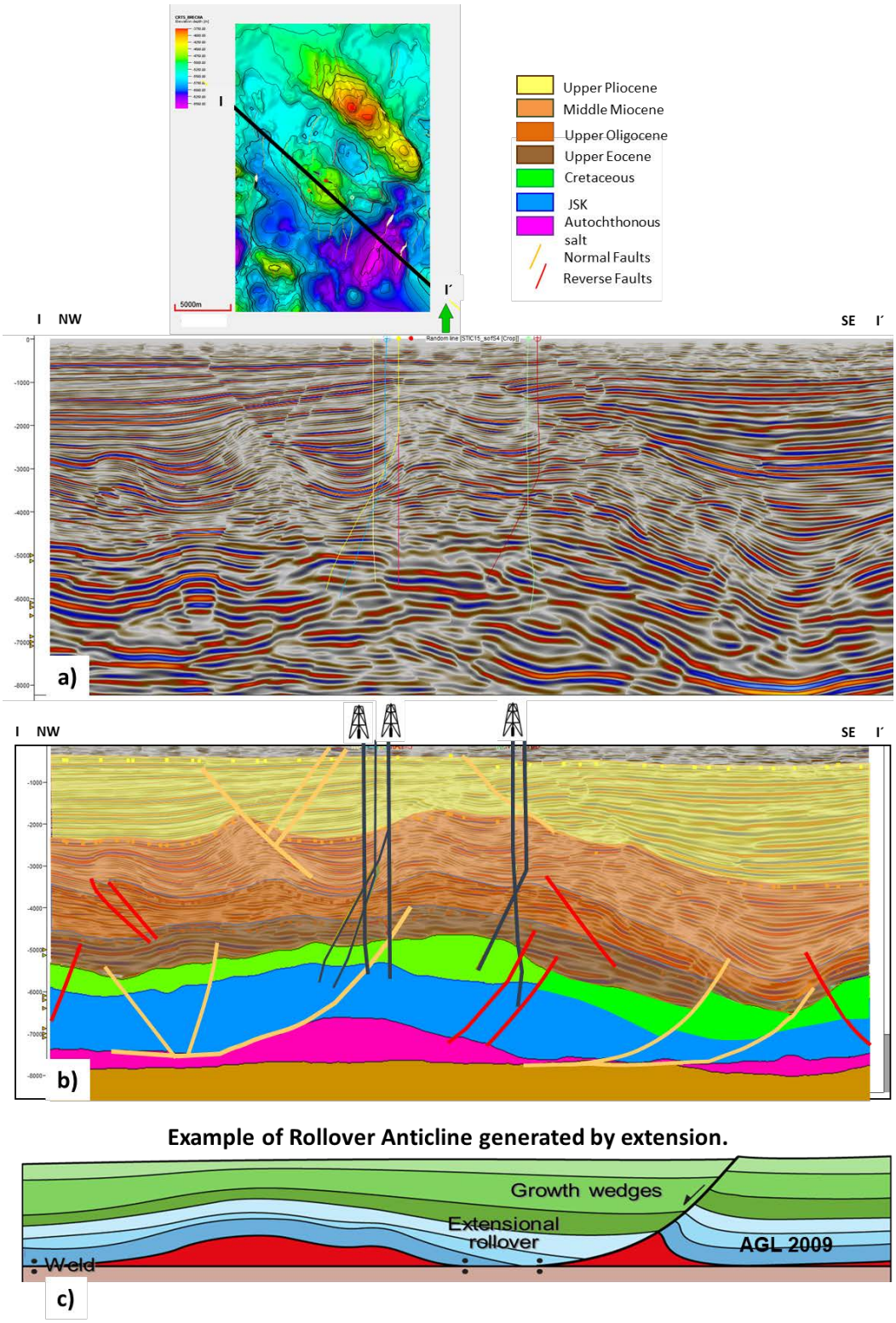


**Figure 7. 2** a) Seismic section I-I´; b) Interpreted structural section I-I´NW-SE parallel to the structure "A" and to the direction of the Extension D1. Observe the structure originated by the extension basin-ward is a Roll-over structure. c) Roll-over schematic analog model (AGL Hudec & Jackson, 2009) compared with "A" structure.

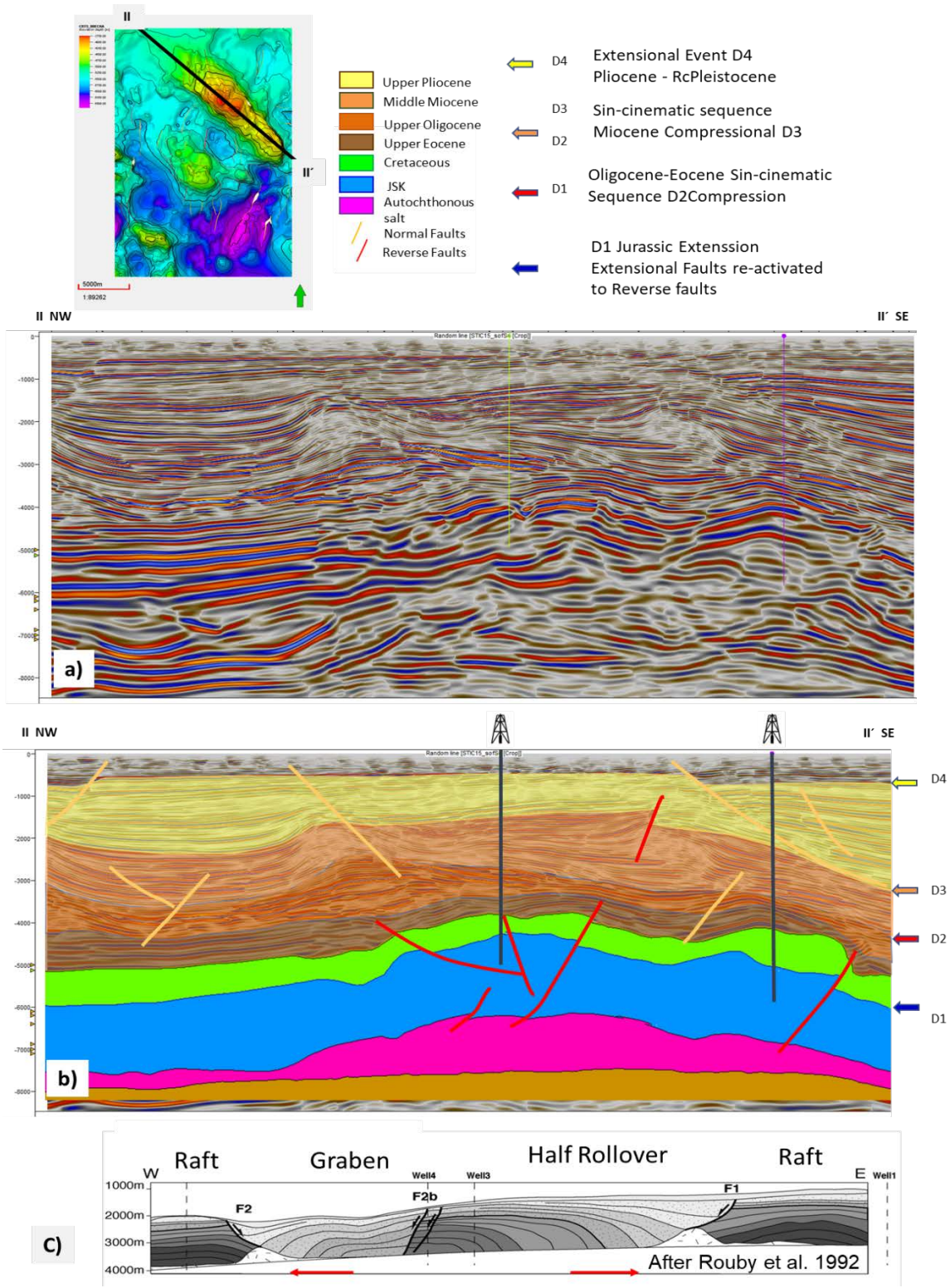


**Figure 7. 3** a) Seismic section II-II´; b) interpreted structural section II-II´ NW-SE parallel to structure B and into the direction of the Extension D1. Observe the structure originated by the extension basin-ward is a Roll-over structure but re-activated after this by the Compressional episodes of D2 and D3 Orogenies.

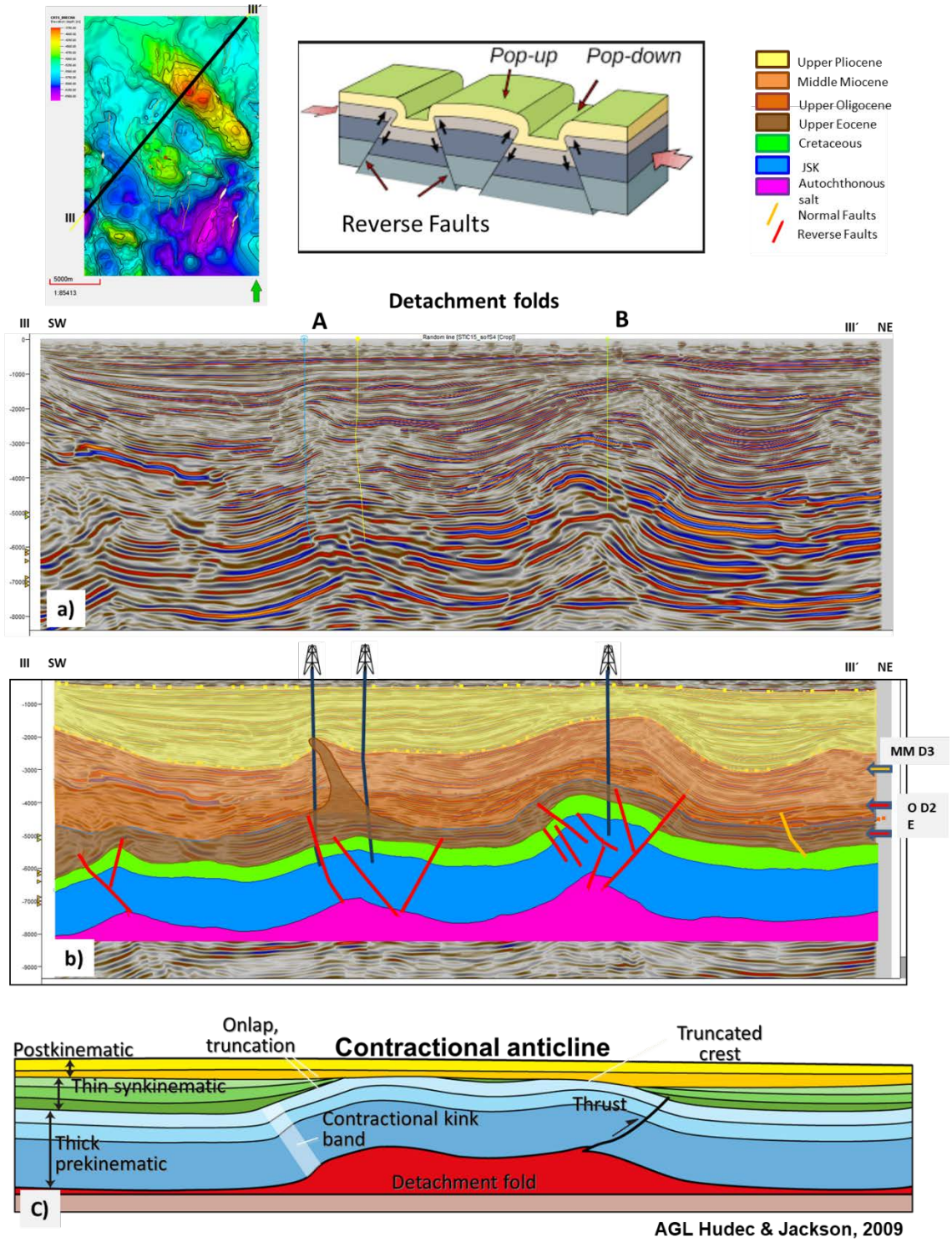


**Figure 7. 4** a) Seismic section III-III´; b) interpreted structural section III-III´ SW-NE perpendicular to both structures A and B, parallel to the direction of the compression in this study area. Observe that the structures are detachment folds forming Pop-up anticline, one (B) more developed than (A) the other structure. These folds were influenced by the two Compressional episodes D2 (Eocene- Oligocene) and D3 (Middle-Upper Miocene) Chiapaneca Orogeny.

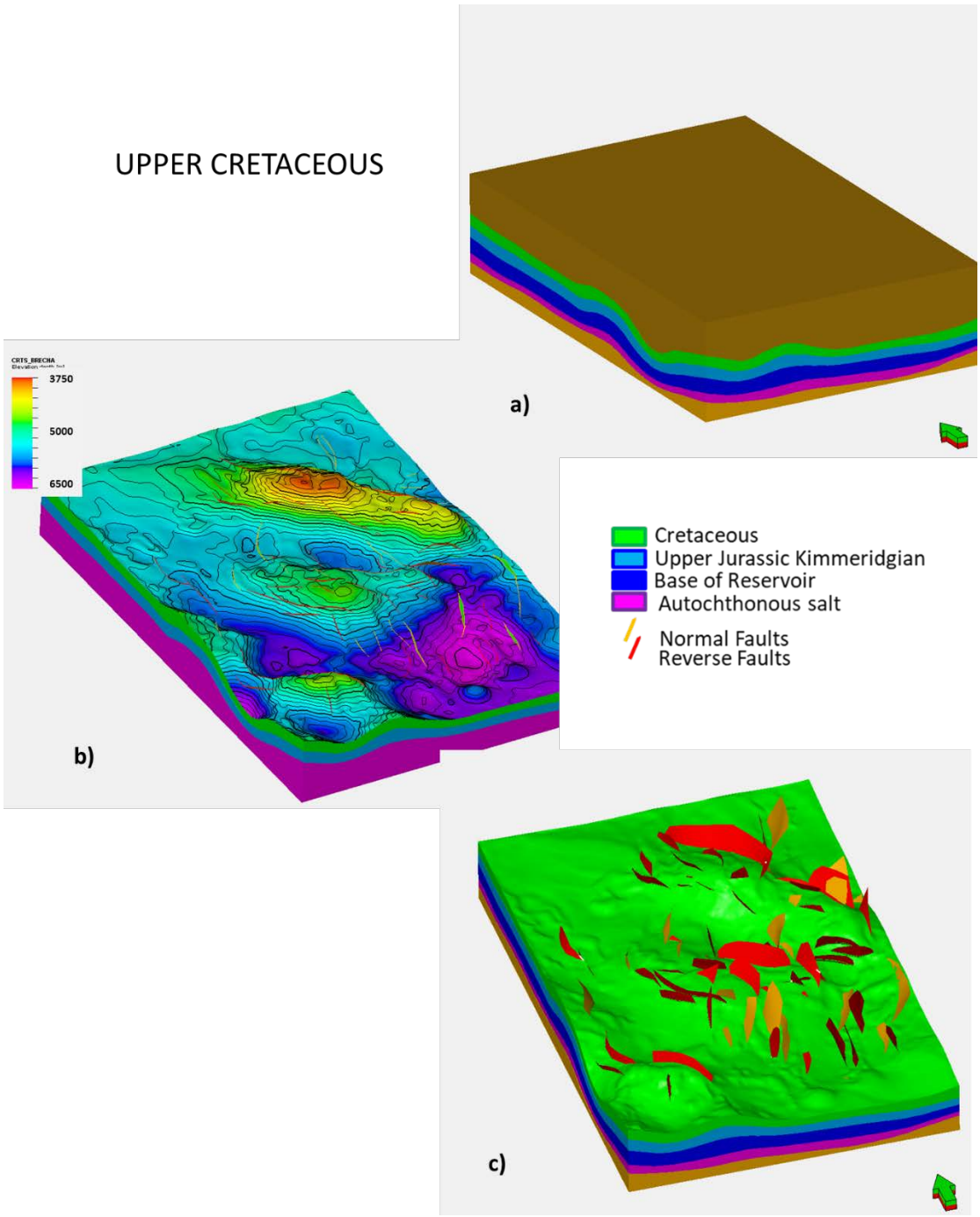


**Figure 7. 5** a) Three D structural model with the four interpreted horizons (Upper Cretaceous, Upper Jurassic Kimmeridgian, Top, and base of autochthonous salt; b) Top of Upper Cretaceous and c) the 100 modeled faults. Top of Cretaceous is shown in green, features in red represent thrust faults and in yellow the normal faults.

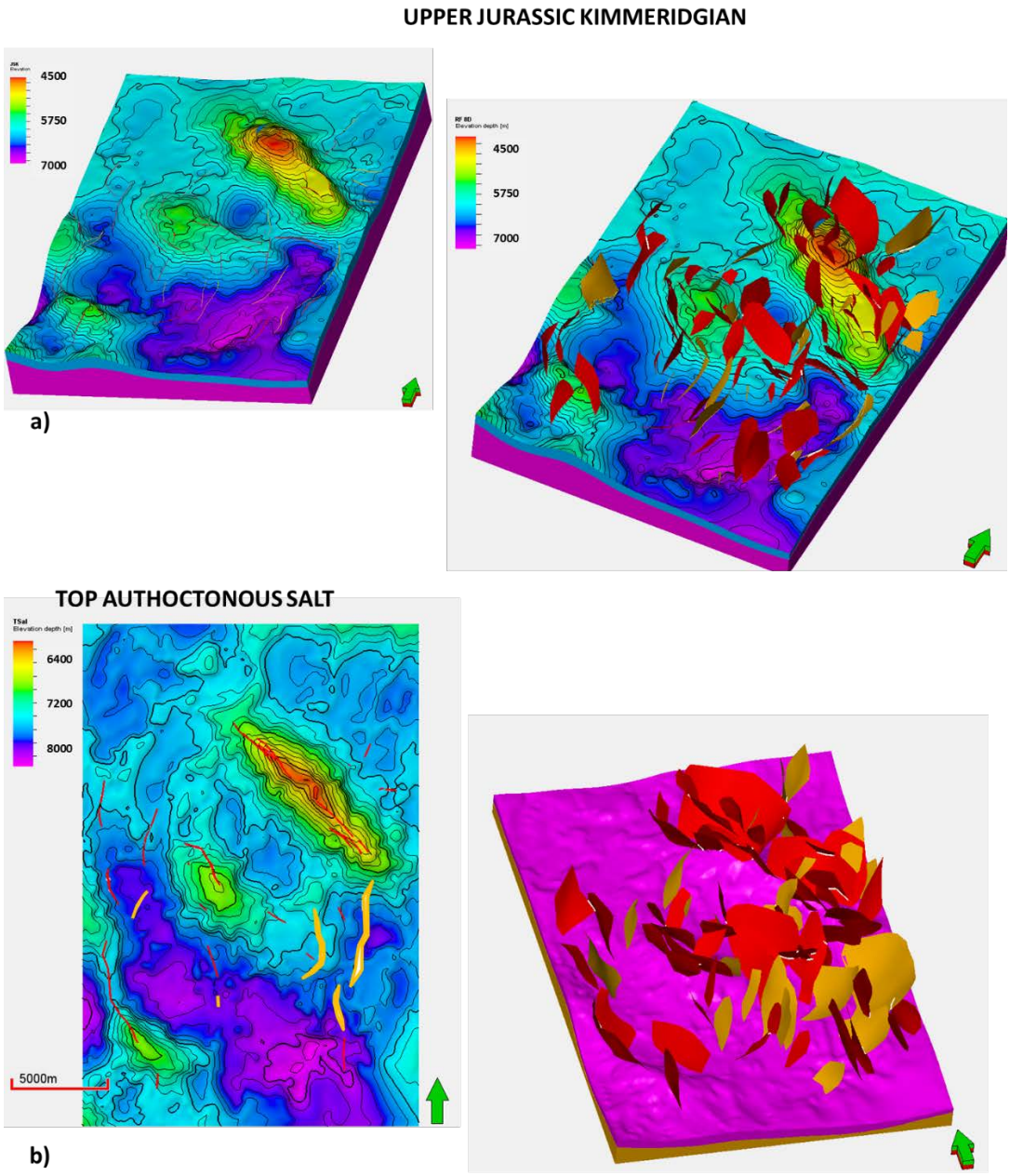


**Figure 7. 6** Three D structural model showing a) the top of Upper Jurassic Kimmeridgian with their modeled faults; and b) pink the Top autochthonous salt. With its 3D model and faults, Red are thrust faults, yellow normal faults.

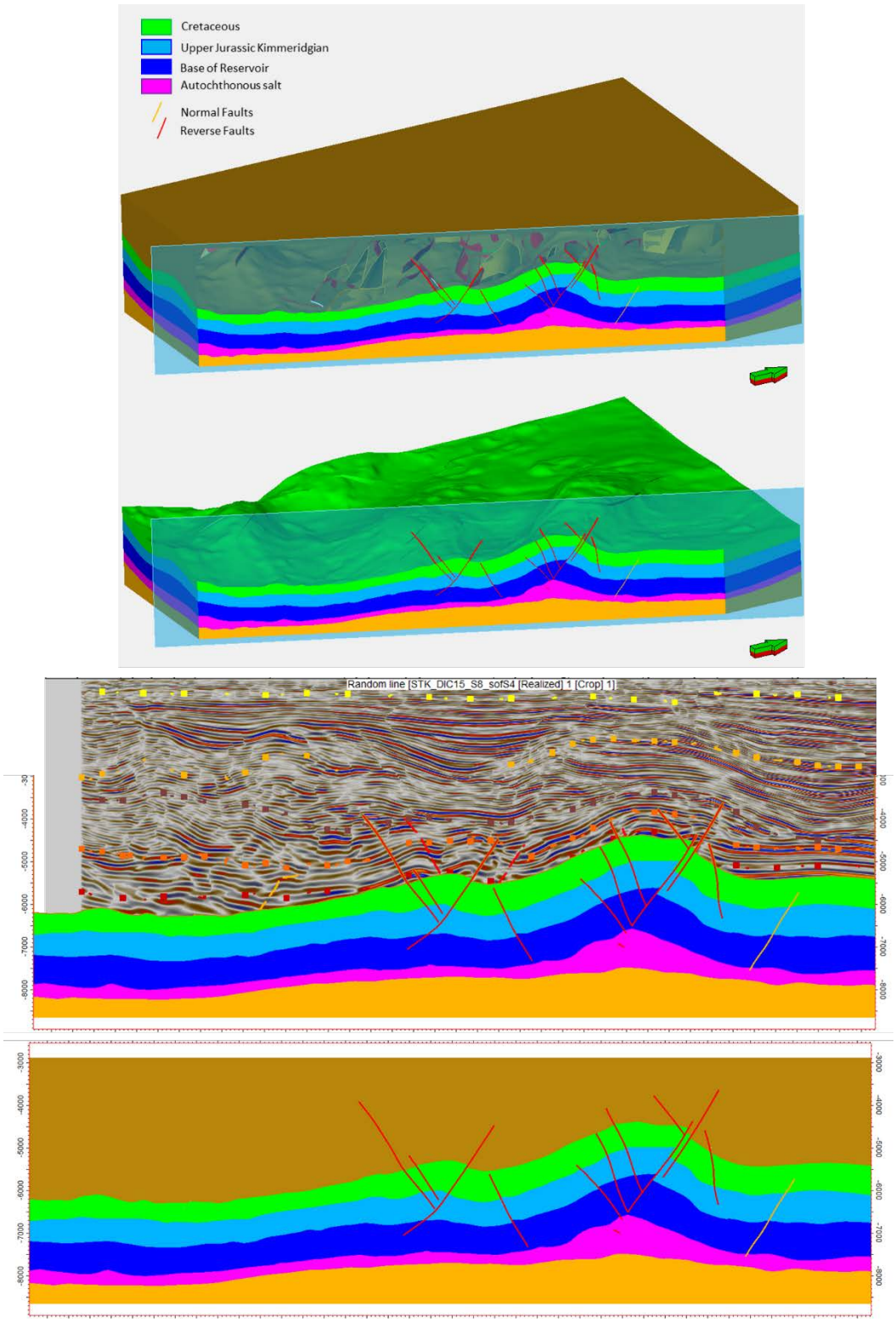


**Figure 7. 7** 3D structural model representing the three interpreted horizons: green top of Upper Cretaceous, light blue the top of Upper Jurassic Kimmeridgian and in pink the autochthonous salt; Dark blue is the base of the Upper Jurassic Kimmeridgian reservoir, comformable to the UJK top. With and without modeled normal and reverse faults.

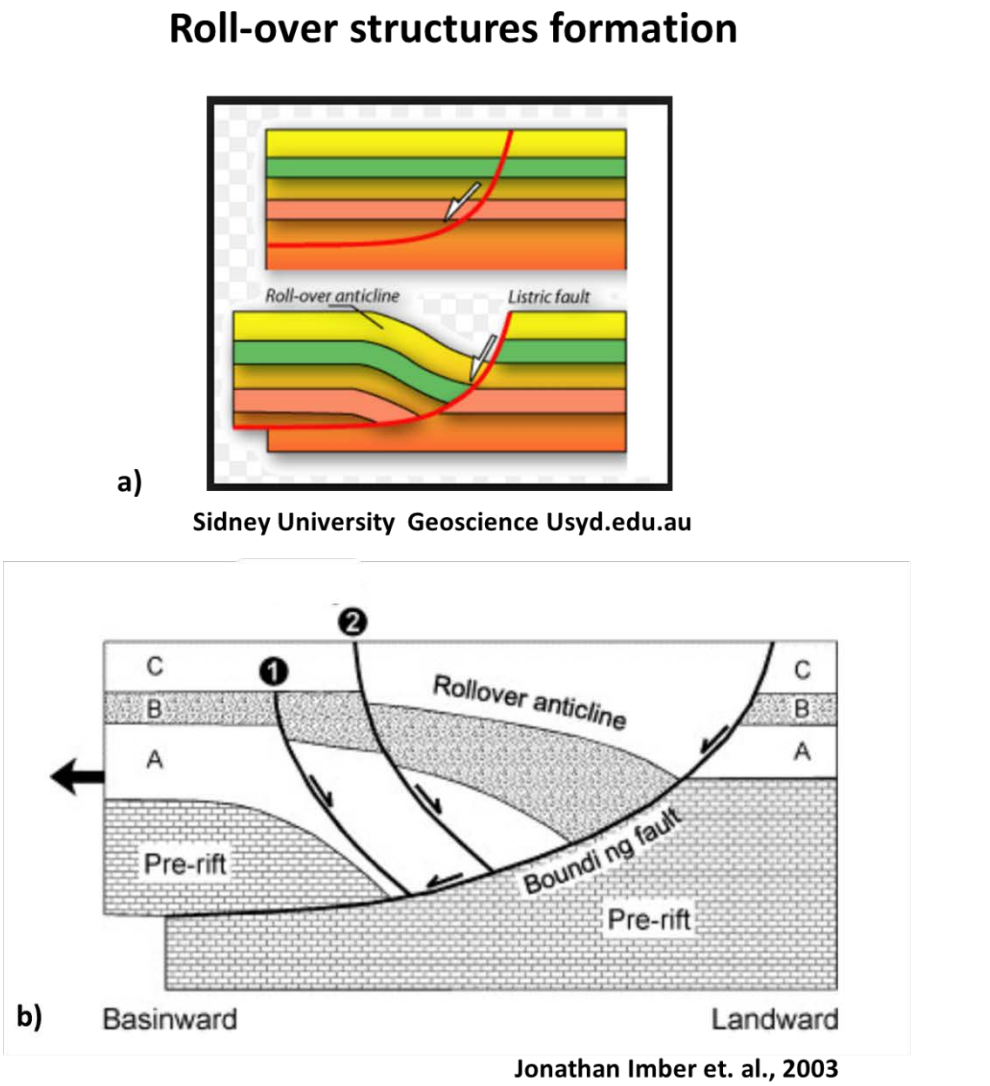


**Figure 7. 8 a)** Mechanism of the roll-over structures formation, showing the first steps of extension forming listric faults and the Roll-over anticline; **b)** Rollover basinward extension of one structure, synthetic and antithetic faults formed on the crest, **c)** a Basin-ward Regional extensional system forming Half-grabens and Tilted blocks over a detachment surface. Moreover,

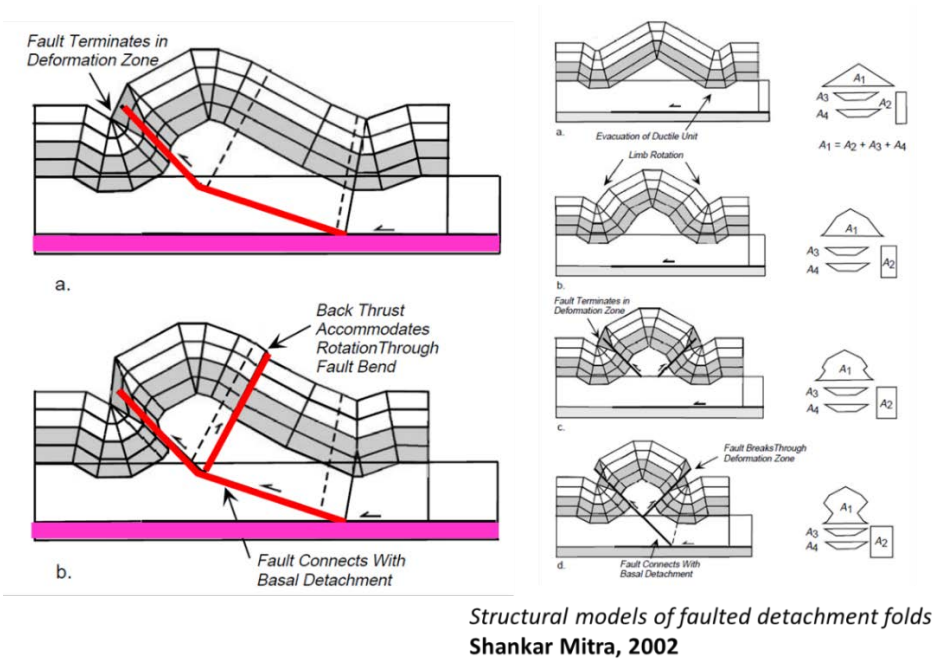


**Figure 7. 9** Structural models of Faulted Detachment folds (S. Mitra, 2002). A Similar Pop-up structure is formed in the B-1 Structure.

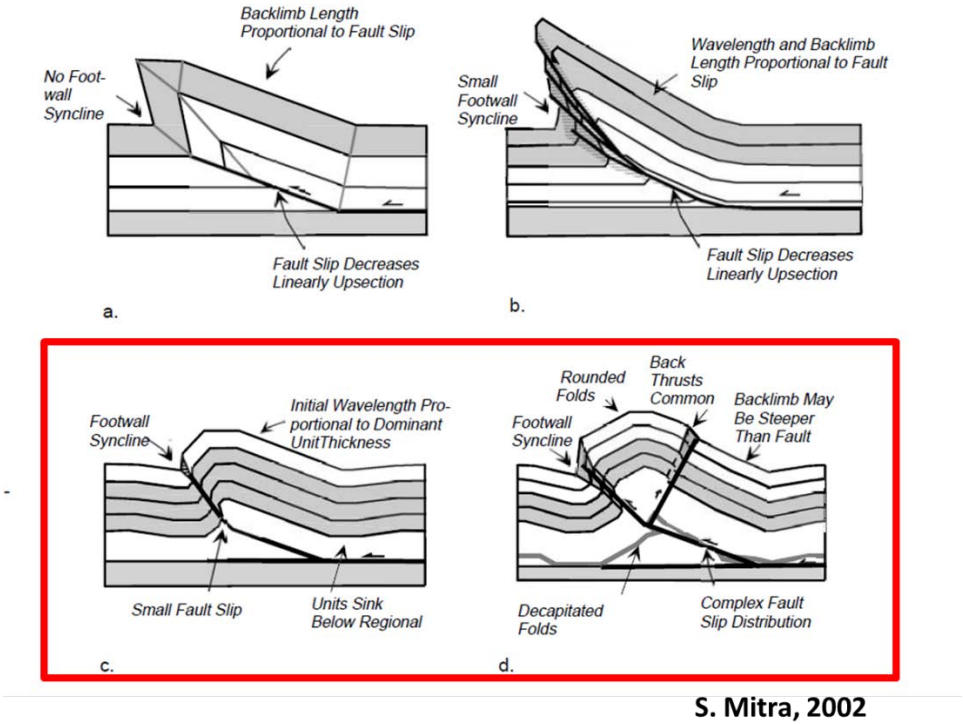


**Figure 7. 10** Comparison between fault-propagation and faulted detachment folds. **(a)** Self-similar fault-propagation fold; **(b)** trishear fault-propagation fold; **(c)** faulted detachment fold (model 1) Like structure A in the study area; **(d)** faulted detachment fold (model 2), Similar as structure B in the study area. (S. Mitra, 2002).

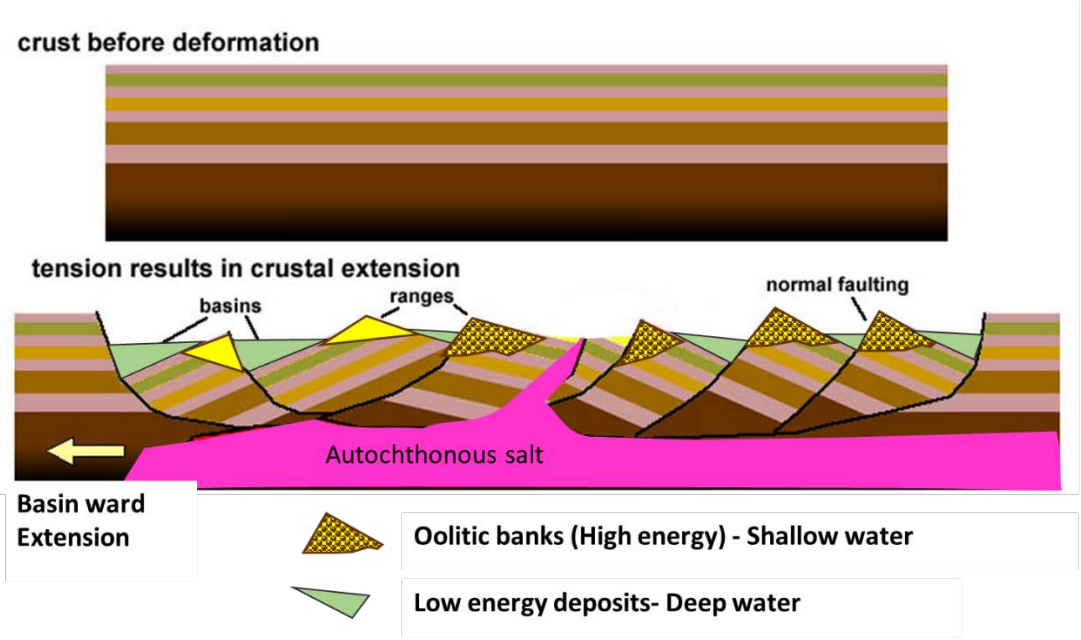


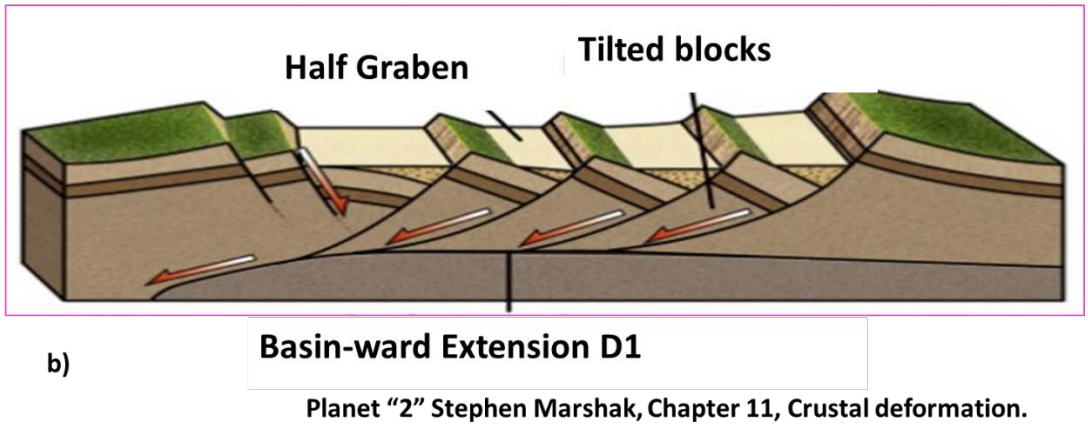


**Figure 7. 11** "Rampa Estructurada" (Structured ramp) after R. Portillo et al. 2017. **a)** Display of the three stages of the extensional linked system (Brun & Fort, 2012). **b)** During the Extensional domain D1, the study area is located in the Extensional stage of the linked system (Geology lecture 12, Mountain Building); **c)** Schematic model of the structured ramp showing high and low energy deposits during the extension of the tilted blocks.

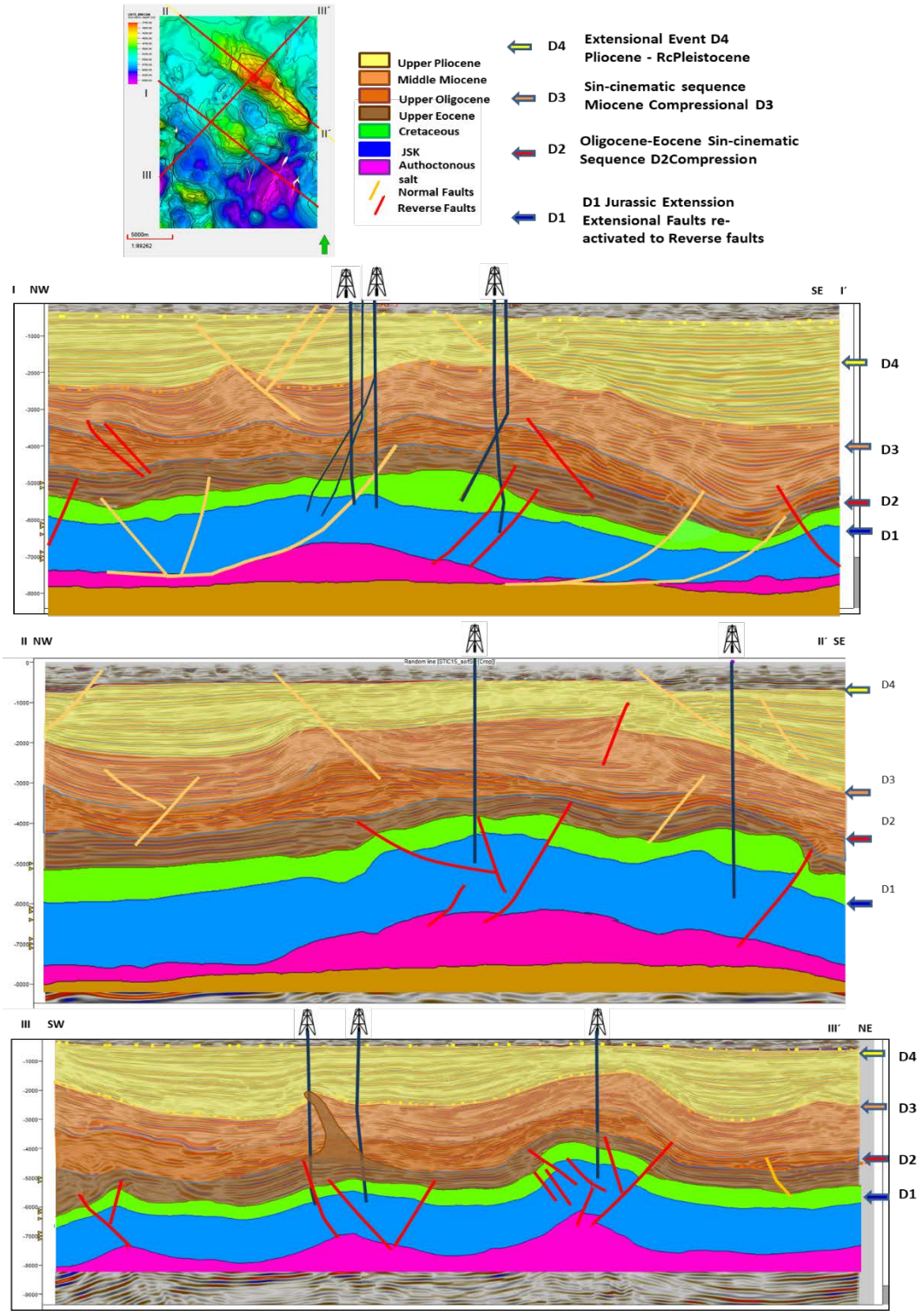


**Figure 7. 12** Three structural sections: I-I´Parallel to Structure A, II-II´, parallel to structure B, both to show the direction of the Extension in the area; and III-III´perpendicular section to both structures, showing their maximum shortening, since the direction shows the principal direction of the Compression events D2 and D3.

## CHAPTER 8. Fracture analysis.

Fractured carbonates have great importance in Mexico since more than 85% of hydrocarbon production comes from naturally fractured carbonate reservoirs, (Monroy Santiago, 2012). In addition, more than 60% of the world´s oil and 40% of the gas reserves are held in carbonates. (Schlumberger, 2018). Some of the most important Mexican carbonate reservoirs are located in the South Gulf Salt Province (SGSP) in Campeche Bay. Accurate analysis of fracture behavior on the area is accordingly of fundamental importance to México´s petroleum industry.

This section analyzes fracture patterns and their relationship to the evolution of the structures. Cores, thin sections, petrophysics, and image logs were integrated to develop the fracture characteristics, focusing exclusively on the Cretaceous basinal carbonate reservoir (**Figure 8. 1**).

### 8. 1 Fracture analysis (small scale).

The multidisciplinary methodology used in the fracture analysis was developed by PEMEX (Mexican Petroleum) and IMP (Mexican Petroleum Institute) by Monroy and Zaldivar 1998 – 2014, and included the workflow of fracture diagenesis and paragenesis analysis by Laubach et al. 2010 and Gale at U.T. Austin. The method includes core analysis integrated with measurement of fracture sets and kinematic indicators (stylolites, striations, foliation or sigma structures). Fractures were color-coded as open, partially open or closed. The fracture analysis was carried out by the fracture group of which I am a member. The information is contained in internal reports compiled from PEMEX 2009-2014.

***Fracture analysis methodology.***

The following steps were followed (**Figure 8. 1)**.

1. Rotation of the cores to true North to ensure correct orientation of the fracture sets using image logs. (Zaldivar, 1998).

2. Graphing of measurements on stereo-plots with fracture sets classified to study their orientation (Figure 8.1 a). When thin sections are absent, the colors assigned are cyan for open with hydrocarbons, dark blue for partially open, and red for closed (J. Zaldivar et al. 2000-2014).

3. Analysis of thin oriented sections (diagenesis and paragenesis). Description and analysis of thin sections defining the nature of the fractures and understanding the relationship between the relative ages of the fracture sets, determining their strikes, spacing, and aperture (**Table 2**). Color classification for diagenesis studies (determined by the observed qualitative conductivity) is as follows in Figure 8.1 b): green for open with good conductivity, yellow for partially open with regular conductivity and red for closed with null conductivity. (Prieto et al., 2014).

**Figure 8. 5** exemplifies the initial three steps of the analysis.

4. Analysis and interpretation of image logs identifying the principal fracture directions within the interest zone and the fracture density curve (**Figure 8. 2**).

5. Petrophysical analysis of the complex (double or triple porosity) porous media in carbonates, reveals in the area matrix and fracture porosity.

***Fracture measurement in cores.***

The application of the fracture analysis methodology on the study area shows some of the results measured for the “A” structure in Figure 8. 3. This figure contains

the fracture rose diagrams for wells A1 and ADL obtained from cores, thin sections, and image log information.

***Implementation of fracture analysis – sample results.***

The methodology described successfully produced accurate and compelling data on the structures within the Cretaceous and Upper Jurassic Kimmeridgian reservoirs. The current analysis addresses only the Cretaceous reservoirs.

Data from well A1 and ADL are discussed below.

***Well A1.***

Well A1 has two cores within the Cretaceous. Core one is located in the Upper Cretaceous, while core two is in the Middle Cretaceous. Fractures in both cores were measured, analyzed and classified. The rose diagrams depicted in Figure 8. 3 show the results. Thin section study was only performed on the second core in well A1; fractures were analyzed and classified according to their observed qualitative conductivity as good, regular or null.

The fracture intensity measured in both cores indicates that core 2 (Middle Cretaceous) has higher fracture intensity (229 measured fractures = 25 fractures/m) than the core 1 (Upper Cretaceous with 82 measured fractures = nine fractures/m). Moreover, the fractures in core 2 present better qualitative conductivity.

***Well ADL.***

Well ADL has core data analysis and image log fracture analysis within the Cretaceous. Two cores were analyzed: core one, located in the Upper Cretaceous and core 2 in the Middle Cretaceous. Thin section analysis was done exclusively in core

number 2. However, only one direction of regular conductivity was detected. The low fracture intensity detected, indicates that the interval of the core was not the best interval within the Middle Cretaceous such as core 2 in well A1. Nevertheless, the best interval was determined later with interdisciplinary studies of image logs and petrophysics.The resulting rose diagrams of the measured and discretized fractures displays in **Figure 8. 3.**

Compared with A1 well, the fracture measurements on well ADL show that core 1 (Upper Cretaceous) and core 2 (Middle Cretaceous) have a very similar fracture intensity (Core 1: 123 fractures = 20 fractures/m vs. Core 2: 112 fractures = 18.6 fractures/m). However, the partially open fractures are more significant in number within the Middle Cretaceous.

Unlike the core fracture measurements, the image logs analysis indicate that the Lower Cretaceous interval shows the maximum fracture density with 180 fractures, Upper Cretaceous coming in second with 76 fractures and the lowest fracture density is present within the Middle Cretaceous with 16 fractures detected. These findings demonstrate greater fracture density within the Lower Cretaceous Period.

***Well B4.***

Well B4 has one core analyzed within the Upper Cretaceous. Fractures were measured, analyzed and classified. The rose diagrams depicted in **Figure 8. 4** show the results. A thin section studied in this core shows the analyzed fractures and classified them according to their observed qualitative conductivity. However, only one direction of good conductivity was detected. The low open fracture intensity detected, indicates that the interval of the core was not the best interval within the Cretaceous.

Nevertheless, the best interval was determined later with interdisciplinary studies of petrophysics.

Fracture measurements in well B4 show similar fracture intensity in connection with A1 and ADL wells, within the Upper Cretaceous, i.e., well B4:123 fractures =13 fracts./m; well A1: 82 fractures = 9 fracts./m; and well ADL: 123 fractures = 20 fracts/m. Nevertheless, it shows only one direction of good conductivity.

Compared with the core analysis, image logs have less sensitivity to detect fractures, because image logs are indirect measurement tools. However, they cover a greater interval, since they can be run along the entire well. On the other hand, core data represent hard and more reliable data but, this data covers a smaller interval. Both tools represent different measurement scales with a different range, sensitivity, and extension. The ideal way to analyze the fracture systems is to employ both tools if possible with calibration between measurements.

### 8. 2 Fault and Fracture comparison.

The most critical faults already interpreted and modeled in the 3D seismic volume (chapter 7), were graphed on rose diagrams and divided into normal and reverse faults. They were additionally classified as faults related to the Mesozoic deformational episodes and into those developed during the Tertiary Period. The graphs facilitated a comparison of fault with fractures from the analyzed cores, thin sections and image logs.

The trends of the major faults interpreted on the 3D seismic and 3D structural model were represented and discretized on rose diagrams according to color: yellow for main Mesozoic normal faults, red for thrust faults and green for normal Tertiary faults.

**Structure "A."**

The most important and representative faults for Structure "A" were projected on the rose diagrams as shown in **Figure 8. 5**.

**Figure 8. 6** shows the main fracture sets in Structure "A" from wells A1 and A4. A1 results were determined from cores and thin sections, A4 measurements come from image logs. **Figure 8. 7** includes wells A1 and A4. It exhibits the plots of the nearest faults to the wells and the open fractures measured within them to clarify the relationship between the fractures recorded on wells and the trend of the structure and faults.

The open fractures trend in well A1 is transverse to the fold axis and are therefore referred to as transverse fractures (Type 1 of Stearns and Friedman, 1972), whereas the open fractures in well A4 are parallel to the fold axis and to the principal regional faults surrounding the zone and are referred to as longitudinal fractures (Type 2 of Stearns and Friedman, 1972).

The open fractures direction in well A1 is related to the extensional transverse fractures created during the compressional episodes by extension parallel to the fold axis (Stearns and Friedman 1972; Nelson, 2001; Jadoon et al., 2005; Li et al., 2018), (**Figure 8. 7**). On the other hand, the open fracture sets in well A4 perpendicular to A1, are extensional longitudinal fractures related primarily to curvature parallel to the fold

axis due to local deformation, they are also enhanced by greater curvature in the vicinity of major reverse faults. (**Figure 8. 7**).

Transverse and longitudinal extensional fractures usually develop a high angle inclination and are considered of excellent conductivity, (Stearns and Friedman 1972; Golf-Racht, 1982; Florez-Nino et al., 2005 and Jadoon et. al, 2006).

***South-east part of structure "A" and "B".***

**Figure 8. 7** shows the south-east area within structures "A" and "B", represented by wells ADL and B4. The open fracture sets (**Figure 8. 6**) in ADL, are parallel to those in well A1, transverse to the trend of the structure. The open fracture set is parallel to the direction of the contractional deformation episodes **Figure 8. 7**. This suggests that the response of the open fractures in well ADL, as in well A1, are generated by extension parallel to the fold axis (Type I), during the compressional episodes D2 and D3. The open fractures direction in well B4 is parallel to that in well A4. These fractures are longitudinal extensional fractures (Type 1) originated by the two compressional episodes D2 and D3.

**Figure 8. 8**, shows a) the fold models related to the fractures type I and type II by Stearns (1969, 1972); b) the model relating these two types with the names of Transverse extension fractures (type I) and Longitudinal extension fractures (type II), (Price and Cosgrove, 1990) and c) the most representative open fracture set in the study area, perpendicular to the fold trend (extensional transverse fractures, created by compression).

The fracture data suggests that both longitudinal and transverse fractures can be open or partially open and increase conductivity within the reservoir. However, the analyzed data denotes that the transverse fractures are more conductive than the longitudinal fractures due to their better quality. This may be related to the present day in situ regional stresses in the areas. Well data in the study area, suggests that the maximum horizontal compressive stress trends approximately parallel to the transverse fractures. This would tend to keep these fractures open and increase conductivity. Additionally, the paragenetic studies indicate that these fracture sets are the latest formed in the area, allowing them to have higher permeability and less fracture- filling cement.

### 8.3 Fracture generation and its relationship with fold deformation.

Based on the structural interpretation of the 3D seismic data, the final structural model for both structures “A” and “B” is represented by faulted detachment folds. These detachment folds resulted primarily by the two compressional events D2 and D3 and caused the formation of the most important structural traps. Detachment folds by two main deformation mechanisms: hinge migration and limb rotation (Mitra, 2003), **Figure 8. 10** and **Figure 8. 11**.

Structures “A” and “B” have developed by detachment folding by both hinge migration and limb rotation during the contractional episodes, and faulted through by thrust faults. Some of the thrust faults are reactivated Jurassic-Early Cretaceous normal faults. The structures have also been affected by late-stage Tertiary extension during episode D4.

Many different relevant factors can control the naturally fractured carbonates, such as the regional and local deformation, the inherence of the closest-faults, lithology, porosity, mechanical stratigraphy and diagenesis (Milad, 2017; Milad, Ghosh and Slatt, 2018). The structural controls are directly related to the kinematic evolution of the folds.

Faulted detachment folds developed above broad salt pillows during deformational episodes. Hinge migration results in the development of longitudinal fractures over parts of the structure. Limb rotation results in local zones of high fracture density of longitudinal fractures in areas with maximum curvature. These zones are located at fixed hinges, where the curvature is the greatest. In the case of structures A and B, areas of highest curvature are typically near the crest of the structure, generating high angle fractures, where maximum curvature exist (Milad and Slatt, 2017). In addition, a local zone of high fracture densities can develop in the vicinity of thrust faults and reactivated normal faults (**Figure 8. 11**).

The transverse fractures are primarily related to extension perpendicular to the fold axis, possibly caused by the plunge of the fold axis. They may also be related to regional extension. These fractures may have developed late in the folding history.

According to the author's observation during the fracture analysis and to Golf-Racht, fractures are related to several states of stresses during the folding history and are being affected by diagenesis during these different stages.

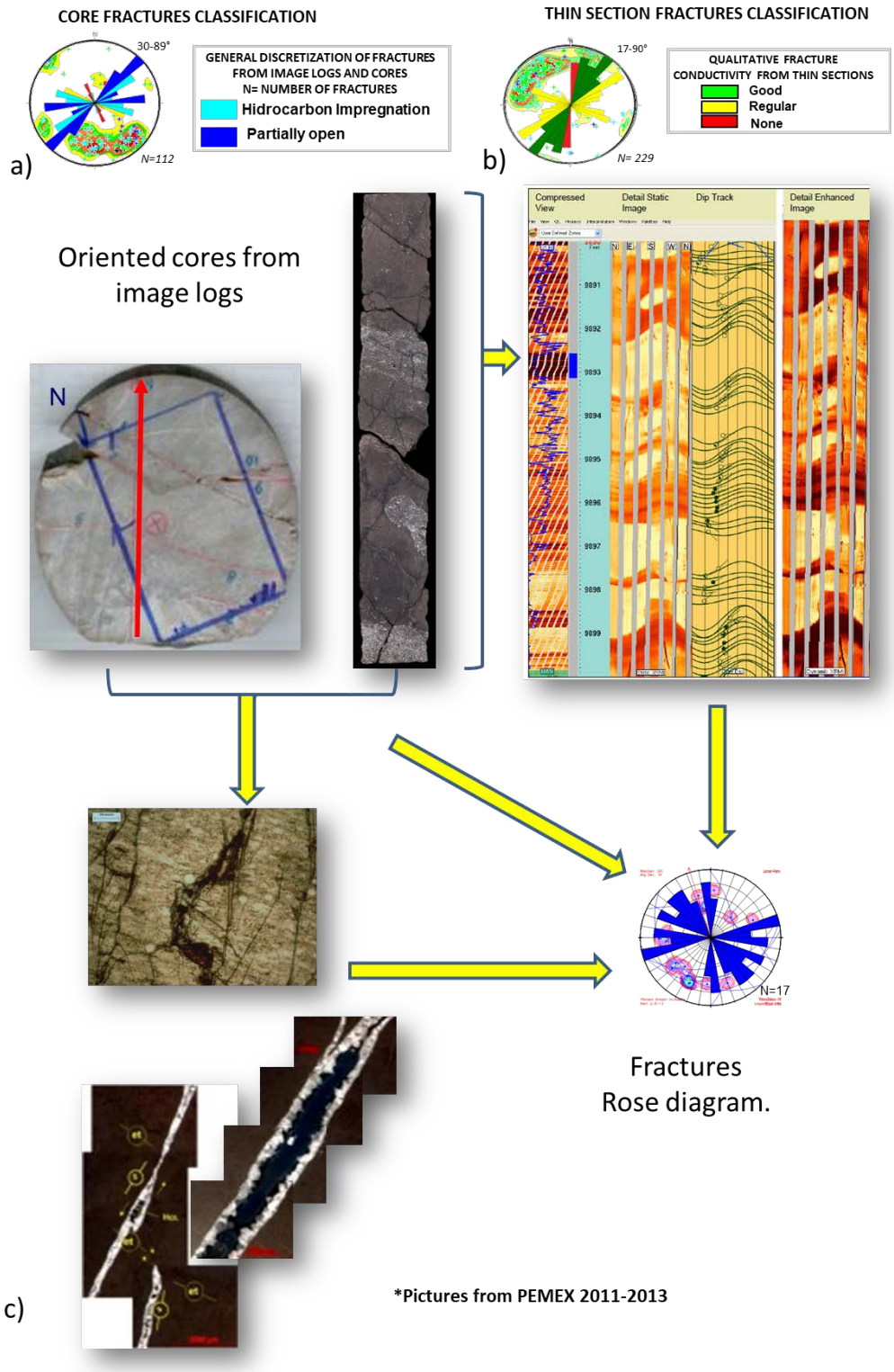


**Figure 8. 1** a) Classification for fractures measured in cores, b) Fractures classified by thin section. c) Methodology and different scales of fracture study: core orientation and measurement, thin sections and image logs analysis. Measurements graphed on rose diagrams. (PEMEX 2008- 2014).

**Table 2 Wells with core data, thin sections, and logs within the study area.**

| Structure | Well | Cret. Cores | Thin Section | Petrophysics | Image log |
|---|---|---|---|---|---|
| A | A1 | Upper | ✔ | ✔ | |
| | | Middle | | | |
| A | ADL | Upper | | ✔ | ✔ |
| | | Middle | | | |
| A | A2 | | | ✔ | |
| | A3 | | | ✔ | |
| A | A4 | | | ✔ | ✔ |
| | A30 | | | ✔ | |
| A | A50 | | | ✔ | ✔ |
| | A100 | | | ✔ | |
| B | B1 | | | ✔ | |
| | B4 | Upper | ✔ | ✔ | |

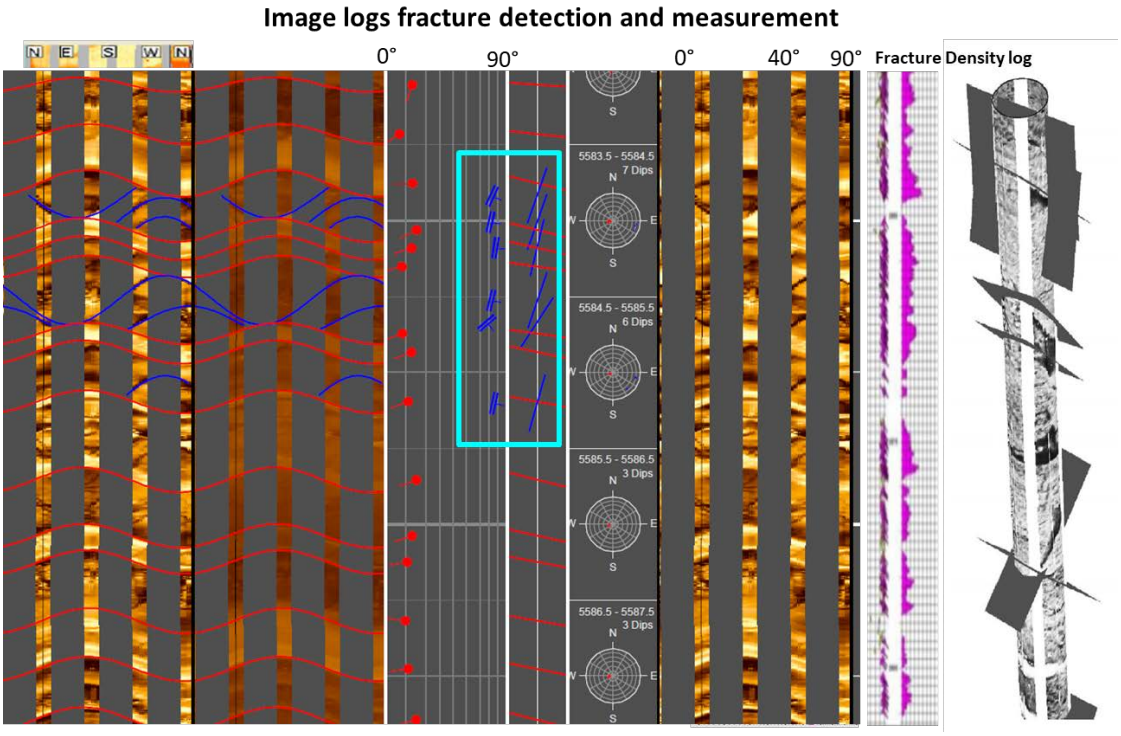


**Figure 8. 2** Image logs fracture detection, measurement, and analysis in one of the wells of the study area.

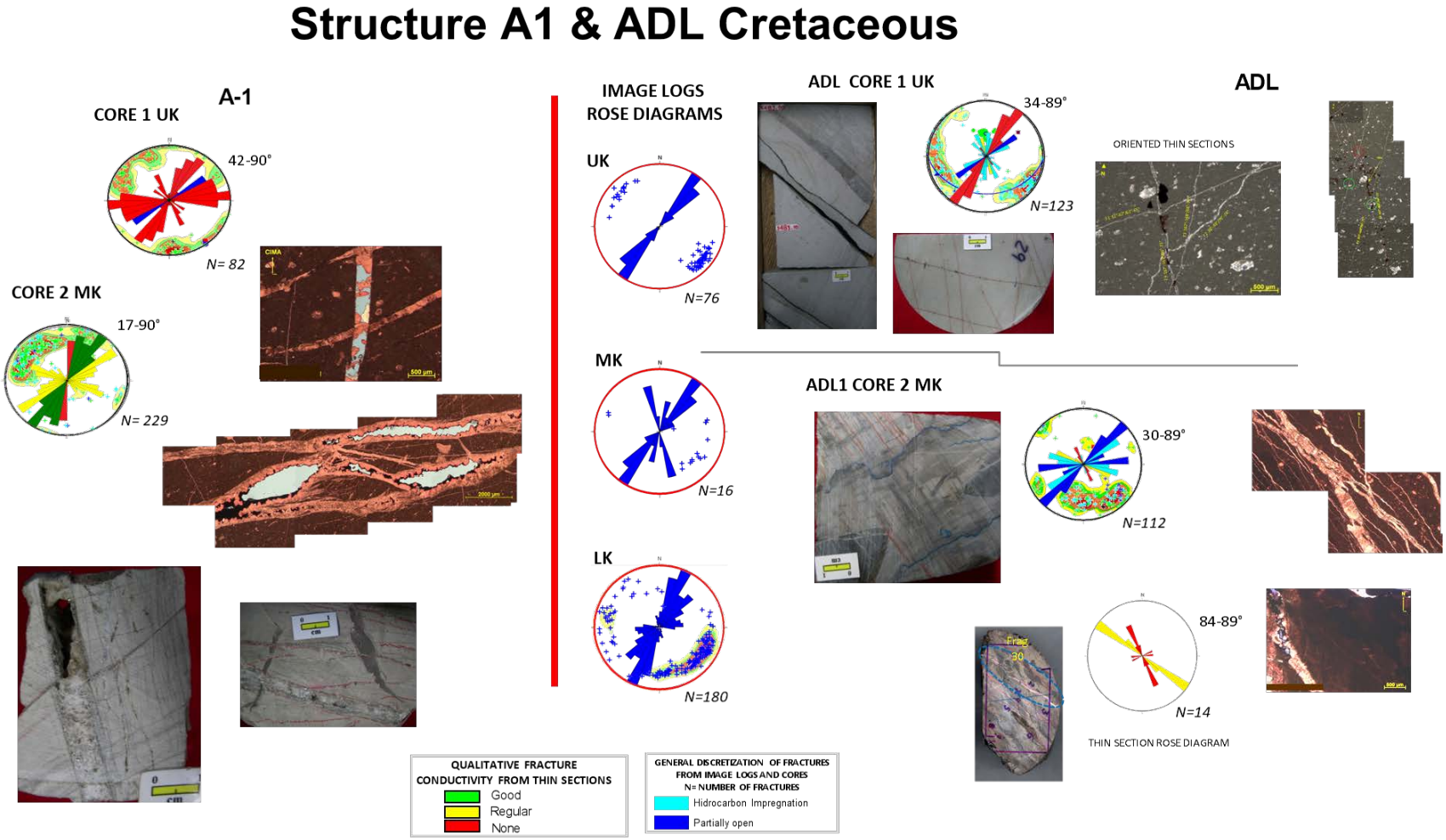


**Figure 8. 3** Fracture analysis of cores, thin sections and well image logs measured in Structure "A" on the wells A1 and ADL. A1 Core and thin section data, ADL core, thin section and image logs data results (Showing the principal open fracture directions on the rose diagrams and evidence of the fracture types in cores).

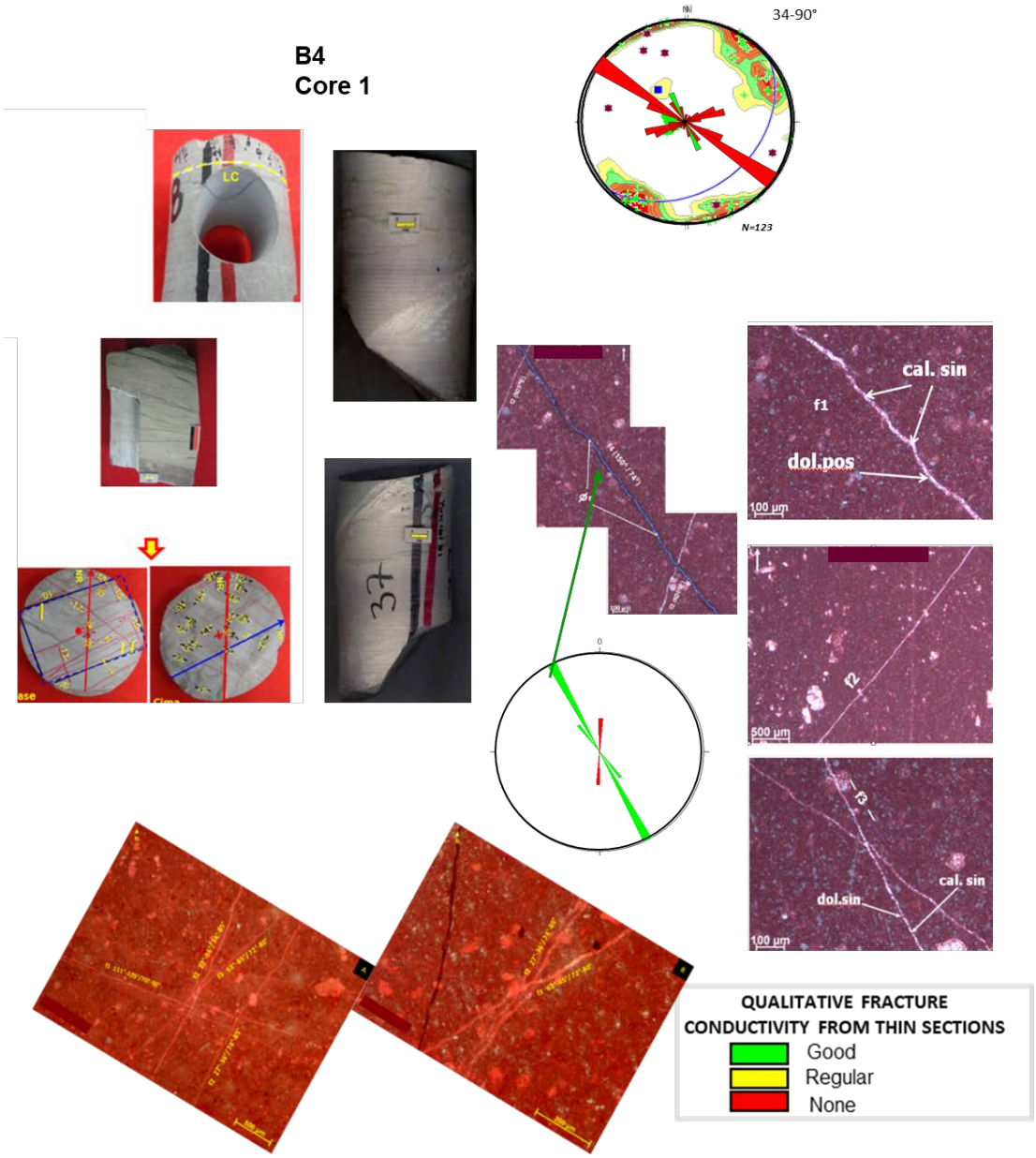


**Figure 8. 4** Fracture measurement and analysis in one core at Structure "B," well B4.

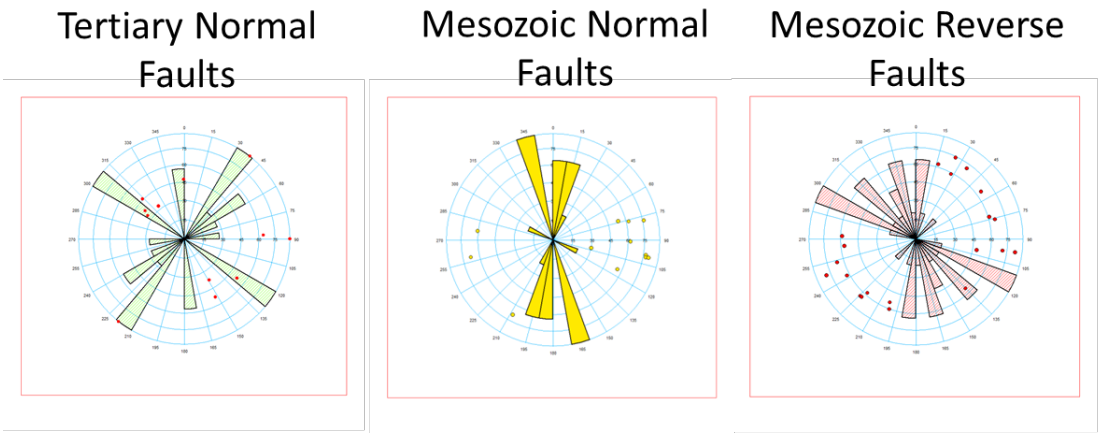


**Figure 8. 5** Rose diagrams projecting the most important faults related Structure "A." Tertiary normal faults, and Mesozoic normal and reverse faults.

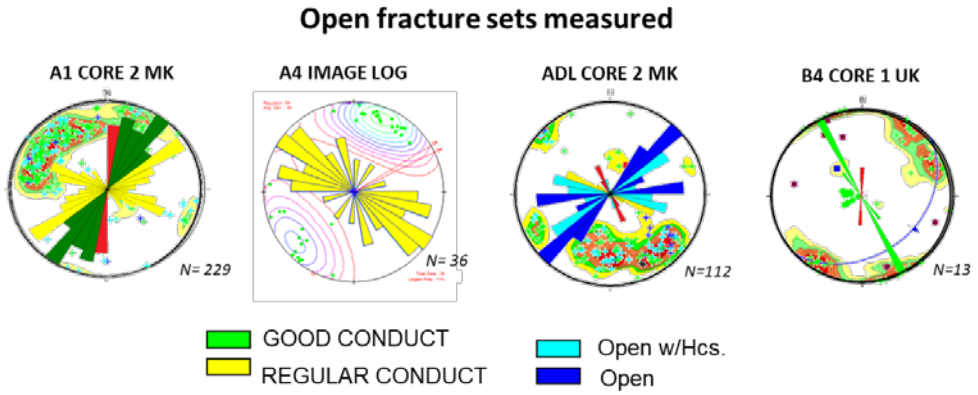


**Figure 8. 6** Open fractures measured in wells: A1 from core in the Middle Cretaceous, ADL from cores and image logs, A4 image logs, both measured for the entire Cretaceous and B1 from the core in Upper Cretaceous.

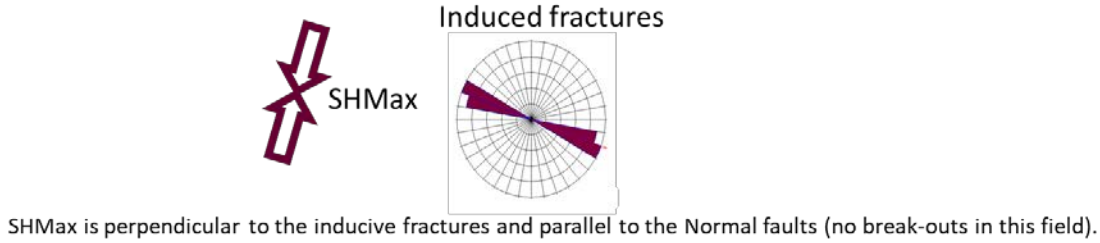


**Figure 8. 7** Induced fractures in Structure "A" and its proportional SHMax perpendicular to the fractures trend. Indicating the actual compressional strength in the study area.

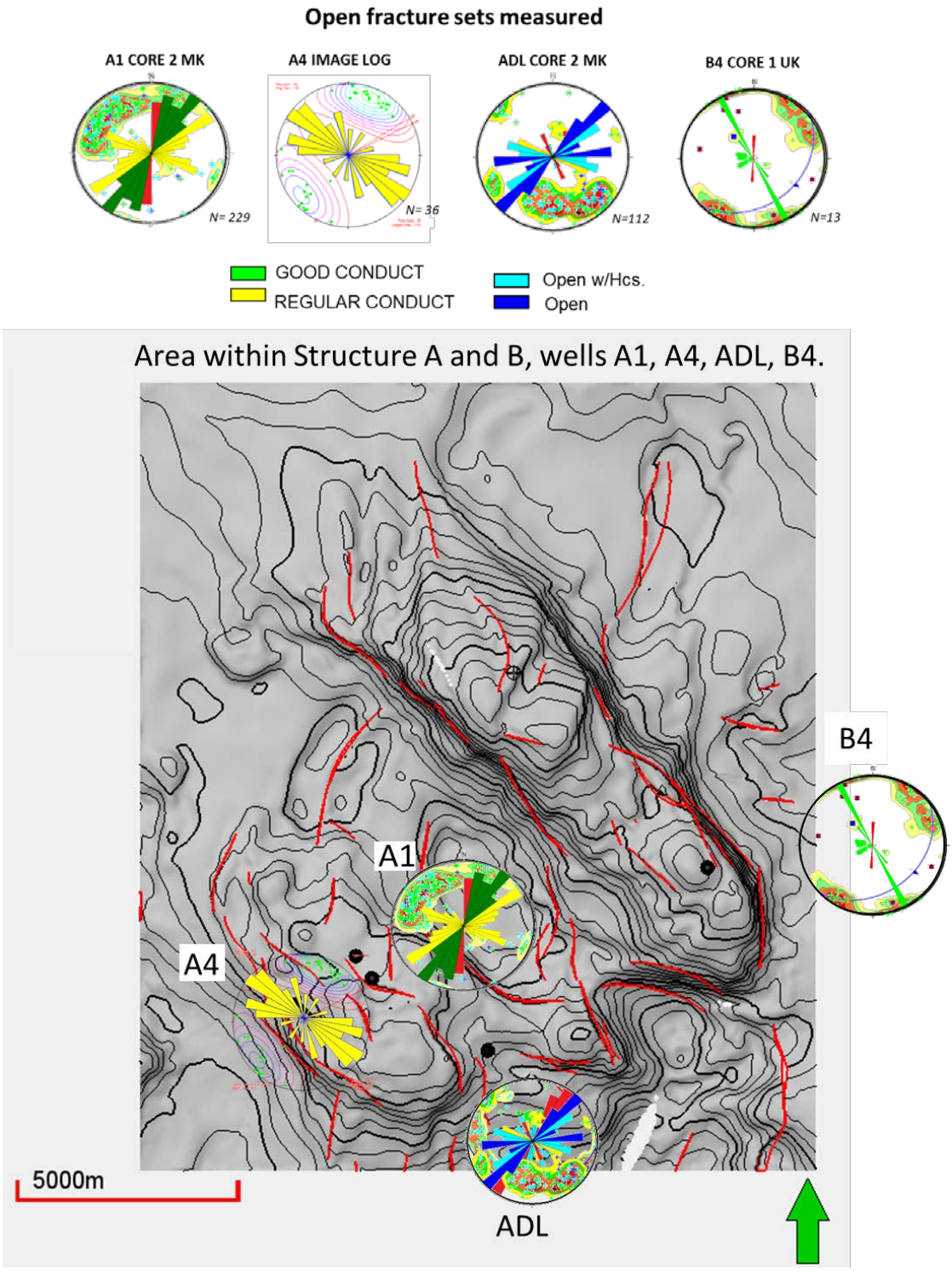


**Figure 8. 8** Rose diagram plots represent the open fracture directions obtained from the core analysis (A1, ADL and B4), image logs (A4) and the closest normal and reverse faults to this structures.Upper Cretaceous map showing the principal faults interpreted (red lineaments) and the open fracture sets measured in wells A1, A4, ADL, and B4.

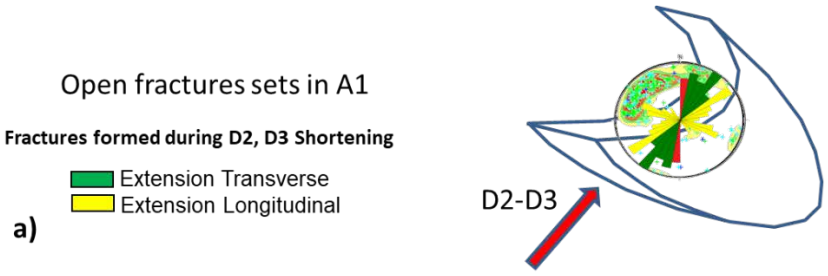


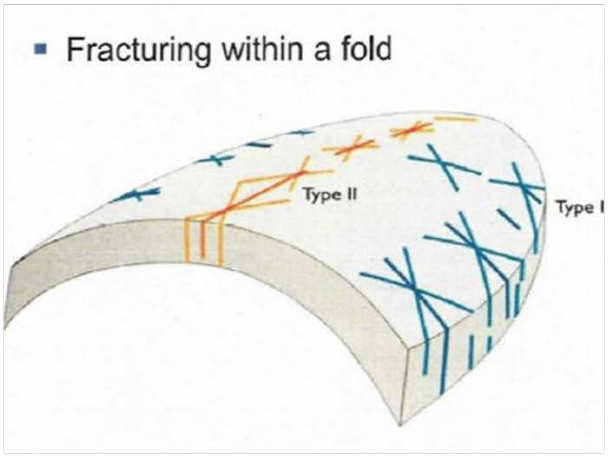


b)

(Modified after Stearns and Friedman, 1972)

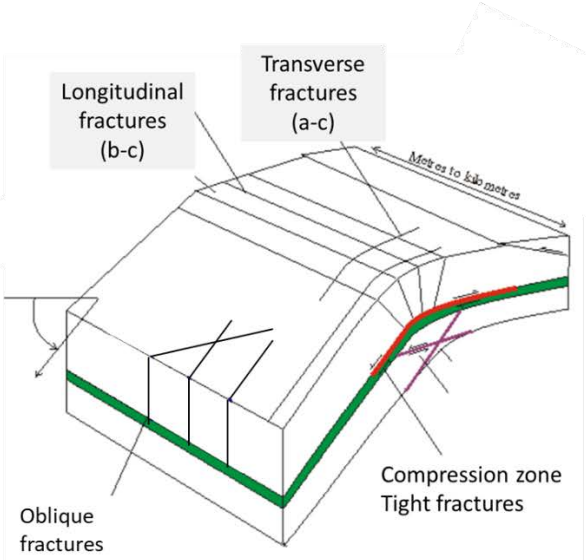


c)

Based on Price and Cosgrove, 1990.
(Modified by uwe.ac.uk/geocal/totalgeology)

**Figure 8. 9** Principal open fractures systems in well A1 compared with a) Stearns and Friedman 1972 fracture model within a fold, differentiating them as Types I and II. b) Price and Cosgrove 1990 Same sets of fractures classified in transversal, longitudinal and share compared with the tectonic axes of an open fold. (b) Classification of significant open fracture systems in Structure A as Extension -Tension Type I, relating them to the deformation events of the region.

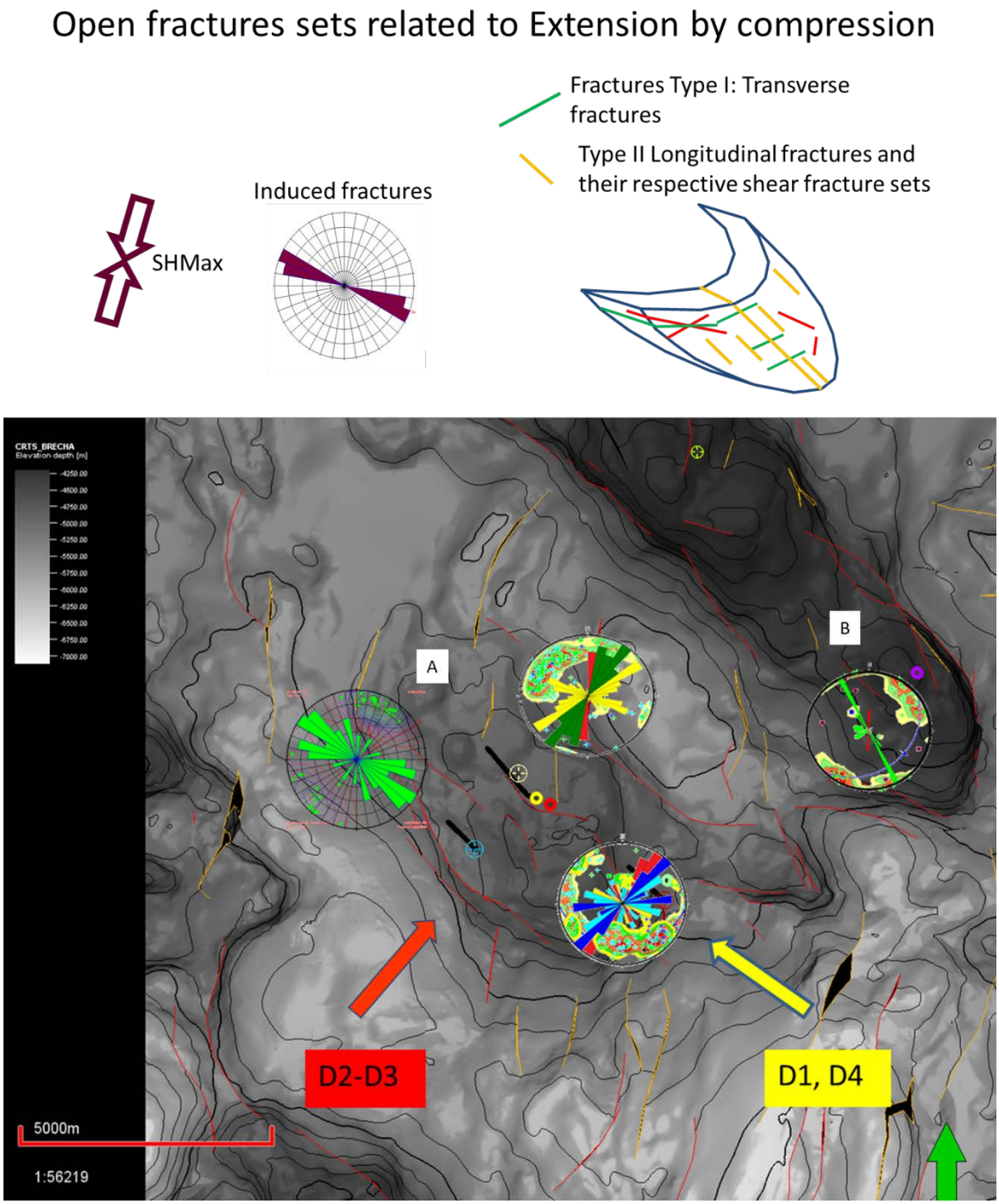


**Figure 8. 10** Top of Upper Cretaceous Map showing the open fractures sets in structures A and B compared and related with the SHMax Maximum horizontal stress and the extensional fractures created by compressional episodes D2 and D3.

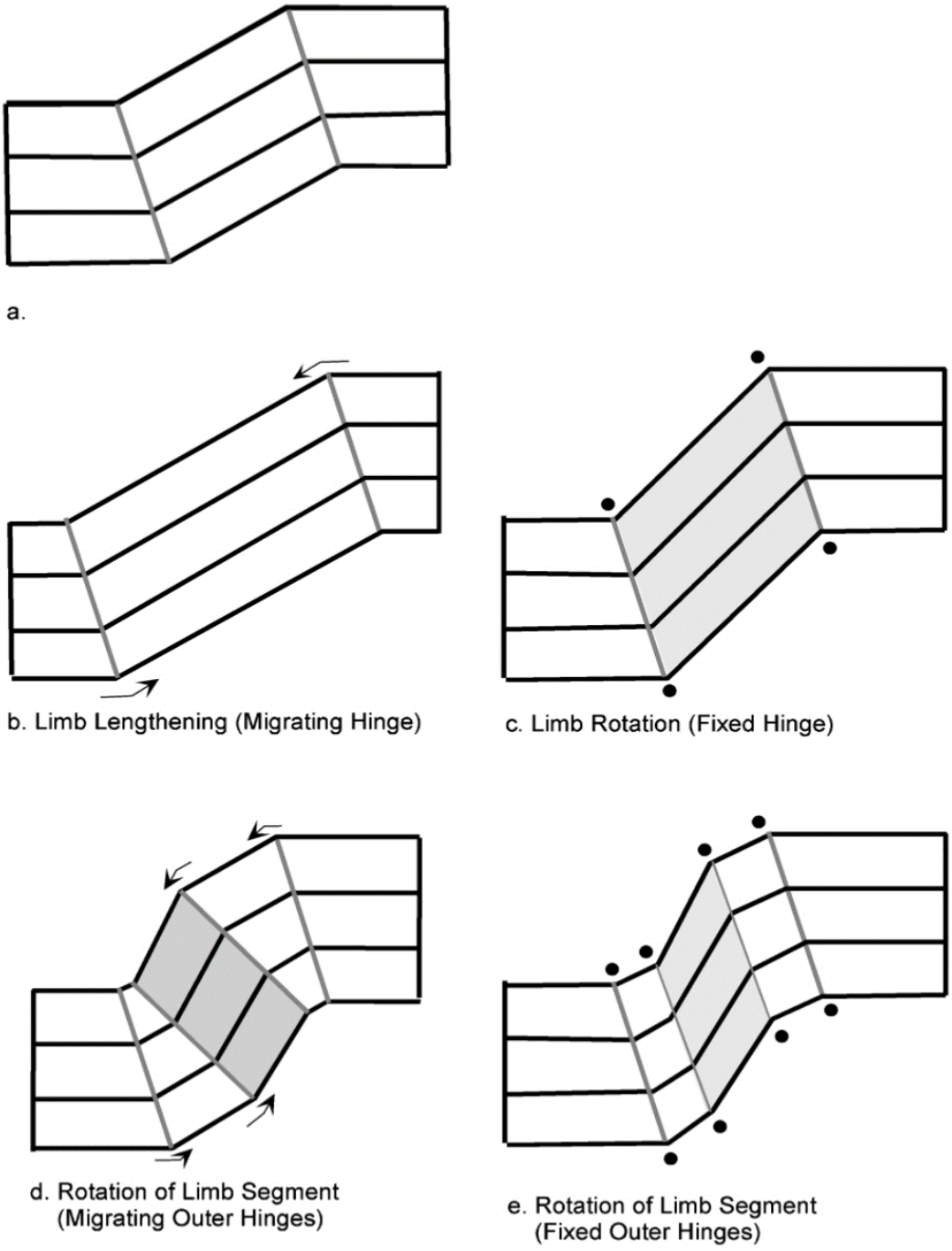


**Figure 8. 11** Comparison between a) hinge migration and b) Limb rotation around fixed hinges mechanisms generated after compression, forming during a detachment fold model. (adapted from Rafini and Mercier 2002 by Riadh Ahmadi 2007, 2013). Lines 1–5 show the evolution of the fold limb schematically in the pre-growth strata.

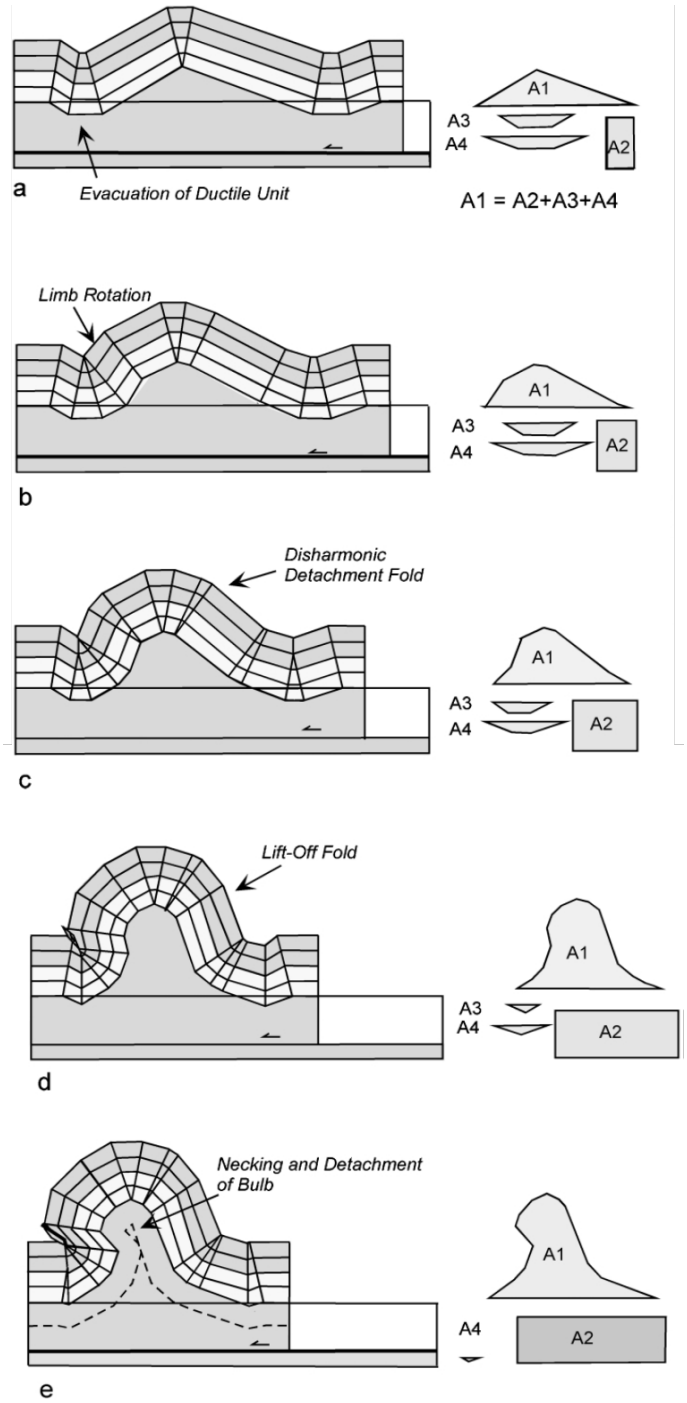


**Figure 8. 12** Stages of the evolution of a detachment fold model. (Mitra, 2003). a) Initial development of a low amplitude detachment fold, similar evolution as "A" structure in the study area. b–d) Growth of fold from a disharmonic detachment fold to a lift-off fold by rotation of limb segments and migration of material from the synclinal area to the fold limbs. The limb rotation may initially occur without appreciable internal deformation, and subsequently by shear between fixed hinges. Similar evolution stages for "B" structure in the study area. e) Late stage deformation results in overturning and necking of beds and the formation of a detached bulb.

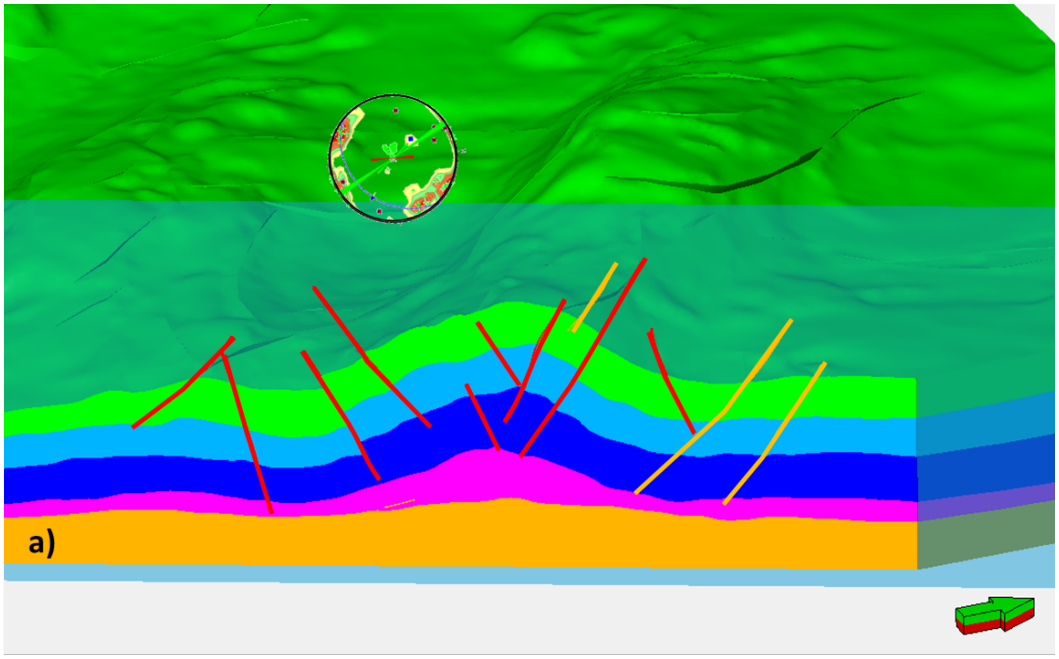


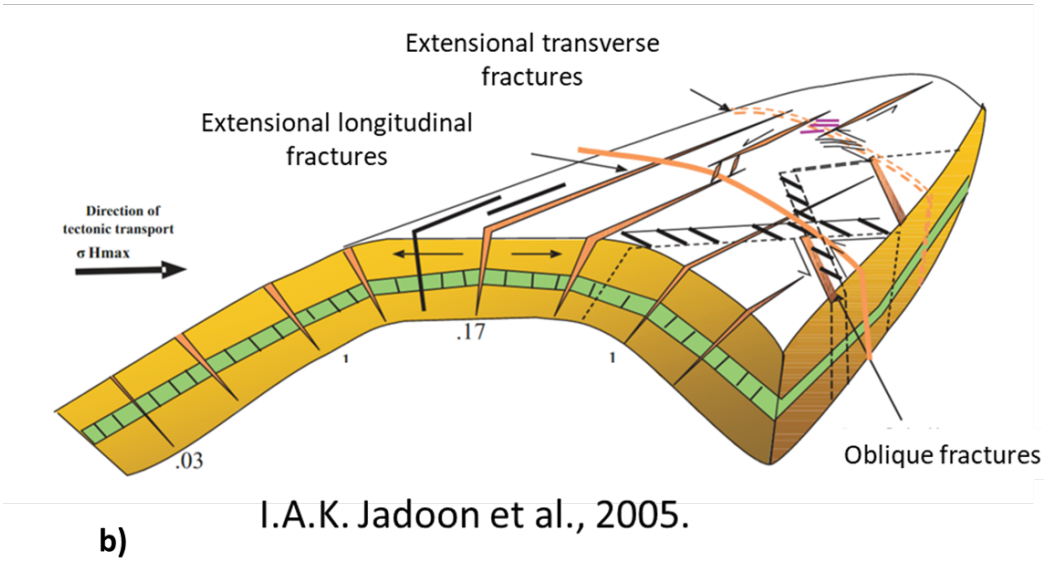


**Figure 8. 13** Comparison between the most developed structure of the study area: "B" and a model structures relating the analog extensional fracture types formed along and across the fold (longitudinal and transverse).

## CHAPTER 9. Conclusions.

Interpretation of the structural geometry, fault orientations, and related fracture distribution is conducted on two structures (A and B) in the South Gulf Salt Province (SGSP) in Campeche Bay, Mexico. The structures are located in the most important developed hydrocarbon province in Mexico.

The structures have a complex structural history and were affected by four major episodes of deformation. These are (1) upper Jurassic to early Cretaceous gravitational extension, D1, forming roll-overs in structure "A" and salt pillows in structure "B"; (2) Eocene-Oligocene compression (D2), followed by (3) Middle-Upper Miocene compression (D3), both resulting in the formation of faulted detachment folds, and (4) late Miocene to Recent extension (D4).

The stratigraphy of the Upper Jurassic Kimmeridgian period in the area is divided into six cycles, the most productive of which are cycles four, five, and six. The facies consist of dolomitized mudstone-wackestone to packstone-grainstone of ooids with fracturing and related dissolution. The Cretaceous stratigraphy is divided into ten cycles, with cycles five through ten (Middle through Upper Cretaceous) being the most productive. Fractured mudstone-wackestone, occasionally recrystallized or brecciated make up some of the reservoirs.

A 3D model of the Mesozoic reservoir units has been built to display the structural geometry. The model is based on 3D seismic data combined with the guidance of geometric attributes, i.e., Fault Likelihood and Tracking. Four horizons were modeled: top of Upper Cretaceous, Top of Upper Jurassic Kimmeridgian, top and

base of autochthonous salt. In addition, 400 faults were interpreted, with 100 of them included in the 3D model.

The study area is characterized by the presence of salt diapirism and faulted detachment folds (structures “A” and “B”). D1 and D4 extensions and D2-D3 compressions resulted critical for the formation of structural and stratigraphic traps within the fractured carbonates reservoirs of the Upper Jurassic Kimmeridgian and Cretaceous.

Fracture analysis was applied to the Cretaceous reservoirs. Integrating cores, thin-section and image log data. According to the fracture measurements, the Middle Cretaceous has the highest fracture density. The open fracture trends were transverse and longitudinal to structures “A” and “B”. The two open directions were formed due to extension during the compressional episodes D2 and D3 corresponding with types I and II according to the classification of Stearns (1972). The transverse set of fractures has the best conductivity in the study area. Additionally, these open fractures sets are parallel to some of the normal Tertiary faults (D4), and to the present day maximum horizontal compressive stress, suggesting that this fracture trend posses the best probability to be open. The Cretaceous reservoirs of the study represent type I and II of Nelson´s classification for fractured reservoirs, where the fractures provide the essential permeability to the reservoir.

The understanding of the most deformed zones and the integration of the structural geology analysis with multidisciplinary studies are critical for new prospects location.

## References


Angeles-Aquino, F. J., 2006, Monografia Petrolera De La Zona Marina. IN SPANISH. Monograph Of The Marine Zone Oil: Boletin de la Asociacion Mexicana de Geologos Petroleros, p. 69.

Angeles-Aquino, F., and A. Cantu-Chapa, 2001, Subsurface Upper Jurassic stratigraphy in the Campeche Shelf, Gulf of Mexico: The Western Gulf of Mexico Basin. Tectonics, Sedimentary Basins, and Petroleum Systems., v. 75, p. 343–352.

Cantú-Chapa, A., 2009, Upper Jurassic Stratigraphy (Oxfordian and Kimmeridgian) in Petroleum Wells of Campeche Shelf, Gulf of Mexico: AAPG Memoir, v. 90, no. 2001, p. 79–91, doi:10.1306/13191079M902804.

Cantu-Chapa, A., and R. Landeros-Flores, 2001, The Cretaceous-Paleocene boundary in the subsurface Campeche Shelf, southern Gulf of Mexico: The Western Gulf of Mexico Basin. Tectonics, Sedimentary Basins, and Petroleum Systems., v. 75, no. Figure 1, p. 389–395.

Chopra, S., and K. J. Marfurt, 2015, Is curvature overrated? No, it depends on the geology: First Break, v. 33, no. 2, p. 45–55, doi:10.3997/1365-2397.2014021.

Davis, D. M., Engelder, T., 1985. The role of salt in fold-and-thrust belts. Tectonophysics 119, 67-88.

Florez-Nino, J. M., A. Aydin, G. Mavko, M. Antonellini, and A. Ayaviri, 2005, Fault and fracture systems in a fold and thrust belt: An example from Bolivia: AAPG Bulletin, v. 89, no. 4, p. 471–493, doi:10.1306/11120404032.

Golf-Racht, 1982, First part: Fundamentals of fractured reservoir engineering. Chapter1: 1-30 p.

Grajales-Nishimura, J. M., E. Cedillo-Pardo, C. Rosales-Domínguez, D. J. Morán-Zenteno, W. Alvarez, P. Claeys, J. Ruíz-Morales, J. García-Hernández, P. Padilla-Avila, and A. Sánchez-Ríos, 2000, Chicxulub impact: The origin of reservoir and seal facies in the southeastern Mexico oil fields: Geology, v. 28, no. 4, p. 307, doi:10.1130/0091-7613(2000)28<307:CITOOR>2.0.CO;2.

Grajales Nishimura, J. M., E. Cedillo Pardo, C. Rosales Dominguez, D. J. Moran Zenteno, W. Alvarez, P. Claeys, J. Ruiz Morales, J. Garcia Hernandez, P. Pedilla Avila, and A. Sanchez Rios, 2000, Chicxulub impact: The origin of reservoir and seal facies in the southeastern Mexico oil fields (vol 28, pg 307, 2000): Geology, v. 28, no. 12, p. 1152, doi:10.1130/0091-7613(2000)28<307:CITOOR>2.0.CO;2.

Hale, D., 2012, Fault surfaces and fault throws from 3D seismic images: SEG.

Jadoon, S. K., A. H. Bhatti, A. Ali, and I. A. K. Jadoon, 2005, Fracture Characterization

and Their Impact on the Field Development: no. November, p. 1–12, doi:10.2118/111053-MS.

Li, Y., G. Hou, K. R. Hari, Y. Neng, G. Lei, Y. Tang, L. Zhou, S. Sun, and C. Zheng, 2018, The model of fracture development in the faulted folds: The role of folding and faulting: Marine and Petroleum Geology, v. 89, p. 243–251, doi:10.1016/j.marpetgeo.2017.05.025.

Magoon, L. B., T. L. Hudson, and H. E. Cook, 2001, Pimienta-Tamabra (!)-A giant supercharged petroleum system in the southern Gulf of Mexico, onshore and offshore Mexico: AAPG Memoir, v. 75, p. 83–125.

Marfurt, K. J., 2006, Robust estimates of 3D reflector dip and azimuth: Geophysics, v. 71, no. 4, p. P29, doi:10.1190/1.2213049.

Marfurt, K. J., V. Sudhaker, A. Gersztenkorn, K. D. Crawford, and S. E. Nissen, 1999, Coherency calculations in the presence of structural dip: Geophysics, v. 64, no. 1, p. 104, doi:10.1190/1.1444508.

Milad, B., 2017, The Effect of Karsting on Natural Fracture , Hardness , and Brittleness of the Hunton Limestone and Paleo- Deposition of the Woodford Shale : A Study Using 3-D Seismic , Outcrop , Well Log , and Core Data *: v. 51417.

Milad B., Ghosh S., and S. R., 2018, Comparison of rock and natural fracture attributes in karsted and non-karsted Hunton Group Limestone : Ada and Fittstown area , Oklahoma and Much More Comparison of rock and natural fracture attributes in karsted and non-karsted Hunton Group Limestone : A: no. April, p. 69–86.

Milad, B., and R. Slatt, 2017, Integrated 3-D Seismic , Outcrop , and Core Data for Characterization of Natural Fractures of the Hunton Limestone and the Woodford Shale in Central Oklahoma *: v. 51382, p. 1–3.

Mitra, S., 2003, A unified kinematic model for the evolution of detachment folds: Journal of Structural Geology, v. 25, no. 10, p. 1659–1673, doi:10.1016/S0191-8141(02)00198-0.

Mitra, S., 2002, Structural models of faulted detachment folds: AAPG Bulletin, v. 86, no. 9, p. 1673–1694, doi:10.1306/61EEDD3C-173E-11D7-8645000102C1865D.

Monroy Santiago, F., 2012, Interrelationships Between Carbonate Diagenesis and Fracture Development : Example From Monterrey Salient , Mexico and Implications for Hydrocarbon Reservoir Characterization: p. 369.

Murillo-Muñetón, G., J. M. Grajales-Nishimura, E. Cedillo-Pardo, J. García-Hernández, and S. García-Hernández, 2002, Stratigraphic Architecture and Sedimentology of the Main Oil-Producing Stratigraphic Interval at the Cantarell Oil Field: The K/T Boundary Sedimentary Succession: Proceedings of the SPE International

Petroleum Conference and Exhibition of Mexico, p. 643–649, doi:10.2118/74431-MS.

Nelson, R. A., 2001, Geologic Analysis of Naturally Fractured Reservoirs: 351 p.

Padilla y Sanchez, R. J., 2007, Evolución geológica del sureste mexicano desde el Mesozoico al presente en el contexto regional del Golfo de México: Boletín de la Sociedad Geológica Mexicana, v. LIX, no. 1, p. 19–42.

Prieto, C. U., S. Di-Dio-Balsamo, F. Monroy-Santiago, and N. A. Olaez, 2014, Methodology to Integrate Multiscale Fracture Analyses in Fractured Systems Modeling: Application to Reservoirs of Southeastern Mexico*.

Qi, Xuan; Marfurt, K., 2017, Aberrancy.

R. Portillo, R. Peterson, D. C., 2017, Rampa Estructurada, influencia en el ambiente sedimentario durante el Jurasico superior, porcion Pilar de Akal., *in* CMP Congreso Mexicano del Petroleo: p. 1–19.

Rivera, R. S. S. et al., 2011, Tectonic Evolution of the South Gulf Salt Province in the Gulf of Mexico: Gulf Coast Association of Geological Societies Transactions, v. 61, p. 421–427.

Salvador, A., 1987, Late Triassic-Jurassic Paleogeography and Origin of Gulf of Mexico: ABSTRACT: AAPG Bulletin, v. 63, no. 4, p. 419–451, doi:10.1306/2F917F19-16CE-11D7-8645000102C1865D.

Stearns and Friedman, 1972, Reservoir in fractured rock. In R.E. King (Ed.), Stratigraphic Oil and Gas Fields-Classification, Exploration Methods, and Case Histories.: AAPG Memoir 16.

Zaldivar, J., 1998, Estudio Genetico del Fallamiento y Fracturamiento en Rocas Carbonatadas para la Caracterizacion de Yacimientos: Mexico, UNAM, p. 172.